New Approaches to Reinforce Cast Aluminum

João Francisco Oliveira Barbosa

FEUP Supervisor:

Prof. Dr. Manuel Vieira

INEGI Supervisor:

Dr. Omid Emadinia

Dissertation submitted to the Faculty of Engineering of the University of Porto for the degree of Master of Science in Material Engineering

DEMM, Faculdade de Engenharia da Universidade do Porto Rua Dr. Roberto Frias,

4200-465 Porto, Portugal

Porto, july 2023

Abstract

The incessant search for better and superior properties leads to the development of composites. These consist of the junction of two distinct materials, in which one reinforces the other, acquiring properties that would be unattainable otherwise. Bearing this, the aims of this study were (1) to produce powder composite and mix it with liquid aluminum, (2) to produce bimetallic composites, and (3) to characterize both base and reinforced alloys.

Throughout this study, bimetallic composites, i.e., aluminum casts reinforced with a steel sheet, and a composite powder consisting of A356 alloy milled chips with 10 wt.% alumina, were produced and studied.

The bimetallic composites were investigated by microstructural, tensile, microstructural and fractography analysis. Through the forementioned characterization techniques, it was found that the implementation of steel sheets, with holes with the aim of improving the bonding, on A356 casts led to a decrease of up to half of both the yield strength and ultimate tensile strength. However, ductility was enhanced by a large amount, even though elongation values were relatively low on the A356 T6 heat-treated base alloy. Furthermore, an intermetallic layer composed of different Al-Si-Fe ternary phases was observed. These were increasingly harder closer to the steel insert. Also, a discontinuity line along in the aluminum matrix along the insert was evidenced, which is hypothesized to be caused by silicon segregation.

When it comes to the composite powder, the alumina had a heterogeneous distribution across the aluminum, and had twice the hardness values of the base alloy.

Keywords: Aluminum Alloys; Casting; Composites; Intermetallic Layer; Reinforcement.

Resumo

A procura incessante por propriedades melhores e superiores leva ao desenvolvimento de compósitos. Estes consistem da junção de dois materiais distintos, em que um reforça o outro, adquirindo propriedades que de outro modo seriam inalcançáveis. Deste modo, como objetivos deste trabalho definiram-se (1) produzir pó compósito e misturar com alumínio líquido, (2) produzir compósito estrutural e (3) caraterizar a liga base e ligas reforçadas.

No decorrer deste estudo, compósitos bimetálicos, i.e., fundidos de alumínio reforçados com uma chapa de aço, e pó compósito que consiste em aparas moídas da liga A356 com 10% em peso de alumina, foram produzidos e estudados.

Os compósitos bimetálicos foram investigados por análise de microestruturas, tração, microdureza e superfície de fratura. Através das técnicas de caraterização supracitadas, descobriu-se que a implementação de chapas de aço, com furos para melhorar a ligação, em fundidos de alumínio originou uma perda de até metade da tensão de cedência e tensão máxima à tração. No entanto, a extensão após rotura melhorou significativamente, embora os valores do alongamento se demonstrem relativamente baixos na liga base A356 tratada termicamente no estado T6. Simultaneamente, diferentes fases ternárias de Al-Si-Fe foram descobertas na camada intermetálica. Estas eram incrementalmente mais duras à medida que se aproximavam do inserto. Por outro lado, uma linha de descontinuidade foi detetada na matriz de alumínio que acompanhava o inserto, que se hipotisa ser causada por segregações de silício.

Relativamente ao pó, a alumina apresentou uma distribuição heterogénea na matriz de alumínio, e valores de dureza de aproximadamente o dobro comparativamente à liga base.

Palavras-chave: Camada Intermetálica; Compósitos; Fundição; Ligas de Alumínio; Reforço.

Acknowledgements

The development of the current work demanded high amounts of dedication, resilience, and time management. However, the work reflected in this document was the fruit of a conjoined effort and support from various people. Bearing this, I would like to express my genuine and deepest gratitude:

To Engineer Hélder Nunes for all the guidance, experience, kindness, and patience exhibited throughout the development of the present work. For always striving to improve the value of my work, and the unconditional availability displayed.

To Dr. Omid Emadinia, for the opportunity, encouragement, and guidance. For all the assistance, and shared knowledge, which surely made me learn a lot.

To Prof. Dr. Manuel Vieira for the opportunity to participate in this project and work directly with INEGI. His experience and mentoring guaranteed the best possible path.

To Engineers Rui Madureira, José Silva and Gonçalo Soares for the help displayed throughout the practical work, more precisely on the composite casting and mechanical tests.

To my parents and my sister, for their unconditional love and support. They always know best.

Lastly, to all of my dearest friends, for all the support and happy moments created both before and during my five years of college. A special thank you to Lúcia, for always seeing the best in me.

I gratefully acknowledge the funding of Project Hi-rEV – Recuperação do Setor de Componentes Automóveis (C644864375-00000002). This research was funded by the Project PAC (PO-CI-01-0247-FEDER-046095), cofinanced by COMPETE 2020 through FEDER and by National Funds through FCT.

I also acknowledge INEGI for the work opportunity, and CEMUP (Materials Center of the University of Porto) for the expert assistance with SEM.

Contents

List of Figures

List of Tables

List of Acronyms

A% - Elongation

CTE – Coefficient of Thermal Expansion

DAS – Dendritic Arm Spacing

DED – Direct Energy Deposition

DRA – Discontinuously Reinforced Aluminum

EDS – Energy Dispersive Spectroscopy

FEUP – Faculdade de Engenharia da Universidade do Porto

HPDC – High Pressure Die Casting

IML – Intermetallic Layer

INEGI – Institute of Science and Innovation in Mechanical and Industrial Engineering

LPSC – Low-Pressure Sand Casting

MMC – Metal Matrix Composite

OM – Optic Microscopy

PIC – Pressure Infiltration Casting

PSD – Particle Size Distribution

R&D - Research and Development

SEM – Scanning Electron Microscopy

SS – Specific Strength

UCS – Ultimate Compression Strength

UTS – Ultimate Tensile Strength

YS – Yield Strength

1 Introduction

1.1 Background and motivation

Nowadays, base materials have not been able to keep up with the component requirements for some industries, such as the automotive industry, for example. For this reason, base materials have been reinforced with other materials, creating what is known as a composite. These allow the manipulation of properties, enhancing the base materials according to the nature and quantity of the different materials used. Due to its' high importance, new ways of fabricating composites are the focus of research all around the world, competing to achieve increasingly better properties.

The present work focuses on producing aluminum-based composites, due to both the low density and relatively good functional properties this material presents. On the same note, different types of aluminum matrix composites are fabricated and evaluated, namely bimetallic composites with a steel sheet, through low-pressure sand casting (LPSC), and composite powder created by planetary ball milling. In turn, these composites are characterized through different micrograph techniques and also mechanically evaluated.

Bearing this, the current work is inserted in the context of two developing projects, namely the PAC project, which stands for Portugal AutoCluster for the Future, and Hi-rEV. PAC is being led by Simoldes – Plásticos, S.A., and focuses on addressing different technological challenges identified in the national automotive industry, in an effort to boost competitivity in the sector. This project also focuses on conjugating national automotive companies with various research and development (R&D) representative entities such as INEGI, where the present work is being developed. On the other hand, project Hi-rEV has the intent to position the national automotive cluster on the global value chains of the future car, through industry mobilization around development, testing and demonstration of new generation technologies, processes, and products.

1.2 Objectives

The main focus of this dissertation is to study new ways, or improve pre-existing ones, of producing aluminum composites, more specifically through liquid processing. These processes include LPSC of bimetallic composites, and stir casting, after producing composite powder with the use of planetary ball milling equipment. Furthermore, all composites fabricated are characterized. The most crucial stages are listed below.

- Literature review, procuring to deepen the experimental knowledge obtained, which comprises of: the different classifications of composites, as well as the plethora of composite liquid processing techniques, focusing more on stir casting and infiltration, and the various strengthening mechanisms that promote the property increase in composites.

- Produce A356 aluminum alloy composite casts, with steel sheets enclosed inside the cast, through LPSC. Produce composite powder, with A356 chips and 10 wt.% alumina, by planetary ball milling. Perform different characterization on the forementioned composites, which includes both optical (OM) and scanning electron microscopy (SEM), and hardness tests for both composite types. For the bimetallic composites, tensile tests and fracture surface analysis will also be carried out. Hot dipping procedure optimization parameters shall be studied as well, aiming to achieve a better bond between steel and aluminum. Finally, different measures are going to be performed on the latter composites, namely density and porosity, as well as intermetallic layer (IML) thickness.

1.3 Dissertation Structure

The current dissertation will consist of five different chapters, namely:

1. **Introduction:** Contextualization and scope of the dissertation are given, including the principal objectives.
2. **Literature Review:** Academic and theoretical basis in which the main topics of the current study are approached.
3. **Materials and Methods:** All the materials used, as well as the different procedures and test conditions are presented and thoroughly described.
4. **Results and Discussion:** Consists of an extensive description and analysis of the obtained results.
5. **Conclusion and Future Works:** In this chapter, the study’s most substantial conclusions are presented, accounting the acquired results and proposed objectives. Additional work that can be performed to improve and solidify the quality and robustness of this study was also presented in this section.

2 Aluminum Matrix Composites

Composites are a combination of, at least, two macroscopically different constituents or phases with a distinguishable interface between these. Their properties should also be significantly different than either of the constituent phases' individual properties due to interactions amidst them. With this in mind, there are two main protagonists in this type of material, namely the matrix and the reinforcement. The matrix corresponds to the continuous integrant, which is usually present in larger quantities, in charge of binding and protecting the reinforcement from both handling and the environment. Reinforcement, as opposed to the matrix, is commonly present in lower proportions and has, in most cases, higher strength, hardness and stiffness, therefore being responsible for enhancing the matrix's properties. Consequently, matrices can be classified according to their material class, that is metallic, ceramic, or polymeric. This study will focus essentially on metallic matrix composites, also known as metal matrix composites (MMCs) [1-3].

On this note, MMCs, as the name suggests, have a metallic matrix which can be reinforced with different types of materials such as other metals or ceramics. These reinforcements, in turn, can be classified according to their composition, shape or type, and size [4–6]. Composition classification includes ceramics, carbon-based reinforcements such as graphene and graphite, metals, and others [6]. On the other hand, shape or type classification consists in classifying the reinforcements as continuous fiber-reinforced composites, discontinuous or short fiber-reinforced composites and particle-reinforced composites, as demonstrated in Figure 1 [6]. Continuous fiber-reinforced composites can also go with the denomination of structural composites. At last, when it comes to size, reinforcements can be either on a micro or nano scale [6]. It is also important to state that the MMCs' mechanical properties are dependent on the amount, shape, size, and distribution of the reinforcement phase, as well as the base mechanical properties of the matrix material [4].

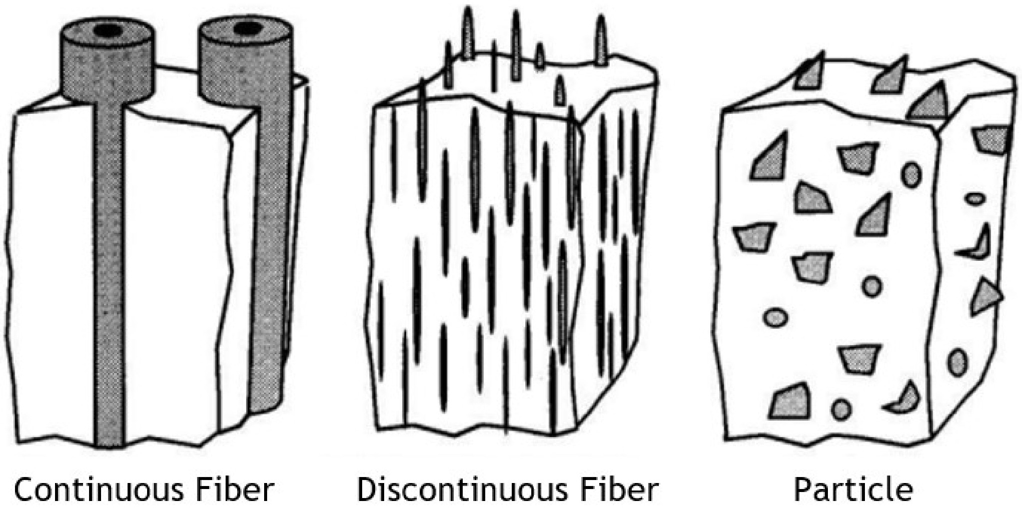

Figure 1 – Composite reinforcement classification [6].

Comparing metals with other matrix materials, such as polymers and ceramics, when addressing composites, there are some differences when it comes to property combinations and processing methods. For example, ceramic matrix composites are often produced to increase the toughness, while MMCs are built when the goal is to increase the strength and stiffness [7]. The prime culprit of this is the intrinsic differences between these types of materials as matrices and not because of the reinforcement class, as one would think. This is especially noticeable in properties such as conductivity. Since ceramics and polymers do not possess free electrons, both electricity and heat conductivity will be significantly lower than most metals [3, 8, 9].

One other important detail when considering producing and studying composites is the matrix/reinforcement compatibility. In other words, interfacial reactions between the composite constituents are of the utmost importance. In some cases, such as when producing Al-Steel bimetallic composites [10], intermetallic compounds are formed in the interface, ultimately deteriorating the composite properties, since these can also act as preferential sites for crack nucleation [11].

Conventionally, the matrix in MMCs is usually of a relatively ductile, low-density nonferrous alloy such as aluminum, the material of this work [7]. This is due to the fact that, in most cases, reinforcements will lower the ductility and fracture toughness of the matrix, making it imperative to have a ductile matrix material [11]. Aluminum matrix composites are of particular interest because of the combination of light weight, corrosion resistance, and functional mechanical properties. One other favorable characteristic of aluminum is its’ melting point, which is sufficiently high to allow it to be used in plenty of applications but also low enough to accommodate practicable processing temperatures [7].

As forementioned, according to the shape or type classification, the composites can either be continuous, if the reinforcement is comprised of various thin multifilaments or thick monofilaments, or discontinuous, if it consists in chopped fibers or particles, and aluminum matrix composites are no exception. Discontinuously reinforced aluminum (DRA) composites have proven advantageous due to being easier to manufacture with lower production costs and having somewhat more isotropic properties than their counterpart. On the other hand, more expensive continuous fiber reinforcements lead to a higher performance, being more commonly used in the aerospace industry to satisfy structural needs requiring high stiffness and strength [4, 12]. It is possible to observe a chart representing this in Figure 2 [4].

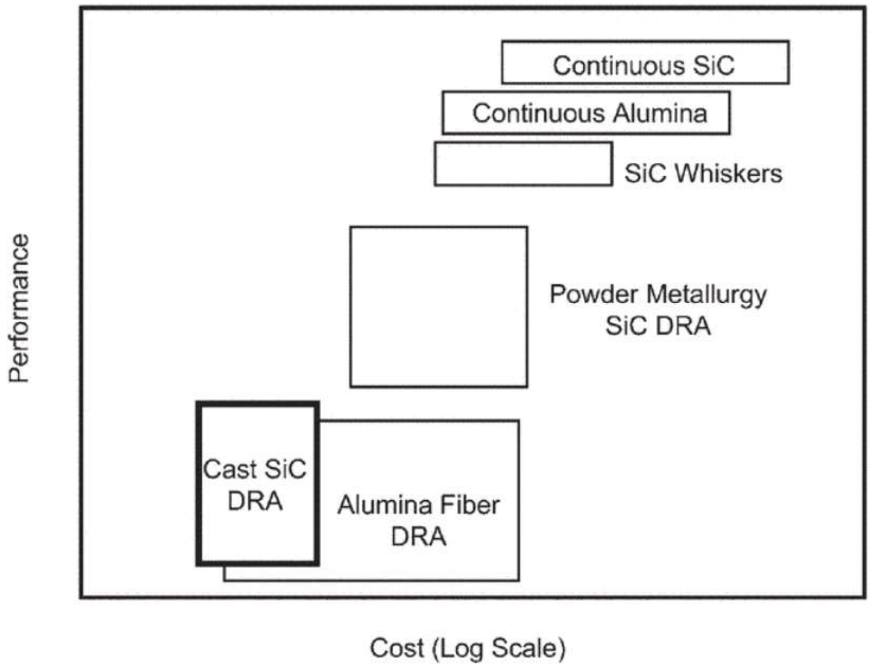

Figure 2 – Performance/Cost relation of different aluminum composites [4].

MMCs can be made through different two big families of processes, namely powder metallurgy and casting, and both have their own advantages and disadvantages [4, 6]. Focusing more on casting processes for producing aluminum composites, Al-Si alloys, such as the A356 alloy, are of particular interest due to their higher fluidity, provided by a larger content of an Al-Si eutectic [11, 13].

2.1 DRA composites

Discontinuously reinforced composites, as previously mentioned, have two main advantages favoring their production, when comparing to their counterpart. They can be manufactured using already-existing equipment, which leads to cheaper production, and also the properties can be partly tailored to match specification demands. The distribution of the reinforcement and the bond quality, between the whiskers or particles, and matrix, are the utmost important factors, since these will ultimately dictate the final product properties [4, 14]. In fact, the matrix is the principal load bearing component of the composite, while the reinforcements' application focus is to restrain the matrix deformation [15]. Additionally, it is crucial to state that in these kinds of composites, load transfer occur straight from the matrix to the dispersoid [4].

When it comes to DRA particle or whisker cast composites, the most widely used reinforcements are silicon carbides, SiC, and alumina, Al_2O_3 [4, 12]. Although, due to particles being in contact with molten aluminum, there is usually a reaction between the reinforcement and the molten alloy. Moreover, in the case of SiC, a detrimental phase, Al_4C_3, is formed at the interface [11]. The formation of this aluminum carbide causes a weakening of the material, and diminishes the melt fluidity and corrosion resistance of the casting.

Regarding the production of aluminum A356 and Al_2O_3 composites, Sajjadi et al. [16] stated that increasing the reinforcement quantity (wt.%) leads to overall higher yield (YS), as well as ultimate tensile (UTS) and compressive strength (UCS) due to a higher load transfer from the soft matrix to the hard reinforcement particles. However, this reinforcement quantity increase will also lead to higher porosity, lower ductility, and lower liquid metal flow, due to the existence of more Al_2O_3 surfaces from which pores can nucleate. Moreover, the authors also verified that there is a maximum micro Al_2O_3 content that can be added, namely 5 wt.%, from which point further increasing the reinforcement quantity will generate a decrease of the forementioned properties due to agglomeration and more porosities and defects.

Also, Al-Si alloys have some concerns regarding the formation and propagation of cracks. Yang et al. [17] noticed that pores cause an exceptionally damaging result in the mechanical properties of these alloys, more specifically elongation (A%) and UTS. This is due to higher strain accumulation on the Al-Si eutectic regions caused by the formation of microcracks on the edge of the pores under lower values of tensile stress. This, coupled with the fact that microcrack propagation is preferential along the eutectic zones, may ultimately cause a premature fracture of the material. This was summarized and schematized by the authors in Figure 3 [17].

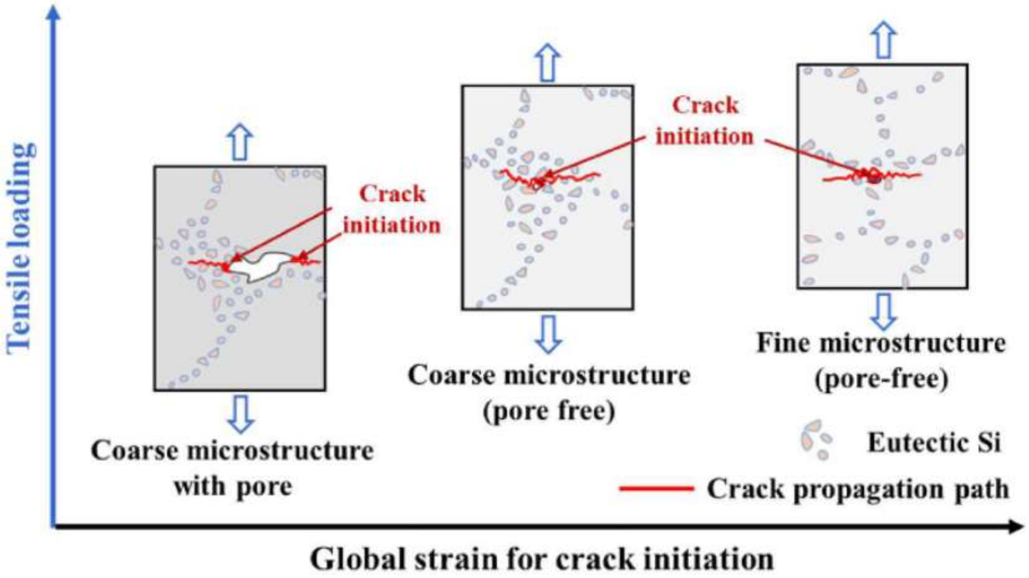

Figure 3 - Scheme of the crack propagation path on Al-Si alloys when tensile loaded [17].

When it comes to processes to produce DRA cast composites, it is possible to use practically any conventional casting method. However, one of the biggest concerns when producing these types of composites is the mixing between both phases, which will be addressed later on [4, 12].

2.1.1 Reinforcement Characteristics

Regarding DRA reinforcements, and focusing on powder, this is usually an assembly of a numerous quantity of small particles within a range of particle size distribution.

Furthermore, as it is the case with many other variables, it is important to have an accurate reinforcement characterization. This is to, simultaneously, have a better understanding of the properties generated in the final component and better traceability of the process. While there are many powder properties that can be determined, for liquid processing composite production there are a selective few that should be focused on. These include the size, shape, and powder composition [18].

Starting off with the size, there are two size classifications that should be considered. These include particle size, portraying the size of representative single particle, and particle size distribution (PSD), which stands for the overall size of the powder as a bulk. PSD can be contemplated as one of the most relevant properties since it allows the overall comprehension of the powder behavior. Moreover, it can be determined by a plethora of techniques, some more complex than others, sieving being the most common and simple [19, 20].

Moving on, the form of the different powder particles can be defined through the particle shape. The most common shapes are flaky, spherical, acicular, and irregular. These, alongside most of the other normalized shapes can be seen in Figure 4 [21]. Furthermore, spherical powder shape is considered the best, due to being able to confer a higher mechanical property replicability and flowability, which facilitates compacting [18]. SEM is possibly the most recurrent method used to obtain this characterization [20].

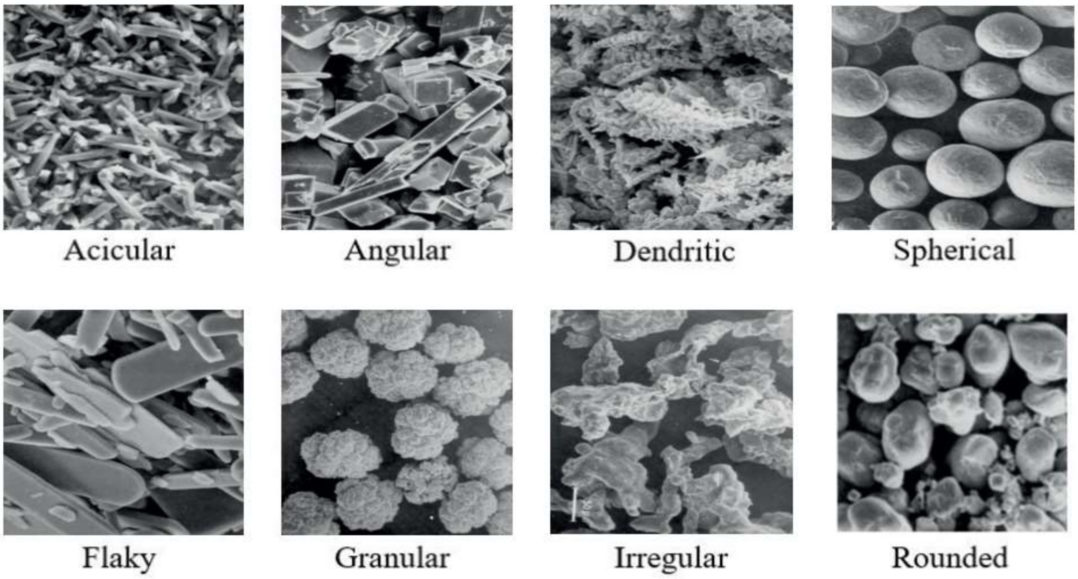

Figure 4 - Powder shape classification according to ISO 3252:2019 [21].

Lastly, when it comes to the chemical composition of the powder, it is important to accurately characterize it. For example, ceramic powders, such as Al_2O_3, have a substantial lack of wetting [7, 12]. Analysis of the powder can be made through different kinds of procedures that are implemented depending on the specific property that needs to be analyzed. This is shown in the chart in Figure 5 [22]. At last, although there are other techniques available, the most commonly used method to acquire this characterization is inductively coupled plasma optical emission spectroscopy [18].

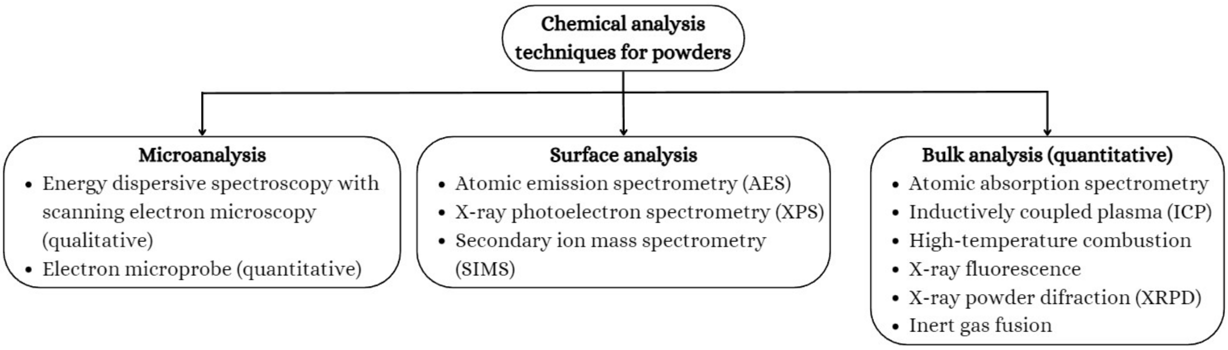

Figure 5 - Powder chemical analysis techniques. Adapted from [22].

2.1.2 Processing

Ceramic reinforced MMCs are also very difficult to process or machine, being important to try to apply near net shape techniques. Liquid processing has some vantages when producing these types of composites, namely a better bonding between matrix and reinforcement, and matrix microstructural control. Also, this kind of processing is very simple and presents low processing costs [23]. However, metal matrix reinforced systems are known for having bad wetting between both intervening phases, namely the matrix and the reinforcement. To compensate for this factor, in casting processes of discontinuously reinforced MMCs, external mechanical forces are necessary to allow the combination of both phases [7]. Although stir casting will be the main focus of this study due to being one of the simplest and most widely used processes, a scheme of the different mixing processes to produce composites can be seen in Figure 6 [7, 12].

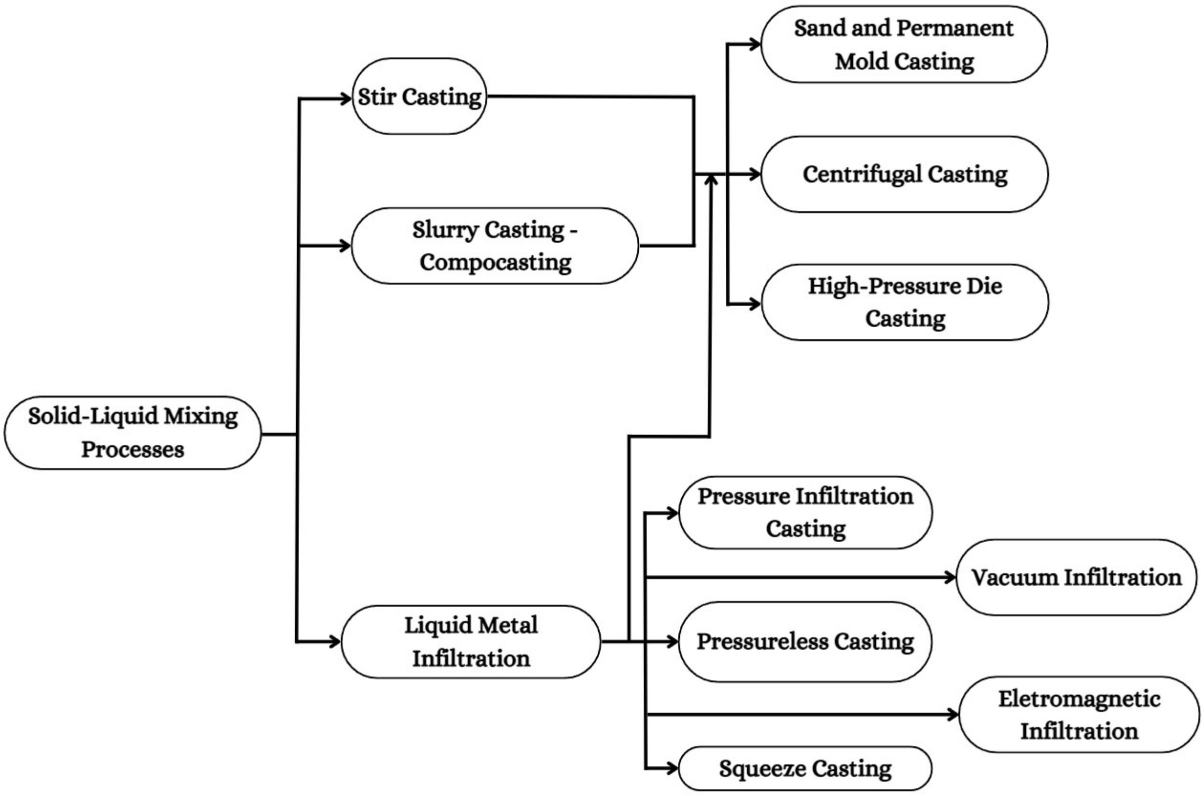

Figure 6 – Liquid state composite fabrication processes.

Mixing solid and liquid phases, especially powder particles in liquids, can be difficult, as one of the most concerning issues is the dispersion these will exhibit in the liquid environment. This translates to the difficulty of a solid phase, a powder, of being incorporated in a liquid medium while achieving a distribution of fine particles amidst the liquid. Bearing this, the quality of the final results of this kind of mixture is controlled by function of the shear rate, cohesiveness of the powder, contact angle, surface tension, viscosity, and the different interactions between both phases. Wetting, something that is also commonly mentioned, is directly related to the contact angle, and is heavily influenced by the surface, or interfacial, energy. Ultimately, low, or poor wetting will lead to a weak bond between phases [24–26].

2.1.2.1 Stir Casting

Stir casting is a group of composite fabrication processes that consist in adding the reinforcement, as loose particles, or whiskers, into continuously stirred molten metal. A scheme of the stir mixing process can be seen in Figure 7 [5]. This equipment usually contains a heating source, to keep the molten metal at the desired temperature, a motor, to allow the mixing, impellers, connected to the motor, to stir the melt, and inert atmosphere or vacuum for reasons that will be presented in the next paragraph [7].

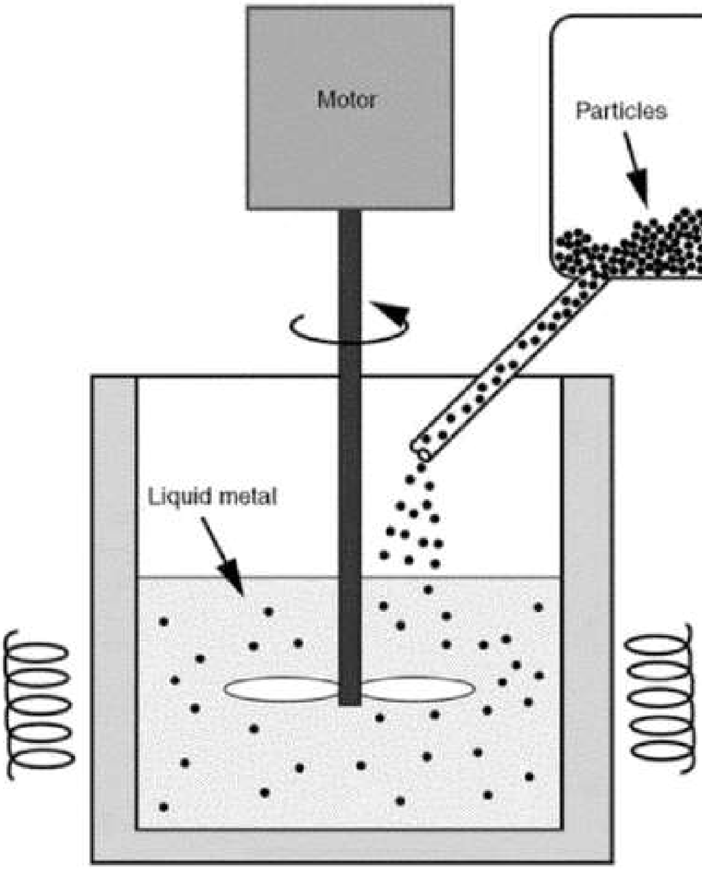

Figure 7 - Stir casting scheme [5].

The stirring movement will install high shear forces to both strip adsorbed gases and promote wetting of the reinforcement, by reducing surface tension and allowing the formation of a molten metal coating. Utilizing vacuum or an inert atmosphere is also something that should be considered, since this is essential in preventing gas uptake and entrapment, and eliminating the gas boundary layer at the melt surface which will ultimately facilitate the entry of the reinforcement in the molten metal. Although stirring will usually also induce a more homogeneous distribution of the reinforcement and adequate melt circulation, the quality of these is dependent on the mixing technique and impeller design. However, segregation or settling of the reinforcement, particle agglomeration or, on the other hand, particle fracture, and uncontrolled interfacial reactions may present as complications [5, 7, 12].

Stir mixing and casting have many different stages. Starting off with melting, most crucible furnaces are apt for aluminum MMCs. When using cover gas, as it is typical for cast MMC manufacture, the crucible must be loaded with said gas before inserting the ingots. In turn, these ingots are heated to a temperature greater than 200 ºC to avoid melt contamination by undesirable moisture. Moreover, each and every furnace equipment, including thermocouples for temperature control, should be coated, and extensively preheated and dried prior to being used. Moving on to the stirring phase, it has already been indicated that stirring the melt is necessary to prevent an uneven distribution of the reinforcing particles. However, to prevent vortex development at the melt's surface, the mixing motion must be adjusted. It is also important to take care not to break the melt's surface, as this would contaminate the bath with slag. The process of fluxing and degassing, the next step in stir mixing and casting, consists essentially in administering a mixture of argon and sulfur hexafluoride, SF_6, gases. At the melt surface, a thick, frothy slag typically forms during this phase. The degassing process should involve constant removal of this dross. After degassing, in order to allow any leftover bubbles to rise to the top of the melt, it should be left to remain without stirring for about 30 to 45 minutes. Furthermore, it is particularly crucial to stir the melt just prior to pouring. Next, in the pouring step, when the liquid metal is being moved from the furnace to the pouring unit, maintaining an inert atmosphere cover or stirring action is neither feasible nor required. Moreover, it is advised to thoroughly agitate the bath, skim off any dross in the furnace, and afterwards transport the metal to the pouring ladle. In order to prevent gas entrapment during pouring, it is crucial to keep turbulence in the metal stream at a minimum. This is especially important when using tilting furnaces, although these are not endorsed for composite production. At last, when it comes to the gating systems in castings, their basic rules are also valid for casting MMCs. If these systems are inadequately built, gas will become trapped in the liquid, leading to an increased quantity of porosities in the final casts [12].

The existence of reinforcement is something that will unavoidably affect the microstructure of the matrix. This is because of a plethora of reasons, which include the fact the particles behave as a solute and diffusion barrier, promote heterogeneous nucleation, impact the conductivity, viscosity and fluidity of the melt as well as bestow thixotropic properties. Simultaneously, the reinforcement will limit fluid convection, control morphological instabilities, affect dendrite arm coarsening, and reduce grain size as well as the quantity of latent heat [12].

As previously mentioned, the constituents that form MMCs don't have good wetting by nature. This lack of wetting is even more critical when reinforcing these systems with ceramic particles. Although, there are ways of enhancing this property by recurring to coatings on the reinforcement, such as nickel or copper coatings onto graphite particles. These coatings are multi purposed, since they simultaneously protect the reinforcement throughout handling, improve wetting, and prevent particle agglomeration. Also, wetting agents can be added into the bath in order to increase wettability. For example, in order to improve the wettability of Al_2O_3 particles in a A356 aluminum metal bath, magnesium can be added [7, 12]. Also, particle fracture during stirring can be problematic. This is due to the fact that, as the particle size decreases, the surface energy increases, decreasing wetting, resulting in higher difficulty to disperse and not agglomerate the particles. Furthermore, the prolonged contact between liquid and reinforcement can result in excessive interfacial reactions that will lead to an increase of viscosity of the melt, which will ultimately make casting harder. Also, during casting, metal will not solidify all at the same time. This can prove to be a concern due to an advancing directional solidification front, from the outer walls of the cast to where metal is being fed. Because of this, segregation of the reinforcement may occur, due to pushing of the particles through the solidification front. In turn, ultimately, the last solidifying zones will be particularly rich in reinforcement [4, 7].

One other factor that is required to produce intact and undamaged castings is the fluidity or viscosity of the melt with the reinforcement. As a rule of thumb, increasing the reinforcement content leads to a lower fluidity, or increased viscosity, due to interactions amongst the phases, leading to higher shear resistance. More precisely, increasing ceramic particles content, such as SiC and Al_2O_3, decreases the spiral fluidity of the melt in a linear manner. Simultaneously, temperature, shape, size, flocculation degree, and segregation of particles in the melt all have direct influence on this property [7, 12].

Sajjadi et al. [27] used a novel 3-step stir casting process that consisted in pre-heating Al_2O_3 particles to 1100 ºC for 20 minutes in an inert atmosphere, followed by injection of these into the melt with argon inert gas and then stirring the melt. This led to a homogeneous distribution of the Al_2O_3 micro particles in comparison to the, usually unsuccessful, Al_2O_3 incorporation into aluminum melt. Furthermore, a stirring speed of 300 rpm seems to be the ideal value due to lower turbulence, which in turn leads to lower porosities, and adequately dispersed particles.

The usage of high stirring speeds, more accurately 900 rpm, and high Al_2O_3 reinforcement content, up to 30 wt.%, was carried out by M. Kok [23]. Kok verified that when increasing the Al_2O_3 content, and lowering the particle size, higher porosity was obtained, due to increasing surface area. Also, after pouring, a 6 MPa pressure was applied to the mold for 30 seconds, which simultaneously allowed the increase of particle wettability and decreased porosity content.

2.1.2.2 Slurry Casting – Compocasting

Compocasting is similar to stir casting in the way that it also uses impellers to stir but, in this case, a semi-liquid metal. And thus, slurry fluidity is lower due to the relatively higher solid fractions. To compensate, stirring is carried out at high speeds which, in turn, leads to an inferior viscosity of this slurry due to relatively high shear rates. In fact, this allows to cast with solid fractions around 60% volume at most. When it comes to producing composites via this process, once again it is very similar to the previous one, since the reinforcement material can be added into the slurry prior to casting. Similar to stir casting, the continuous agitation of the impellers reduces viscosity, which in turn leads to enhanced wetting and bonding between the liquid metal and the reinforcement. However, compocasting presents a few advantages when compared to stir casting. These include the trapping of the reinforcement into the slurry, reducing segregation phenomena, a decrease of settling due to the increased apparent viscosity, and an eventual decrease of pouring temperature, which reduces degradation of the reinforced surface [7, 12].

Sajjadi et al. [16] concluded that lower grain size can be obtained, when producing composites by compocasting, due to its better wettability in comparison to stir casting. This is due to the fact that a higher wettability leads to a higher liquid content involving the reinforcement particles and, therefore, lower necessary energy to promote heterogeneous grain nucleation [28]. In turn, the lower grain size on the compocast composites allowed the manifestation of a higher ductility. The superior wettability also originated less porosity in the castings obtained through compocasting.

Vencl et al. [29] registered a coarsening of the structure during compocasting production of A356/Al_2O_3 particle composite, which translates to a grain size increase of the α-Al phase. The authors also evidenced the presence of zones rich in Al_2O_3 and other zones lacking reinforcement content, described as type A clusters, with thin Si particles next to the clusters. Vencl et al. also compared the Al_2O_3 composites (C1) with a base alloy (A356) that was submitted to a T6 heat treatment (A356) and A356/SiC composites (C2) and concluded that the wear resistance of the composites was higher than that of the base alloy. This can be seen in Figure 8. However, if the reinforcement was uniformly distributed across the matrix with a few particle clusters randomly dispersed, in what is detailed as type B clusters, such as in the SiC reinforcement composites, better wear properties could be achieved with the Al_2O_3 composites.

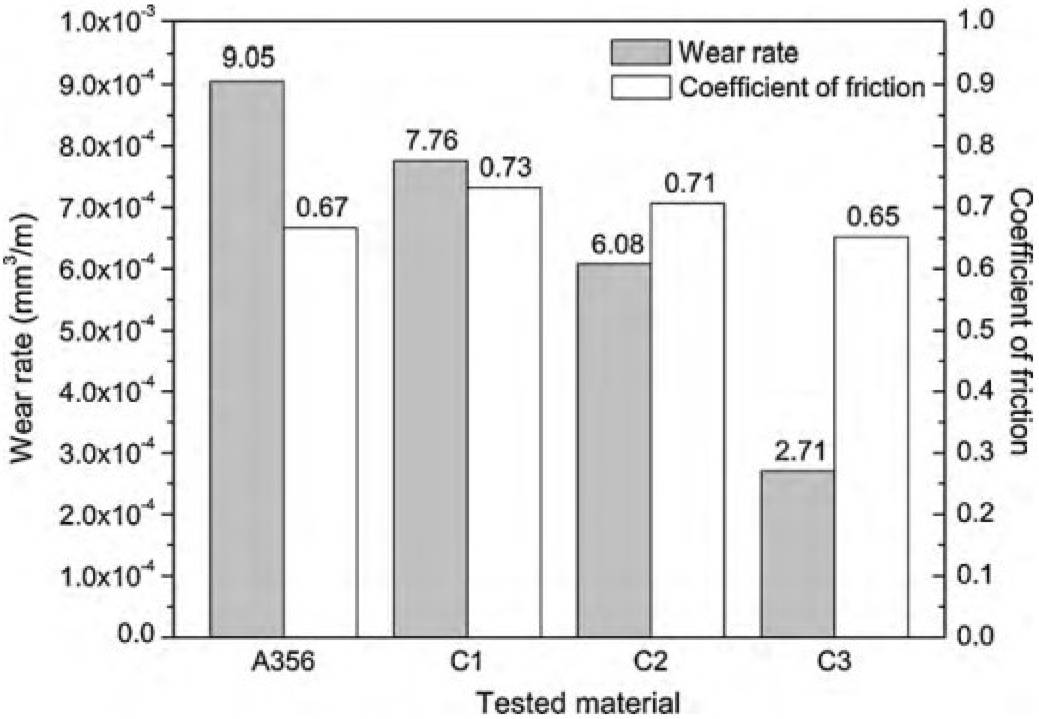

Figure 8 - Wear rate of a T6 heat treated A356 alloy and composites (C1 -10 wt.% Al2O3 particles; C2 – 10% SiC particles; C3 – 10 wt.% SiC and 1 wt.% graphite particles) [29].

2.1.3 Casting Processes

In light of this, as previously mentioned, most casting processes can be used in combination with stir mixing. These include sand and permanent mold casting, centrifugal casting, and high-pressure die casting, each with its own advantages and disadvantages [12].

2.1.3.1 Sand and Permanent Mold Casting

Sand, as well as permanent molds, can be used to pour liquid metal mixed with ceramic particles into. Nonetheless, these castings have some inherent issues. Sand mold casting, in particular, usually has slow solidification rates, which will ultimately lead to particle buoyancy-driven segregation. The higher the difference in density between both phases, the more likely it is that the particles will accumulate on the bottom or top surface of the casting. However, this can be taken into advantage to selectively reinforce surfaces for several tribological applications. Also, it is possible to minimize segregation by using tinier particles, thinner sections and more than one type of ceramic reinforcement [12].

2.1.3.2 Centrifugal Casting

Centrifugal casting consists in pouring molten metal into a spinning die in which, due to the high velocity rotating action, centrifugal forces are applied on the metal, expelling the mixture to the mold or walls. Furthermore, the mold can be revolving on a vertical or horizontal axis, according to the desired component structure [30, 31]. An example of a vertical centrifugal cast scheme can be seen in Figure 9.

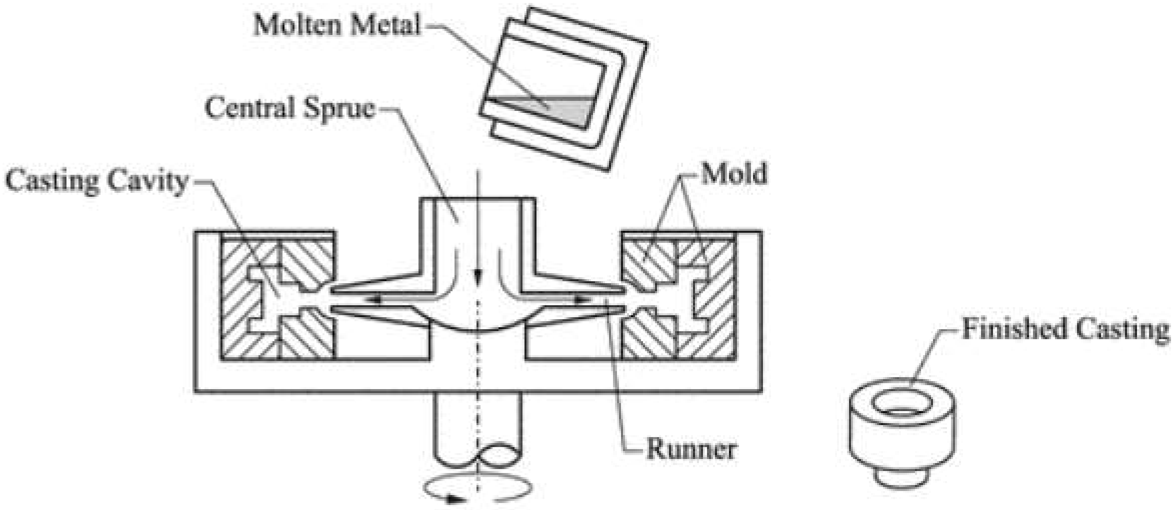

Figure 9 - Vertical centrifugal casting scheme [30].

Particle composite fabrication through centrifugal casting leads to the emergence of two perceptible circumference zones, one particle-rich and the other particle-free, depending on the particle density. If the reinforcement is denser than the liquid metal, as is the case for SiC, the exterior circumference will be particle rich. On the other hand, the particle rich zone will form on the interior if the particles are lighter than the matrix. Once again, taking advantage of the fact, this can be used to purposely create components with a graphite lubricant core or, on the contrary, create wear resistance components due to segregation of the hard particles to the outer surface, with horizontally revolving axis molds [12].

2.1.3.3 High-Pressure Die Casting

At last, high-pressure die casting (HPDC) is one of the very best casting processes for aluminum composite fabrication. This is essentially due to the very high cooling rates induced in this process, which result in an especially fine dendritic structure, almost free of porosities, ultimately leading to relatively good mechanical properties. Also, since the dimensional shrinkage of aluminum MMCs rounds 0.6%, like non-reinforced aluminum, no changes need to be made in both the dies and gating system. Moreover, due to the reinforcement, aluminum MMCs are significantly more viscous which, in combination with the injection pressure, will carry less entrapped gas and turbulence into the die cavity. Also, minimum gate velocities of 30 m/s are recommended in order to best take advantage of the thixotropic behavior aluminum MMCs exert. With this, a practically laminar flow is achieved, which translates to decreased turbulence and causes aluminum MMCs produced by HPDC to have better overall quality than non-reinforced aluminum using the same technique. However, one concern with casting composites through HPDC is the use of hard particles amidst the molten metal during injection, which could negatively impact the die life, due to higher wear. Although, at least in the case of SiC, this can be discarded, since the particles' surface will be entirely wetted in aluminum, which results in only the metal coming in contact with the surfaces of the die during injection. Finally, one other advantage of composite production through HPDC is its high productivity. The combination of lower pouring temperatures coupled with the necessity to remove less heat during solidification, since up to 20% of the composite melt are solid particles, leads to shorter cycle times and also lower die wear and thermal stress [12].

Sevik et al. [32] were able to produce three different particles sizes, namely 44, 85 and 125 µm, Al_2O_3 (5, 10 and 15 vol.%) reinforced aluminum MMCs using a combination of stir and pressure die casting. Through microstructural analysis, shown in Figure 10, the authors verified that a homogeneous distribution of the reinforcement was achieved on the two highest particle size 15 vol.% composites. However, on the smallest particle size, 44 µm, the particles were segregated into the eutectic inter dendritic areas. This happens due to the pushing of the particles throughout solidification into the last solidifying eutectic liquid. Furthermore, through wear test examination wear resistance increased with increasing reinforcement content. Analyzing the wear surfaces, plastic deformation occurred on the matrix, and layer or abrasive deformation of the surface was evidenced on the composites.

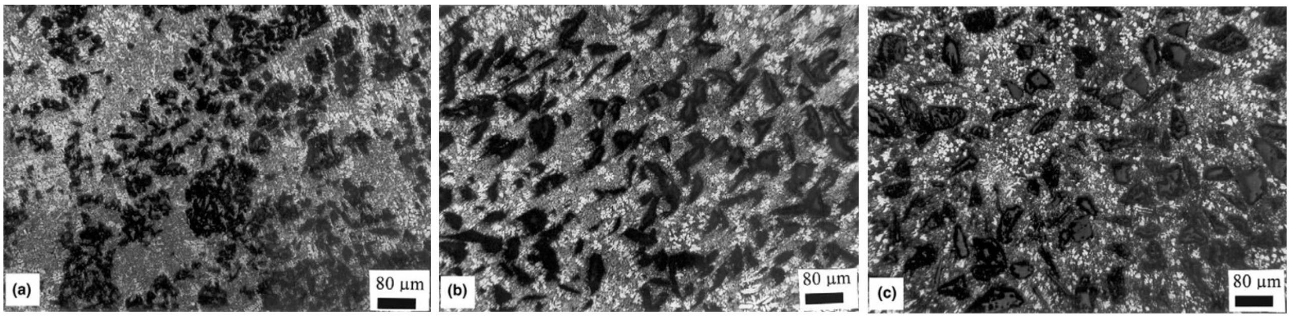

Figure 10: Microstructures of composites with 15 vol.% Al_2O_3: (a) 44 µm; (b) 85 µm; (c) 125 µm [32].

2.2 Bimetallic Composites

Structural or continuously reinforced composites are essentially made of continuous fibers, as opposed to discontinuously reinforced composites. The properties of the continuous composite are directly related to the properties of the reinforcement, making the reinforcement properties the most relevant in this situation. More specifically, the strength will be mainly dependent on the capacity of the matrix to transfer and distribute load to the reinforcement, especially at room temperature. In higher temperature mechanical solicitations, the material constituting the matrix becomes more important due to the fact that the properties will be diffusion controlled [11, 15]. Furthermore, as previously mentioned, these types of composites will have anisotropic properties due to the orientation of the reinforcement. This essentially means that longitudinal and transverse properties will not be the same. In fact, mechanical properties seem to be higher in the longitudinal direction of the fiber [4, 11, 15]. However, in order to achieve a high component performance, good bonding between matrix and fibers is required. The ideal situation is to have a continuous metallurgical bond, consisting of IMLs, to maximize not only the mechanical connection but also the sealing and heat transfer capabilities of the composite. Additionally, the properties of this layer are reliant on the morphology, thickness, and type of phases formed [33]. With this in mind, continuously reinforced composites are usually produced by infiltration methods.

Nunes et al. [34] verified that the insert geometry, as well as its positioning, is something that will have a significant impact on the comportment of the infiltration process. The authors also concluded that for complex geometries, LPSC and centrifugal casting are better when opposed to gravity casting, which seems not capable of consistently infiltrating semi to complex geometries.

Regarding the production of aluminum and steel bimetallic composites. it is important to comprehend what intermetallic compounds may be formed. Kobayashi and Yakou [35] reported that at temperatures below 1000 ºC. a very brittle Fe_2Al_5 layer is formed. On the other hand, less brittle and consequently more fracture resistant, iron aluminides such as FeAl and Fe_3Al are produced at higher dipping temperatures, higher than 1000 ºC. These authors also mentioned that dipping in temperatures that favor the formation of the latter iron aluminides will allow the use of the composite as a structural material, having overall higher wear and corrosion resistance, and also specific resistance.

Xiangfan Fang [36] noticed the formation of two layers on the interface when coating steel with aluminum. The first consisted of a thin layer of iron, aluminum, and silicon, while the second, thicker one, did not contain iron. In the second layer, silicon segregation was verified, leading to different resistance zones. The author also claimed that this difference in material strength on the second layer was responsible for the appearance of a discontinuity line, through which cracks propagated without an increase in tension. This is summarized in the scheme in Figure 11.

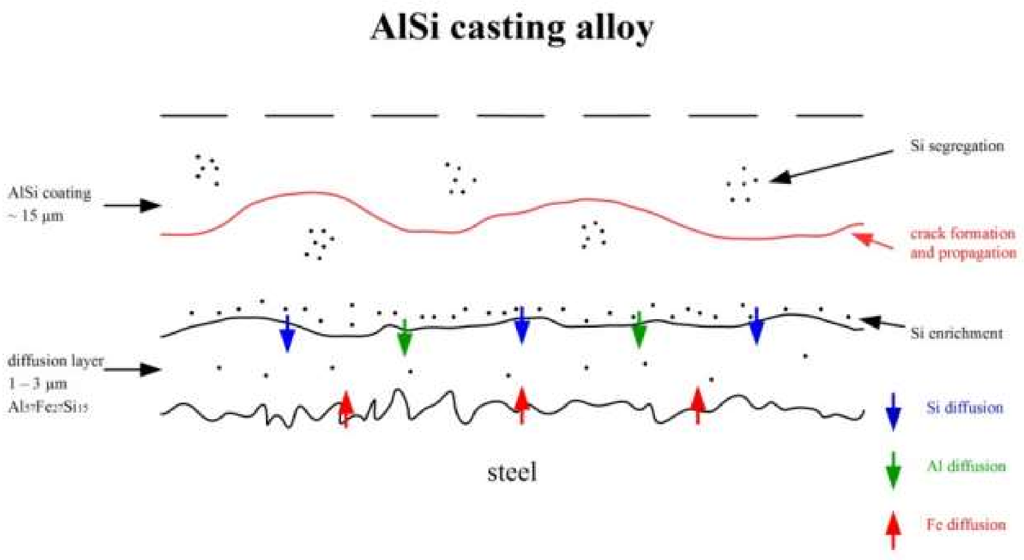

Figure 11 - Crack forming mechanism in Al-Si coatings [36].

As for the hot dipping procedure time, Wang et al. [37] studied its' influence on the aluminum coating. It was verified that increasing the time led to a higher coating thickness, up to around 32 µm. Also, when dipping for 5 and 10 minutes, a gap was verified between steel and aluminum, which was not present when the dipping procedure was carried out for 15 minutes. However, after pouring metal on top of the hot-dipped steel, cracks were present in all the samples, even when implementing heat preservation for up to 30 minutes, due to the different coefficients of thermal expansion (CTEs).

Mao et al. [38] mentions that implementing Ni into the Al-Si alloy bath, when producing aluminum and steel bimetallic composites, will result in a reduced fragility due to the controlled growth of the brittle Al_5Fe_2 phase. Additionally, the authors added different quantities of the Eu element, and concluded that adding 0.1 wt.% of the forementioned rare earth results in the thinnest layer at the interface, lower grain size and highest shear strength. SEM micrographs of the IML with different wt. % Eu contents can be seen in Figure 12.

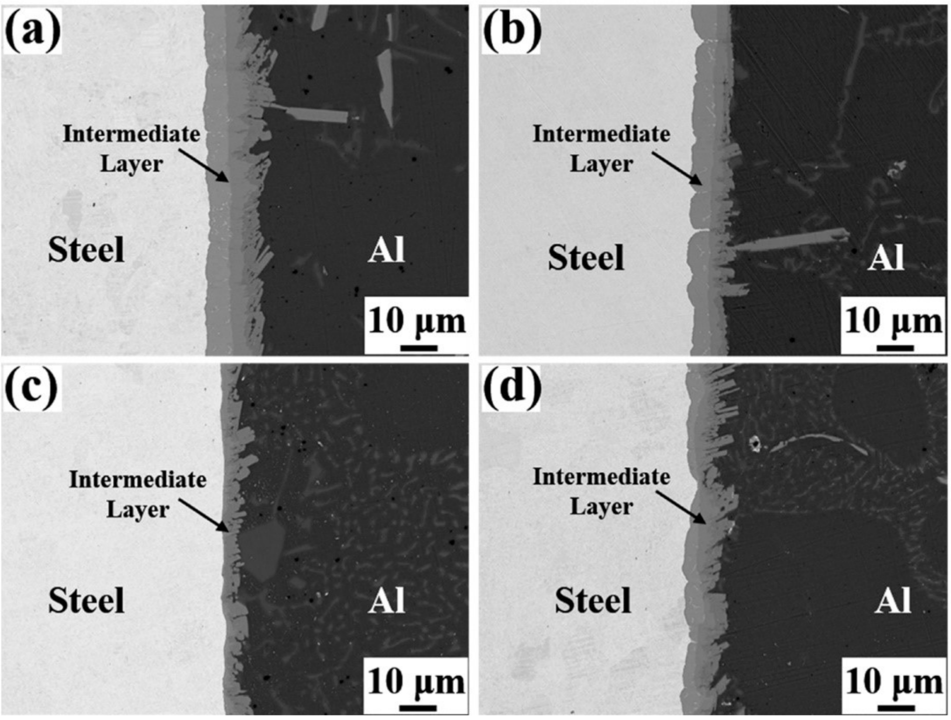

Figure 12 - SEM micrographs of Al/Steel IML with different Eu contents (a) 0 wt. % Eu; (b) 0.05 wt. % Eu; (c) 0.1 wt. % Eu; (d) 0.2 wt. % Eu [38].

2.2.1 Infiltration Casting

Infiltration casting consists in a plethora of casting techniques in which the molten matrix metal will fill a mold which has the reinforcement, in a given preform shape, fixed in space, as opposed to stir casting, where reinforcements are free to roam the molten metal. In these methods, the metal cools as it passes through the fibers or particles. Infiltration casting can be separated into three separate stages, which consist in the assembling of the reinforcement preform, the infiltration of the liquid metal and its solidification. During infiltration it is common to have the formation of a transitory surface film, due to the temperature difference, between the metal and reinforcement. Furthermore, the preheat and superheat temperatures for the fiber and metal, respectively, as well as the infiltration pressure and speed, are the most crucial variables in this process [12]. For instance, in case the molten metal or fiber temperature is too low, castings with a poor infiltration or increased porosity will occur. On the other hand, excessively high temperatures will lead to a deterioration of the properties of the casting due to exaggerated reactions between the fiber and the molten metal. Plunger speed is also to be taken into account, which consists in the speed at which the mold is closed. Very high speeds will cause the deformation of the reinforcement preform on infiltration [12, 39].

Guo et al. [40] were able to increase the wettability of aluminum in steel due to the ultrasound infiltration process that allowed the removal of the superficial oxide layer. The authors also note that the increase in pouring temperature led to an increased thickness of the IML and, therefore, diminished shear resistance due to the brittle nature of the compounds.

2.2.1.1 Pressure Infiltration Casting

Having said that, there are a few variations of this process, as previously exhibited in figure 6. Starting off with pressure infiltration casting (PIC), this involves vacuuming and then using relatively low pressure, between 2 and 10 MPa, to force the molten metal into a mold with a preform, both of which have been preheated to temperatures near the melting point of the matrix metal. This prevents choking by allowing the liquid to flow and fill the mold cavities. After the primary voids have been filled, the pressure can rapidly rise until it reaches a critical value that must be maintained throughout the mold, isostatically filling the final voids. It is also significant to highlight that the use of thin mold walls, which promote rapid cooling, minimize interfacial interactions between the matrix and the reinforcement [4, 12, 41]. As for the pressurizing gas, inert gas is very commonly used due to the fact it reduces the risk of hydrogen absorption [4, 6]. Coupling this with the fact that low pressure is used, liquid velocity of the metal into the mold will usually be below the 0.5 m/s critical value established by John Campbell, thus reducing the risk of mold wear and inclusion incorporation [6, 42]. Additionally, the surface tension forces of the reinforcement are exceeded, and the aluminum is forced into the preform due to the pressure differential between the gas outside the mold and the vacuum in it. Because of this, the pressure differential can only be sustained for a very brief period of time, negating the need for bulky, pricey, and heavy molds. Also, mold pressure will be maintained while directional cooling is applied, which will assist filling shrinkage porosity [12]. At last, a scheme of the PIC process can be observed in Figure 13 [43].

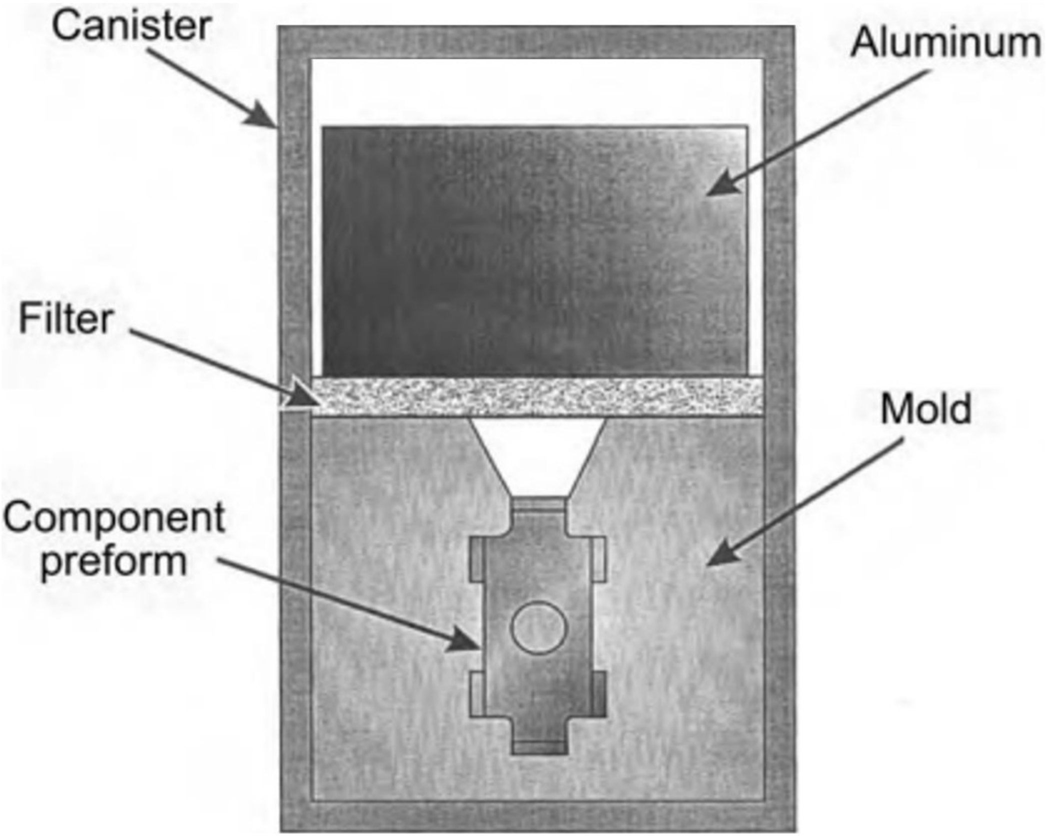

Figure 13 – Top-fill pressure infiltration casting assembly scheme. Adapted from [43].

2.2.1.2 Squeeze Casting Infiltration

Squeeze casting is a process that is commonly described as a combination of two different manufacturing techniques, namely casting and forging. This is due to the fact that the metal is poured into an open mold cavity, and then the mold closes and high mechanical pressures are applied in order to assemble a given component [44].

Adapting this technique to produce composites, in contrast to the last procedure, a premixed suspension of reinforcement contained in the molten metal solidifies as a result of high hydrostatic pressure, with practically no liquid movement during solidification. As a result, using this method allows for the creation of composite castings that are nearly net-shaped and void-free, due to the unidirectional pressure applied. Moreover, since considerable undercoolings are combined with rapid heat extraction, aluminum MMCs made using this method will have an equiaxed and fine grain structure [12]. A scheme of this process can be seen in Figure 14 [4].

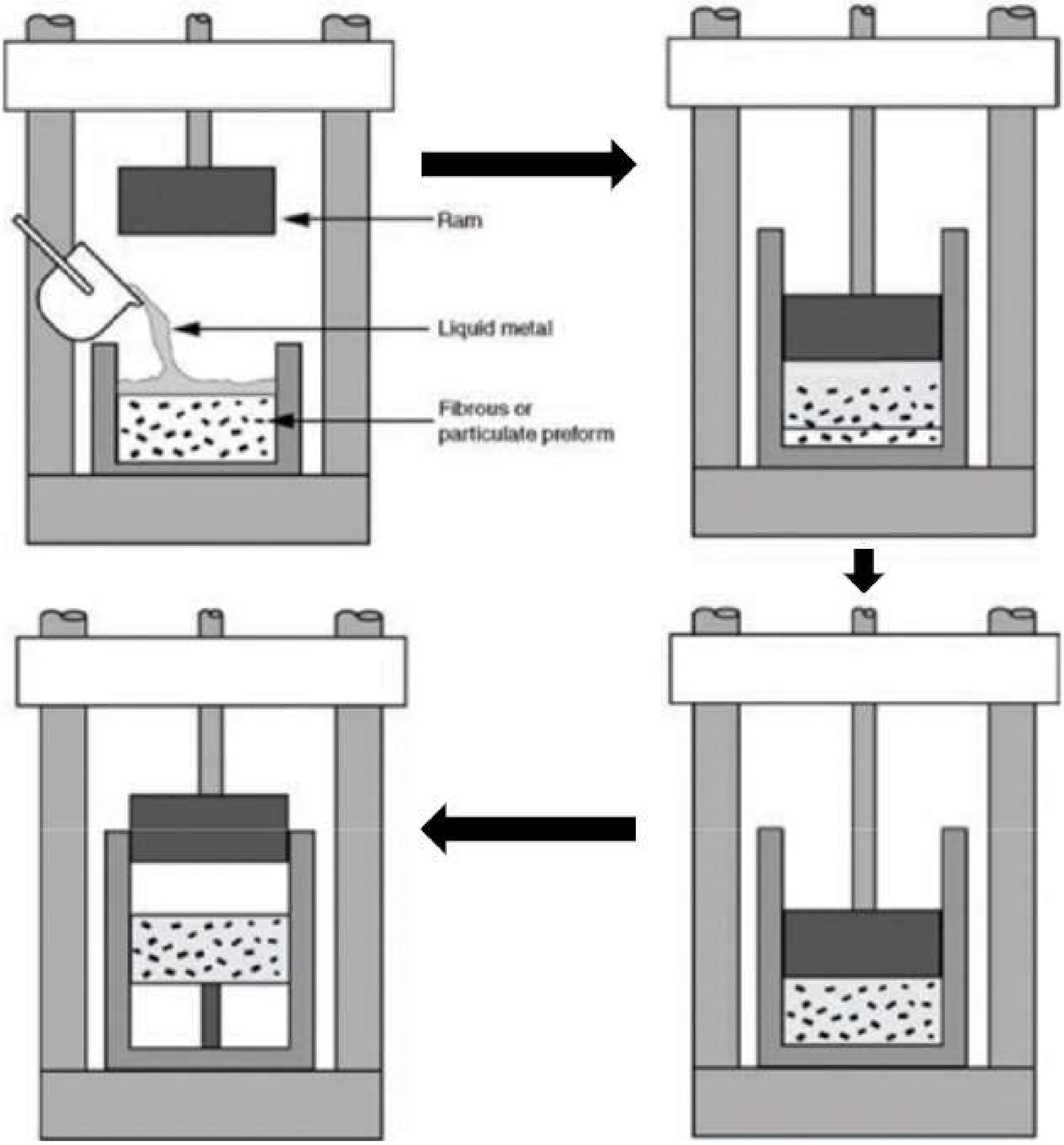

Figure 14 - Squeeze casting infiltration scheme [12].

2.2.1.3 Vacuum Infiltration

Vacuum infiltration is a particular infiltration technique. Composites are created by establishing a negative pressure difference between the preform and its surroundings. This forces the liquid through the preform gaps despite the forces of surface tension, gravity, and viscous drag. Also, it is very common to combine this technique with chemical procedures to enhance wettability. These include modifying the fiber surface or adding certain elements into the matrix, with the objective of enhancing wetting [12].

2.2.1.4 Electromagnetic infiltration

Another peculiar infiltration process is electromagnetic infiltration. Here, as the name suggests, electromagnetic forces are used to allow the liquid penetration of nonwetting preforms. Some of the advantages of this is the absence of necessity of motor driven rams or gas pressure differential. In order to perform this kind of infiltration, high-frequency electromagnetic fields are induced on the metal. In turn, these will react with the eddy currents that are created within the metal. As a consequence of this reaction between the eddy currents and the high-frequency electromagnetic fields, the metal will penetrate the reinforcement preform when it is adequately oriented relatively to the direction of the force [12].

2.2.1.5 Centrifugal Infiltration

Regarding centrifugal infiltration, very similarly to centrifugal casting, MMCs are created via centrifugal forces. These are produced at high rotational speeds that will allow the overcome of the capillary and viscous forces for the metal penetration and flow, respectively, in the preform [4]. This infiltration method is essentially used to infiltrate solid reinforcement preforms where the reinforcement has higher density than the matrix [45], such as aluminum matrix with a steel reinforcement as produced by Nunes et al. [34]. Figure 15 represents a scheme of the centrifugal infiltration process [45].

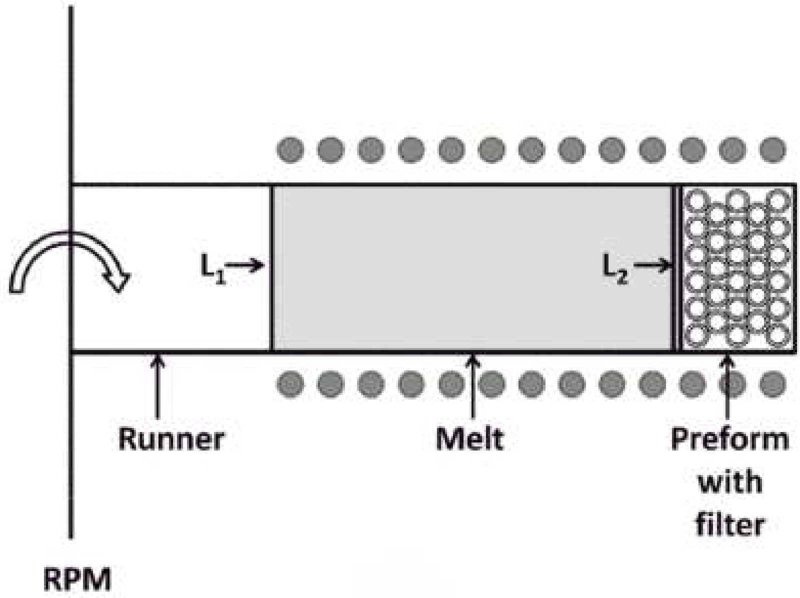

Figure 15 - Centrifugal infiltration scheme [45].

2.3 Strengthening Mechanisms

As previously stated, MMCs have enhanced properties due to the interactions between the metallic matrix and the reinforcement. In aluminum composites, the Orowan, increased dislocation density, load-transfer effect, and grain refinement mechanisms are responsible for the improvement in mechanical properties [46]. One thing all of these have in common is that they all revolve around hindering the dislocation movement by the creation of obstacles. In turn, these obstacles force the dislocations to bend around them, creating a dislocation loop, or cut through them. The obstacles can also change the dislocation to a shape that prevents movement [47].

2.3.1 Orowan Mechanism

The Orowan mechanism states that if second-phase particles are present, such as Al_2O_3 in an aluminum matrix, dislocations will be unable to shear through them, bending between them and rejoining, leaving a dislocation loop around the particles [16]. This dislocation loop promotes an increase in shear stress required to overcome the loop and, in turn, a higher strength of the material [48]. Therefore, in order to move dislocations through an area of hard obstacles, by a looping process, it is necessary to apply a critical stress known as the Orowan stress. This stress can be calculated through equation (1) [16, 48, 49], in which G is the shear modulus, b is the modulus of the Burgers vector, δ corresponds to the inter-spacing between two particles, and r is the particle radius [16].

$$\sigma_{\mathrm{or}} = \frac{0.13Gb}{\delta} * ln\frac{r}{b} \tag{1}$$

It is important to mention that this mechanism is more prominent in nanocomposites, leading to a higher critical stress, because of a finer distribution of the particles across the matrix, which causes a lower spacing between two obstacles [46, 49]. A scheme of this can be seen in Figure 16 [49].

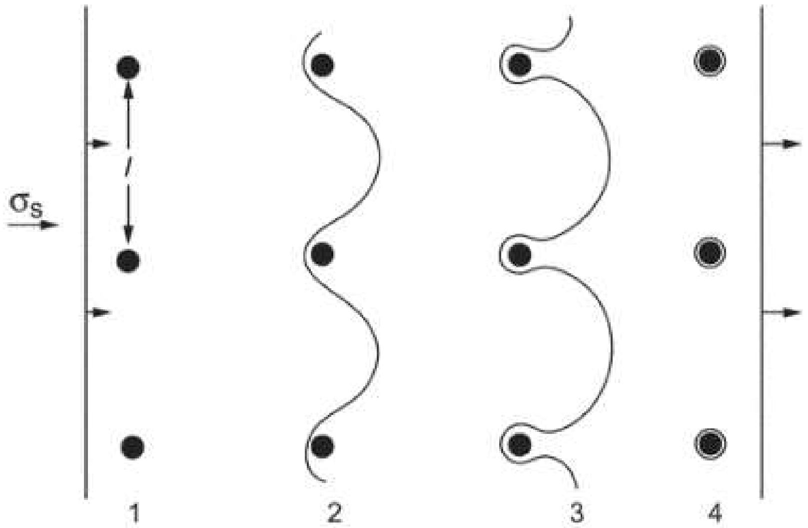

Figure 16 - Orowan mechanism stages [49].

2.3.2 Enhanced Dislocation Density Effect

Regarding the increase in dislocation density, this effect is essentially due to the different CTEs between the matrix and reinforcement material. These CTEs may lead to induced stresses and plastic deformation, producing high-density dislocations, at the interface of the matrix/reinforcement during cooling [46, 48]. Moreover, a fraction of the newly formed dislocations become intertwined and sessile, or immovable, generating an increase in the stress necessary for further deformation due to the formation of a long-range internal stress field that will prevent the mobile dislocations from moving [47]. Equation (2) shows the strength increase granted by the CTE difference, where Δα and ΔT correspond to the difference of the CTE between matrix and reinforcement, and processing and test temperature, respectively, and β pertains to the strengthening coefficient [16].

$$\sigma cte = \sqrt{3}\beta G b * \sqrt{\frac{24 V_{\mathrm{p}} \Delta\alpha \Delta T}{(1 - V_{\mathrm{p}}) b r_{\mathrm{p}}}} \tag{2}$$

2.3.3 Load-Bearing Effect

The load-bearing mechanism consists objectively of a transfer of the load from the lowest-strength part, the matrix, to the higher strength particles from the reinforcement. The strengthening effect of this mechanism can be evaluated by the mismatch strain at the matrix/reinforcement interface and is only possible if there exists a tight cohesion at this interface. However, this effect can be deemed non-relevant when the volume fraction of the reinforcement is low, more accurately at ≤2 vol.% [46, 48].

2.3.4 Hall-Petch Effect

Lastly, reinforcement particles can also act as heterogeneous nucleation sites, in liquid-phase processes such as stir casting, which ultimately leads to grain refinement. Moreover, as grain sizes diminishes, so does the distance between grain boundaries, promoting the necessity for higher amounts of stress required for deformation, which can be justified by a decrease in the mobility of dislocations [46–48]. Having this said, the Hall-Petch equation, equation 3, shows the effect grain refinement has on YS, where d represents the grain size and K is a constant [48].

$$\sigma = \frac{K}{d^{\frac{1}{2}}} \tag{3}$$

Sajjadi et al. [16, 27] evidenced an increase in mechanical properties with increasing reinforcement content in A356/Al_2O_3 particle composites. Even though all the reinforcement mechanisms exerted their effect, the main causes of this, as reported by the authors, were grain refinement and the increase of obstacles through which dislocation have to go through, according to the Hall-Petch and Orowan mechanisms, respectively. Additionally, decreasing particle size from micro to nano particles led to even higher values of 0.2% YS, UTS, and UCS. This was attributed to a superior degree of load bearing, mismatch strengthening and bonding between reinforcement and matrix. The results mentioned can ultimately be seen in Figures 17 and 18.

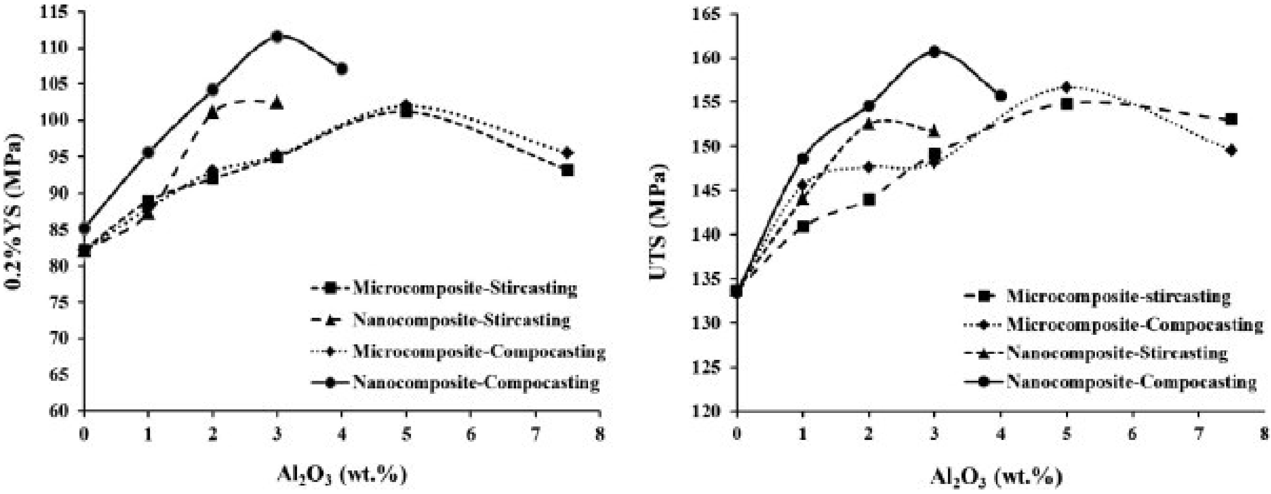

Figure 17 - Yield and ultimate tensile strength of micro and nano Al2O3 composites fabricated by stir- and compo casting [16].

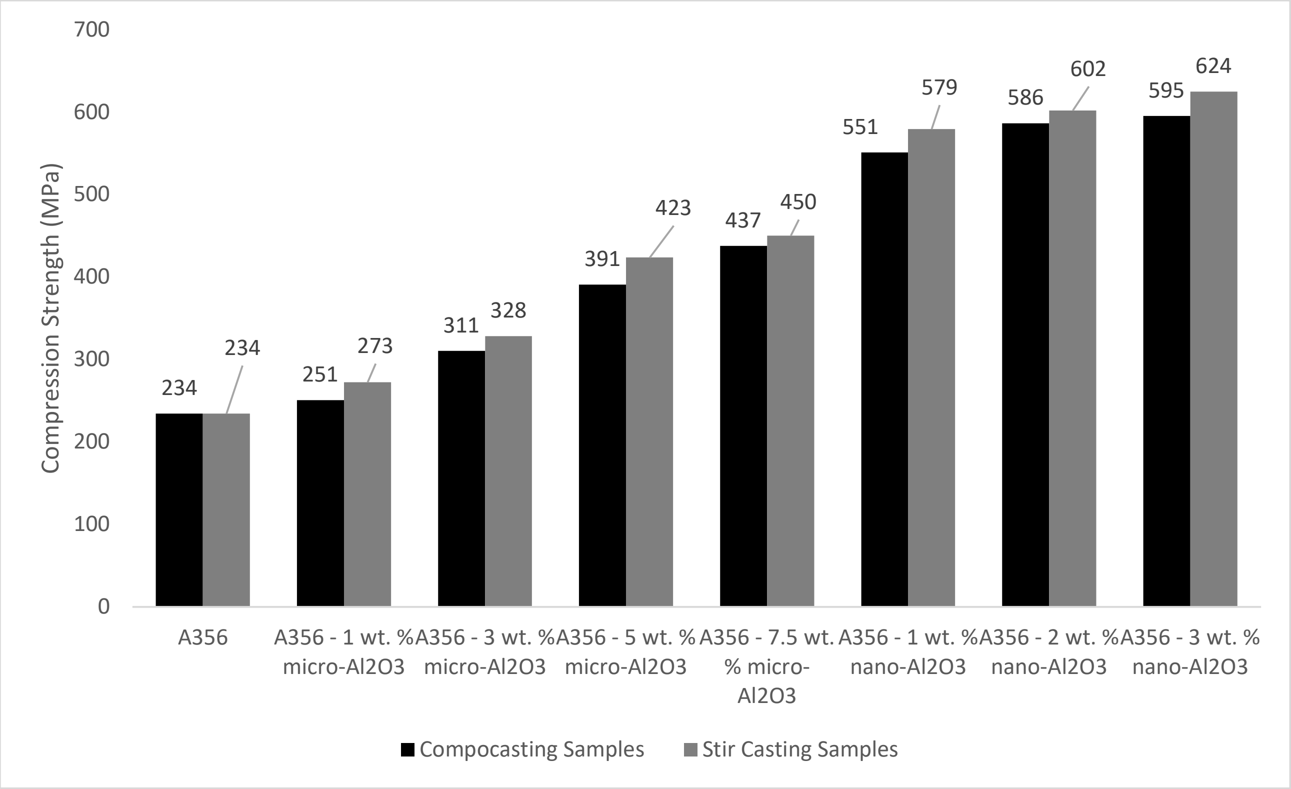

Figure 18 - Compressive strength of micro and nano Al2O3 composites fabricated by stir- and compocasting. Adapted from [16].

3 Materials and Methods

3.1 Materials

3.1.1 A356 alloy and steel insert

The aluminum alloy used for the composites fabricated in this study was the A356 alloy. Its chemical composition can be seen in Table 1.

Table 1 - A356 alloy chemical composition

Element (wt %)	**Al**	**Si**	**Fe**	**Mg**	**Ti**	**Other**
	92.90	6.52	0.10	0.36	0.091	Rest

As for the steel insert composition, it consists of a standard low carbon steel with a galvanization layer.

3.1.2 Alumina particles

When it comes to the Al_2O_3 powder used, it is pure alumina, and its' shape has presented to be granular, which means that each big particle is made up of multiple tiny particles, as it can be seen in Figure 19, taken in SEM.

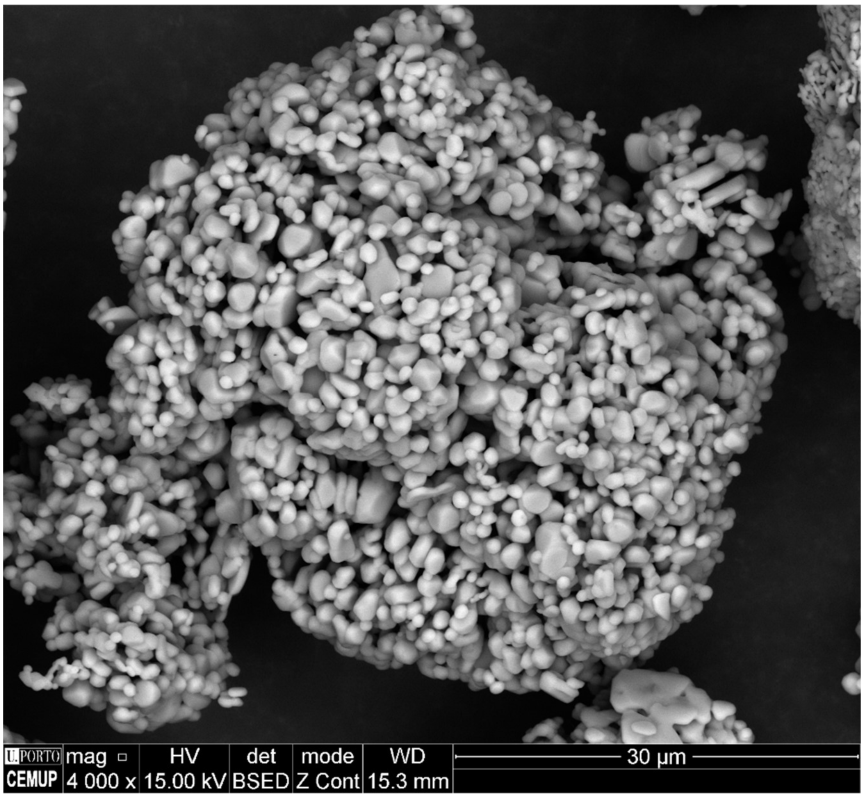

Figure 19 - Al_2O_3 powder particle.

3.2 Reinforcement Preparation

3.2.1 Milling

Reinforcement Al_2O_3 powder was mixed and milled with A356 chips, which were obtained with a manual lathe machine Wabeco D6000, through planetary ball milling, more accurately using a Retsch Planetary Ball Mill PM 100 machine. 25 milling cycles totaling 150 g of Al_2O_3 were carried out, with each cycle manufacturing 6 g. The procedure for each cycle started with the weighting of 60 g of pre-milled A356 alloy chips and 6 g of Al_2O_3, mixing both in the milling container and, afterwards, introducing fifteen 20 mm diameter zirconia balls. This same container was subsequently put into the Retsch machine, and the following parameters were used: 300 rpm, 3-hour total milling time with 2-minute active milling followed by 8-minute rest cycles, to prevent overheating. After each cycle was done, the jar was retrieved from the milling machine and the powder transferred from it into another container, always making sure the proper protection equipment was being used. A tiny powder sample, alongside one of the fifteen zirconia balls, can be seen in Figure 20. As for the pre-milling of the A356 alloy chips, these were milled 15-20 g at a time, for 1 minute at 600 rpm.

Figure 20 - 20 mm zirconia ball with a powder sample.

3.2.2 Compacting

After milling was finished, the powder was compacted in a steel mold with the use of an industrial KPX Instron machine. To achieve this, a force of up to approximately 980 kN was applied to the powder inside the 95x95x80 mm^3 volume mold. Also, the powder was compacted three times, not being able to achieve one uniform block. Therefore, two inconsistent blocks were obtained, and the remaining powder was unable to be compacted. An image of the result after attempting to compact a block can be seen in Figure 21.

Figure 21 – Result after compacting of A356/Al2O3 powder.

3.3 Casting Procedures

3.3.1 Low-Pressure Sand Casting

To produce the bimetallic composites, LPSC was carried out. An image of the setup, more accurately the mold with the inserts, can be seen in Figure 22, along with a technical drawing of the inserts. The A356 alloy was melted at 720 ºC and then modified, with Al-10Sr, and refined, with Al5Ti1B. The goal was to obtain 250 ppm of Sr and 0.15 wt. % Ti. Moreover, 99.9% Ar protecting atmosphere was used, with approximately 120 mbar of pressure, to fill the mold. Different castings were produced, namely base alloy, without any reinforcement, and reinforced with galvanized steel inserts. In turn, these 0.8 mm thick galvanized steel sheets, used as inserts, were put into the sand mold using different conditions. These include no treatment at all, and the hot dip aluminizing surface treatment. The conditions for the hot dip aluminizing treatment included insert pre-heating at 300 ºC, followed by dipping in an A356 molten aluminum bath at 750 ºC for 60 seconds. At last, the inserts were placed into the mold and the casting was carried out. Afterwards, from the different castings, tensile specimens were produced, and the properties were analyzed and compared.

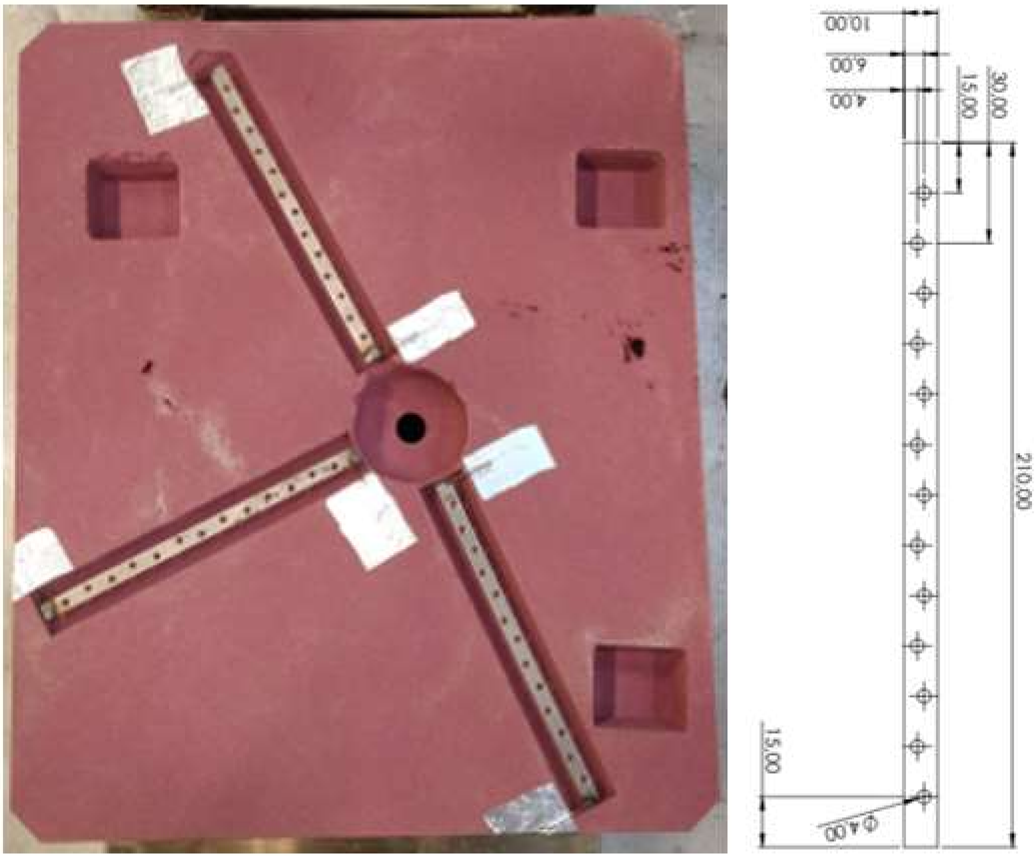

Figure 22 - Mold with placed steel inserts (left) and insert technical drawing (right)

3.4 Hot-Dipping Optimization

In an effort to try and improve the quality of the bonding between both materials, which was found to be not optimal in the upcoming results, an ammonium chloride (NH_4Cl) flux surface treatment was performed, as previously accomplished by Jiang et al. [50]. In light of this, two 80x15x0.8 mm steel sheets were immersed in a 10% NH_4Cl solution, at 80 ºC, for 10 minutes. Afterwards, the sheets were dried in a stove at 120 ºC for 2 hours and then, taken to be dipped in an A356 alloy melt at 780 ºC for 3 minutes. The samples originated from this process are presented in Table 2.

Table 2 - Pre-hot dipping steel sheet conditions

Sample	Conditions
A	Galvanized Sheet
B	Galvanized Sheet + Treatment
C	Non-Galvanized Sheet
D	Non-Galvanized Sheet + Treatment

3.5 Mechanical Tests

3.5.1 Tensile Tests

In order to evaluate the tensile properties of the samples, tensile tests were carried out. This comprises the use of an Instron 5900 R model universal tensile system with a contact extensometer. When it comes to the conditions, a 1 mm/min velocity was used, alongside a 100 kN cell and a 20 Hz acquisition rate. It is also important to note that three section diameters were measured with a Mitutoyo digital micrometer and, consequently, an average section diameter per sample was estimated.

3.5.2 Hardness Tests

Vickers microhardness tests were done with the use of a FALCON 500 INNOVATEST Micro Vickers Hardness Tester. In the case of the structural composite samples, hardness profiles at the interface ± 15 μm were obtained, covering the steel insert, aluminum matrix, and the area between both materials. Three profiles were made in each sample, with an estimated load of 0.029 N (3 gf), for 10 seconds, as mentioned in the ISO 3878:1983 standard.

3.6 Metallography

3.6.1 Metallographic Preparation

With the objective of analyzing the microstructure of the different samples, traditional metallographic preparation was carried out. This involves polishing the various samples with different grits SiC griding paper, with a MESH sequence of 320 – 600 – 1000 – 4000, following the use of 6 and 1 μm diamond suspensions.

3.6.2 Microscopy

Following metallographic preparation, microstructure evaluation was done through both OM and SEM. For the optic microscopy analysis, a ZEISS Axiotech optical microscope allowed the gathering of microstructures in bright field contrast. For SEM observations, a FEI Quanta 400 FED ESEM equipment was used alongside the EDAX Genesis X4M energy dispersive X-ray spectrometer (EDS), from CEMUP, which enabled the chemical composition analysis, using an accelerating voltage of 15 keV, by the standardless quantification method.

3.7 Measurements

Different measurements were also employed. These include density, to determine porosity, IML thickness, and dendritic arm spacing (DAS) measurements. Starting with the density measurement method, a simple Archimedes method was used, with a scale. As for the two latter measurements, these were performed with the aid of the image software ImageJ on the obtained microstructures.

4 Results and Discussion

4.1 Structural Composites

In the following sub-chapters, the structural composite results are scrutinized.

4.1.1 Microstructural Characterization

4.1.1.1 A356 Base Alloy

When it comes to microstructures, it is possible to see one pertaining to the heat-treated base alloy in Figures 23. Some big pores can be seen in Figure 23A, which most certainly influenced the mechanical properties presented further on. However, besides porosities, microstructure is what would be expected, namely eutectic compound, better observed in Figure 24B, made up of Si and Al in between the α-Al dendrites [17, 51]. Also, DAS, pertaining to the distance between secondary dendrite arms, was found to be around 46 μm.

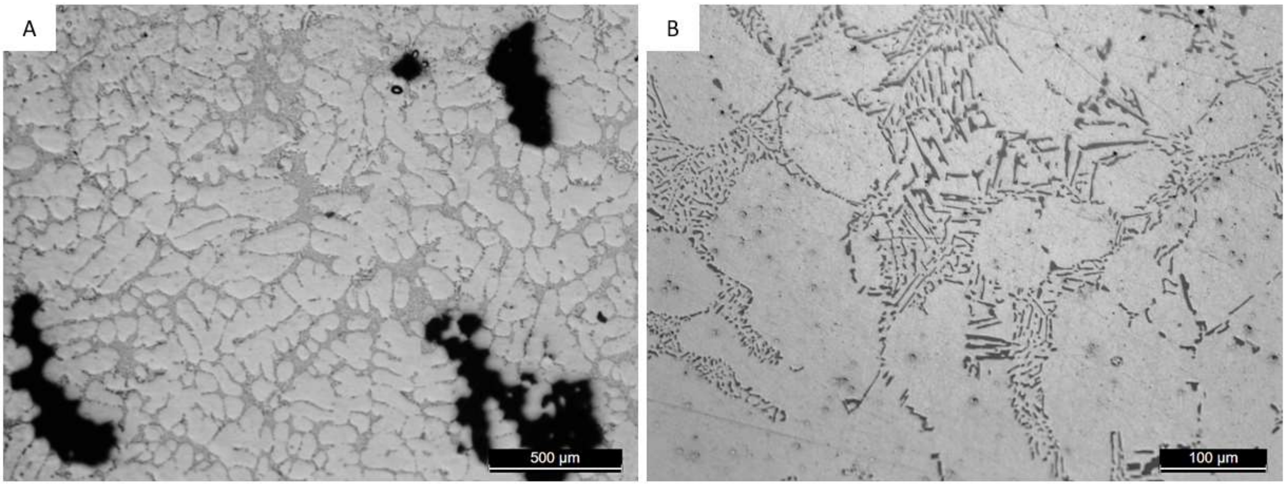

Figure 23 - A356 with T6 microstructure.

Analyzing the SEM results and starting off with the non-reinforced T6 heat treated sample, an α-Al dendritic structure can be seen, alongside eutectic zones, in Figure 24 [17, 52]. Taking advantage of a higher amplification, it was also possible to identify different areas and evaluate their chemical composition, presented in Table 3, with the aid of EDS analysis. It should also be noted that the AlSiFe ternary phase diagram was used to confirm the identified phases, which can be seen in the appendix [53].

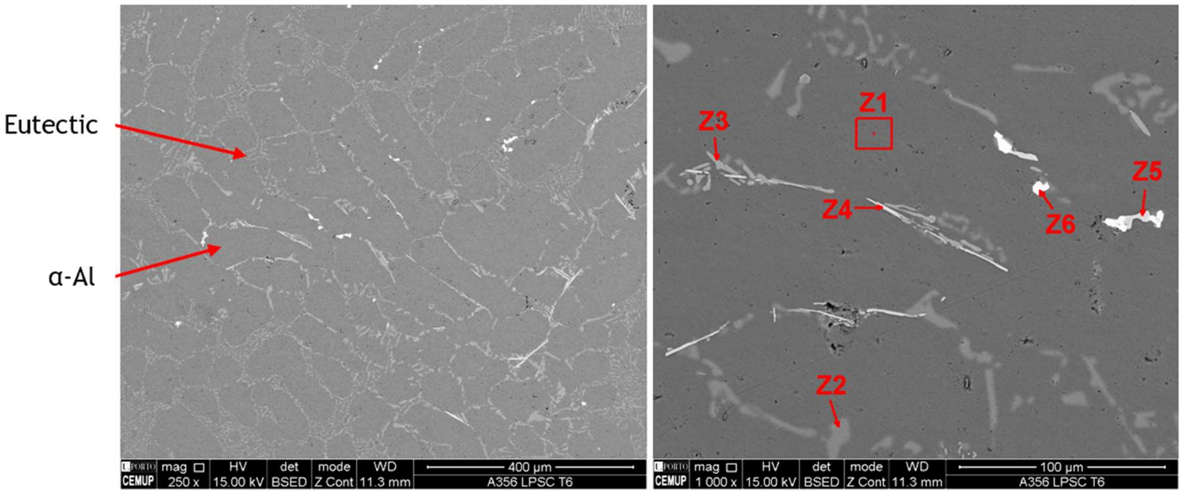

Figure 24 – T6 A356 SEM/EDS microstructures.

Table 3 - T6 A356 EDS chemical analysis on zones Z1 to Z6

Element (at %)	**Al**	**Si**	**Fe**	**Mg**	**Sr**
Z1	99.02	0.98	-	-	-
Z2	2.52	97.48	-	-	-
Z3	56.79	24.30	5.78	13.13	-
Z4	71.36	14.62	14.02	-	-
Z5	51.29	30.24	18.47	-	-
Z6	40.44	37.94	-	-	21.62

Analyzing each zone, Z1 corresponds to the α-Al dendritic matrix, and Z2 to the eutectic compound Si [54]. On the other hand, Z3 and Z4 are both needle-like ternary phases that represent iron aluminides, more accurately $Al_{18}Fe_2Mg_7Si_{10}$ and τ_6-$Al_{4.5}FeSi$, also known as β-AlFeSi, being the difference between these the content of Mg in Z3 [54–56]. The latter phase is known to appear in the form of very fine platelets [57]. Consequently, Z5 is also an AlSiFe ternary phase, concretely τ_4-Al_3FeSi_2, also designated by δ-AlFeSi [56, 58]. At last, Z6 corresponds to a strontium modified phase, probably Al_2Si_2Sr [59]. This is due to the fact Sr was used as a modifier to both reduce the size of eutectic cells and reduce the fiber structure, rounding the eutectic particles.

On Figure 25, three additional zones were identified, namely Z7, Z8 and Z9 and their chemical composition presented in Table 4. The two latter zones correspond to iron aluminides, more precisely τ_6-$Al_{4.5}FeSi$ and $Al_{18}Fe_2Mg_7Si_{10}$ [54–56]. On the other hand, Z7 represents an Mg oxide, MgO, due to the fact that Mg has a lighter atomic density than Si, leading to a darker tone in SEM [60]. Also, it is important to note that some C was detected on Z7, which might be due to contamination, from the polishing procedure for example, coupled with the fact that C measurements are not very precise through EDS analysis.

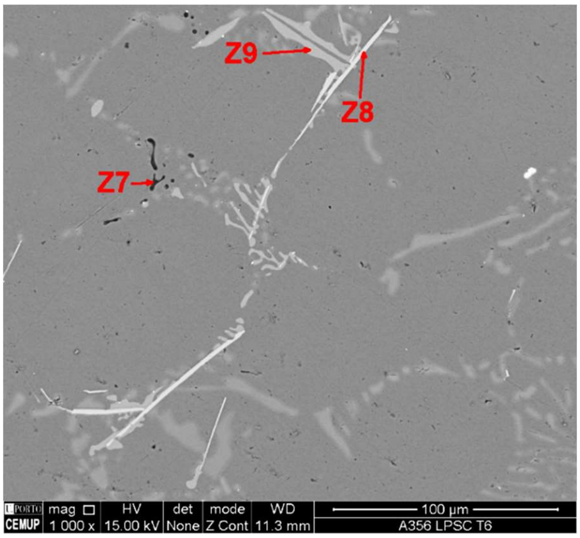

Figure 25 - T6 A356 SEM/EDS microstructure of zones Z7 to Z9.

Table 4 - T6 A356 EDS chemical analysis on zones Z7 to Z9

Element (at %)	Al	Si	Fe	Mg	C	O
Z7	10.68	24.46	-	14.58	11.22	39.06
Z8	66.39	16.98	16.63	-	-	-
Z9	49.44	27.65	6.63	16.27	-	-

4.1.1.2 Bimetallic Composites

Moving to the cold inserted composite sample, its' microstructure can be seen in Figure 26. The steel insert corresponds to the upper portion of the image. At first glance, it appears that there are no significant adhesion problems between aluminum and steel, although this is something that will be confirmed with further analysis. As for the aluminum matrix, it also contains what is expected, eutectic Si in between the α-Al dendrites. However, there is possible to see a discontinuity line close to the insert, along the eutectic, where microcracks are more easily propagated, when the material is mechanically challenged [17].

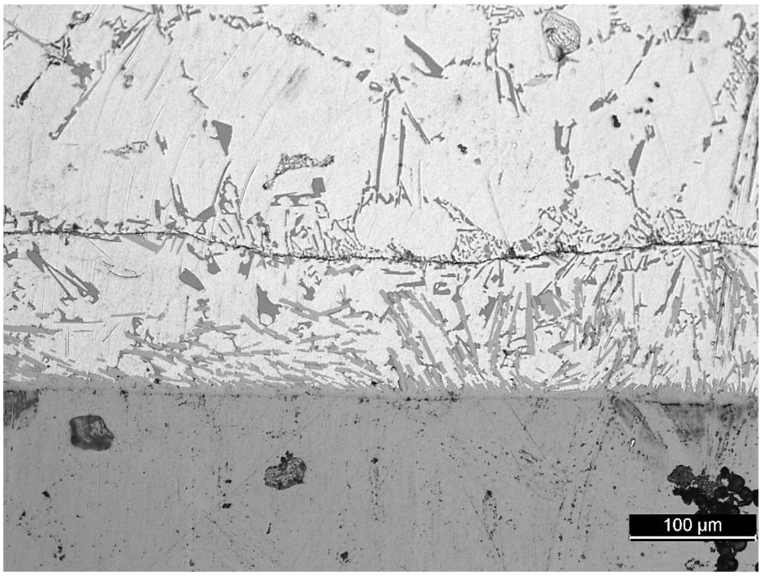

Figure 26 - Cold inserted composite microstructure.

EDS maps of the cold inserted sample shown in Figure 27 demonstrate the presence of expected elements, such as Al, Fe, Si and also Zn, since the steel sheets are galvanized. Bearing this, zinc seems to have spread out across the layer between the insert and the aluminum, due to the temperature at which the latter is poured, causing the zinc to be dissolved into the bath. The EDS maps also show traces of magnesium, which probably correspond to magnesium oxides, or magnesium rich, aluminides as previously evidenced.

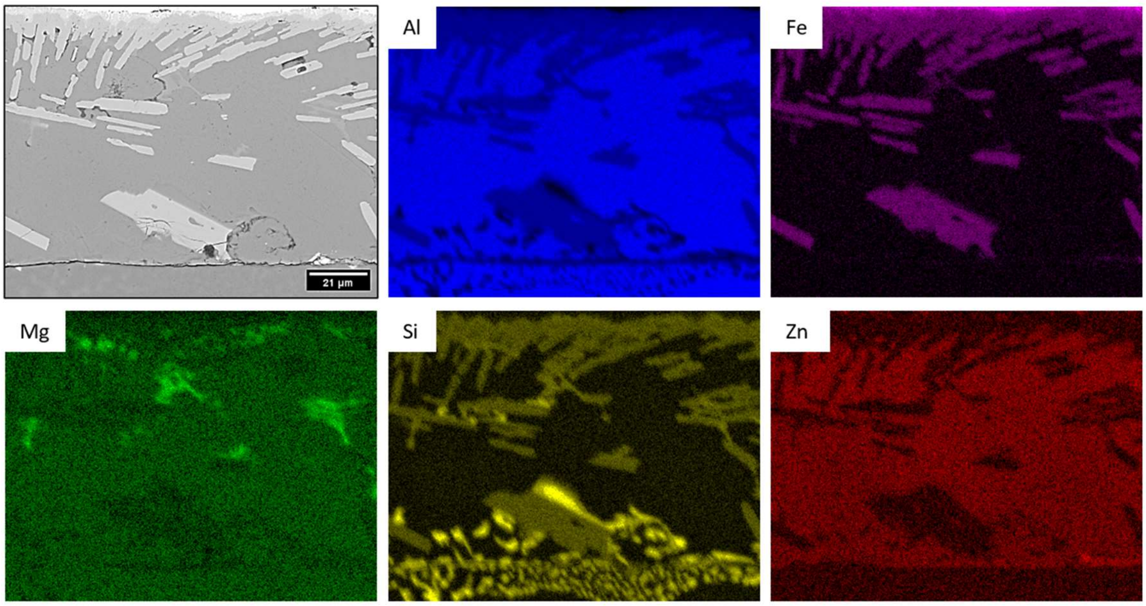

Figure 27 - Cold inserted composite EDS color maps.

Figure 28 represents an interaction zone between the steel insert, in white, and the overall α-Al matrix, in grey. As previously reported, in the aluminum matrix, close to the insert, there seems to be present a discontinuity line along the eutectic. This is due to what was concluded by Xiangfan [36], namely the Si segregation, paired with the eutectic near the aluminides.

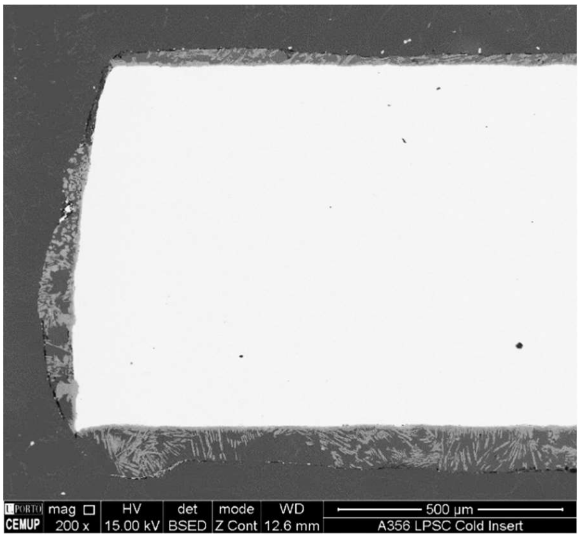

Figure 28 - Cold inserted composite SEM microstructure.

In order to have a better understanding of both the morphology and chemical composition of the compounds in the interface, higher amplifications were utilized alongside EDS analysis, having obtained the results that follow in Figures 29 and Table 5.

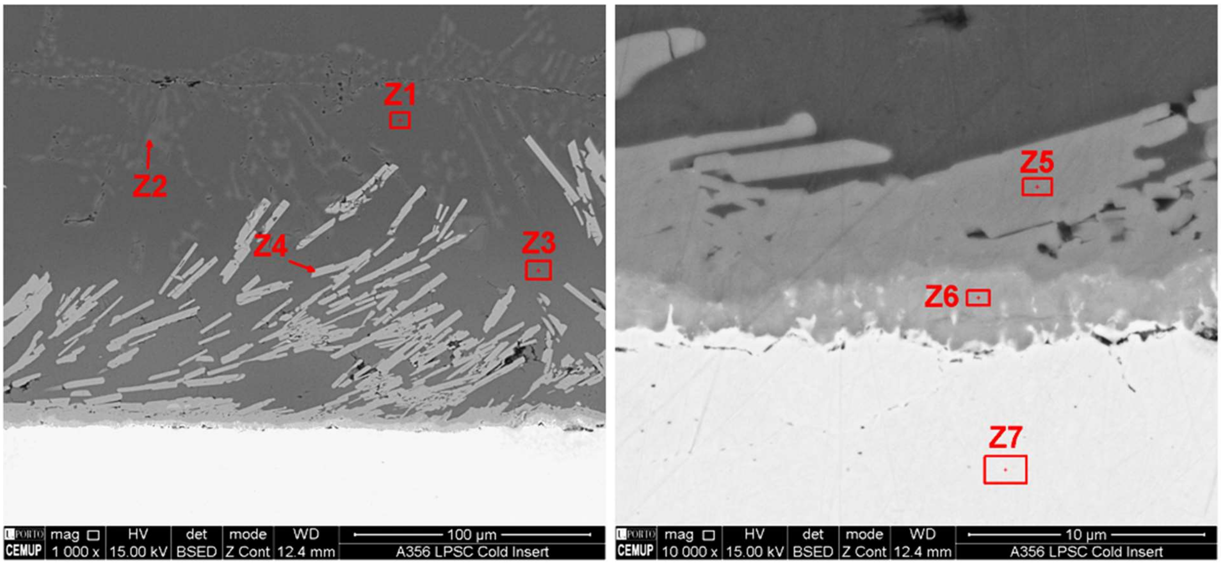

Figure 29 - Cold inserted composite SEM/EDS microstructures.

Table 5 - Cold inserted EDS chemical analysis on zones Z1 to Z6

Element (at %)	Al	Si	Fe	Zn
Z1	98.83	1.17	-	-
Z2	54.64	45.36	-	-
Z3	95.39	1.15	-	3.46
Z4	64.13	18.04	17.83	-
Z5	63.79	18.31	17.91	-

Z6	64.36	5.05	29.12	1.47

Going over the different areas, Z1 corresponds to the α-Al matrix, and Z2 to the α-Al and Si eutectic, similar to the non-reinforced sample [54]. On the other hand, Z3 has a chemical composition alike Z1, leading to believe that this area also corresponds to α-Al matrix with some Zn [61]. In turn, this zinc content in Z3 is due to the diffusion of Zn from the galvanized steel insert into the aluminum matrix. Moving over to the areas Z4, Z5 and Z6, these correspond to iron aluminides, with the iron content increasing the closer to the insert. These aluminides are, respectively, τ_2-Al_3FeSi, for Z4 and Z5, and η-Al_5Fe_2 [56, 58]. Finally, area Z7 represents the steel insert. It should also be added that, despite traces of Mg being found in the EDS maps, this element was not evidenced in any of the phases through chemical analysis.

Advancing to the next sample, the hot dipped reinforced one, microstructure can be seen in Figure 30. Once again, aluminum dendrites with eutectic silicon in between them are present, as well as a discontinuity line across the eutectic near the interface.

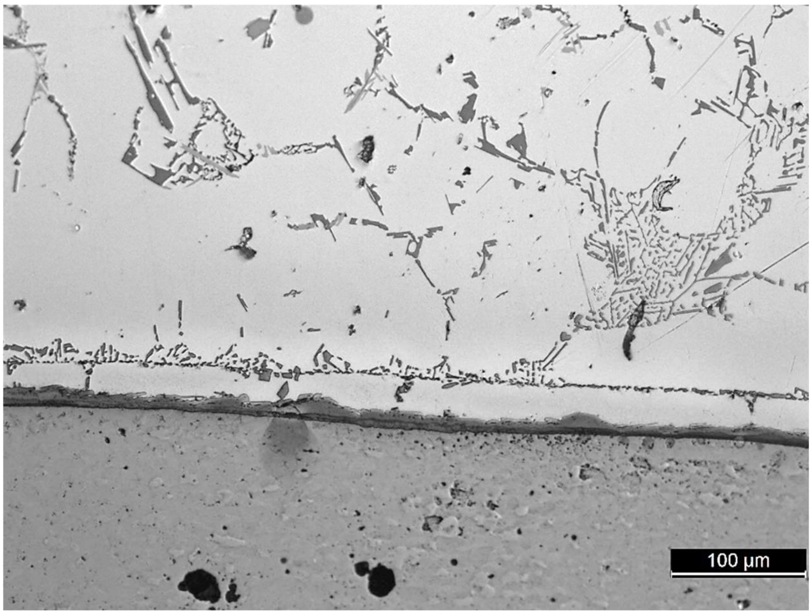

Figure 30 - Hot dipped inserted composite microstructure.

EDS maps for the same previous elements can be seen in Figure 31. However, in this composite there seems to lack the presence of Mg rich phases. Moreso, Zn from the galvanized steel seems to be absent from the maps. This can be attributed to the hot dipping treatment prior to the pouring, that may have caused this element to dissolve into the Al melt, especially since aluminum has a high solubility of Zn.

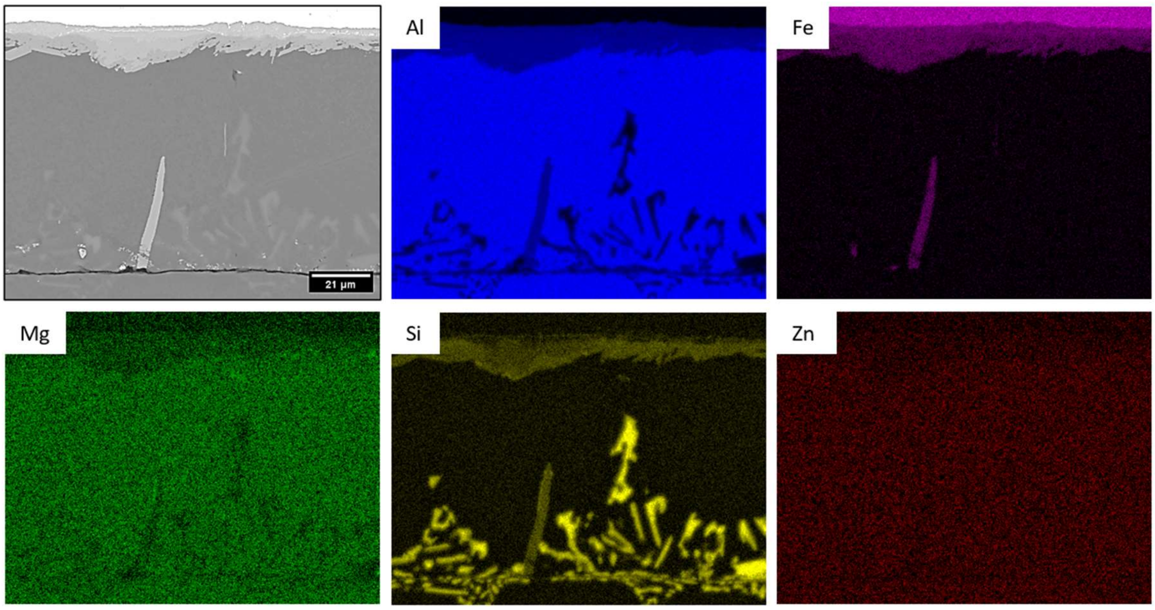

Figure 31 - Hot dipped inserted composite EDS color maps.

An image of the hot dipped insert composite interface can be seen in Figure 32a. Moreover, in Figure 32b, a discontinuity line is evidenced on the eutectic in the aluminum matrix, corresponding to the black horizontal line. This line, as evidenced in the previous sample, exists due to Si segregation, as suggested by bibliography [36]. Also, it is important to note that the discontinuities are observed along the eutectic where microcrack propagation is easier [17]. The chemical composition of the areas in Figure 32c is presented in Table 6.

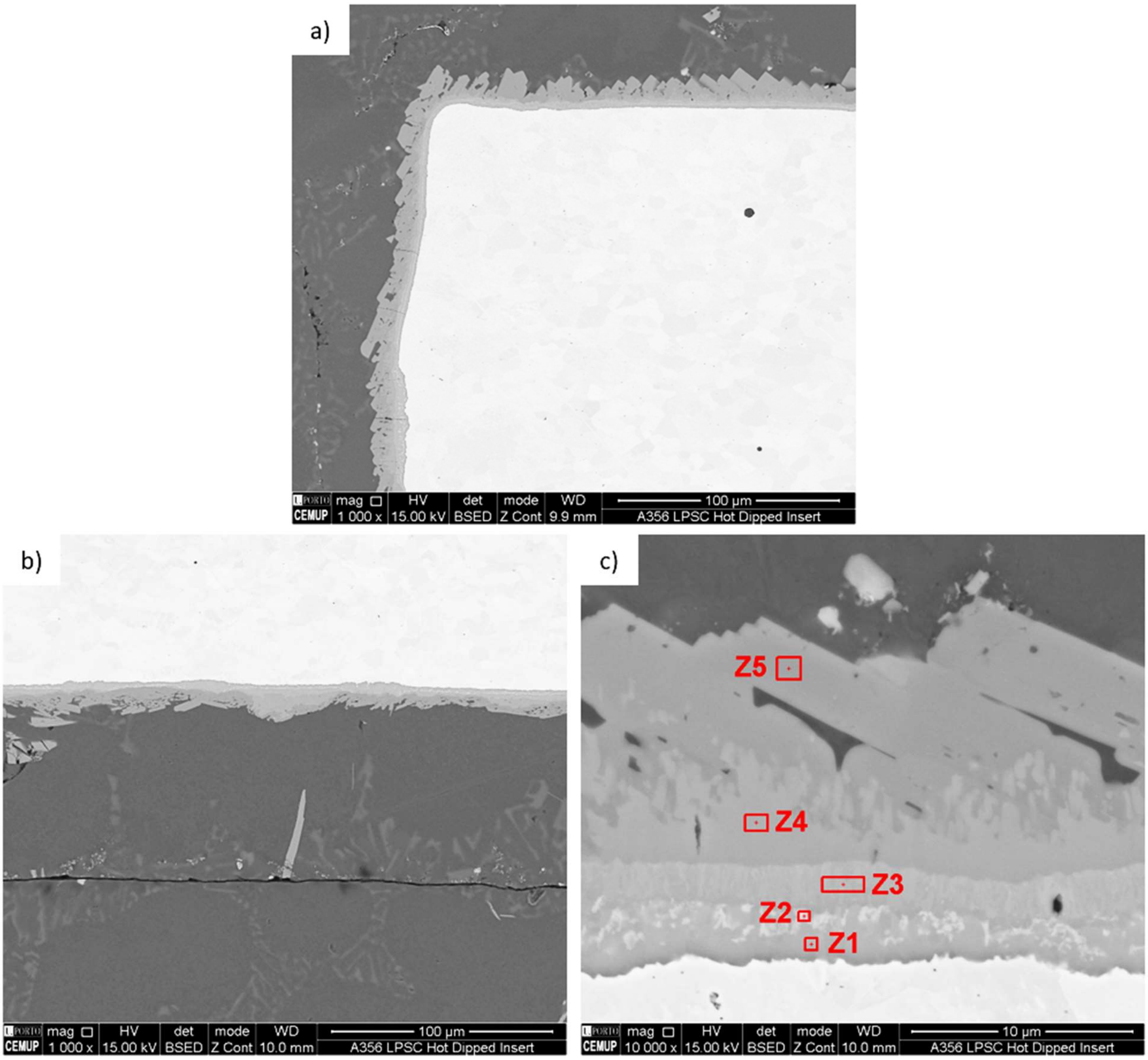

Figure 32 – Hot dipped inserted composite a) SEM microstructure; b) Discontinuity line present near interface; c) SEM/EDS microstructure.

Table 6 - Hot dipped inserted composite EDS chemical analysis on zones Z1 to Z5

Element (at %)	**Al**	**Si**	**Fe**
Z1	62.56	6.30	31.14
Z2	58.14	12.15	29.72
Z3	59.93	14.37	25.70
Z4	65.53	13.24	21.23
Z5	64.46	19.19	16.35

Analyzing the results, it appears that all 5 areas correspond to different stoichiometry iron aluminides. Starting off with Z1, this probably pertains to η-Al_5Fe_2, with an atomic percentage similar to a zone previously mentioned in the cold inserted sample [55, 58]. Moving on to Z2 and Z3, these zones probably correspond to the ternary phase

τ_{11}-$Al_4Fe_{1.7}Si$ [55, 56]. When it comes to Z4, as well as Z5, these two zones are also ternary phases. Moreover, Z4 probably consists of τ_5-$Al_{7.4}Fe_2Si$, and Z5 of τ_2-Al_3FeSi [55, 56, 58]. It is also important to mention that the hot dipping treatment to the galvanized steel insert appeared to have promoted the dissolution of all the zinc into the aluminum bath, since minimal of this element were present in the EDS analysis.

Bearing this, the relatively high silicon content on the iron aluminides can be explained due to different concentration gradients of this element. Since molten aluminum had way more Si when compared to steel, diffusion of this element from the aluminum to the interface occurred. Moreso, the formation of different stoichiometry AlFeSi compounds can be justified by a chain of reactions, where Fe_mAl_n and $Al_xFe_ySi_z$ are the different phases formed, such as [40]:

$$L \rightarrow Fe_mAl_n + L' \rightarrow Al_xFe_ySi_z \tag{4}$$

4.1.1.3 Hot-Dipping Optimization

Microstructures from the optimized samples, portrayed in Table 2, can be seen in Figure 33. From these images, it appears the application of the NH_4Cl treatment led to the absence of the discontinuity line in the aluminum matrix, pointing to a lack of Si segregation. Also, a thinner and more regular IML seems to have been formed in the treated samples, regardless of the presence of the galvanization layer on the sheet. Furthermore, SEM analysis was carried out to better understand the phenomena associated with the treatment.

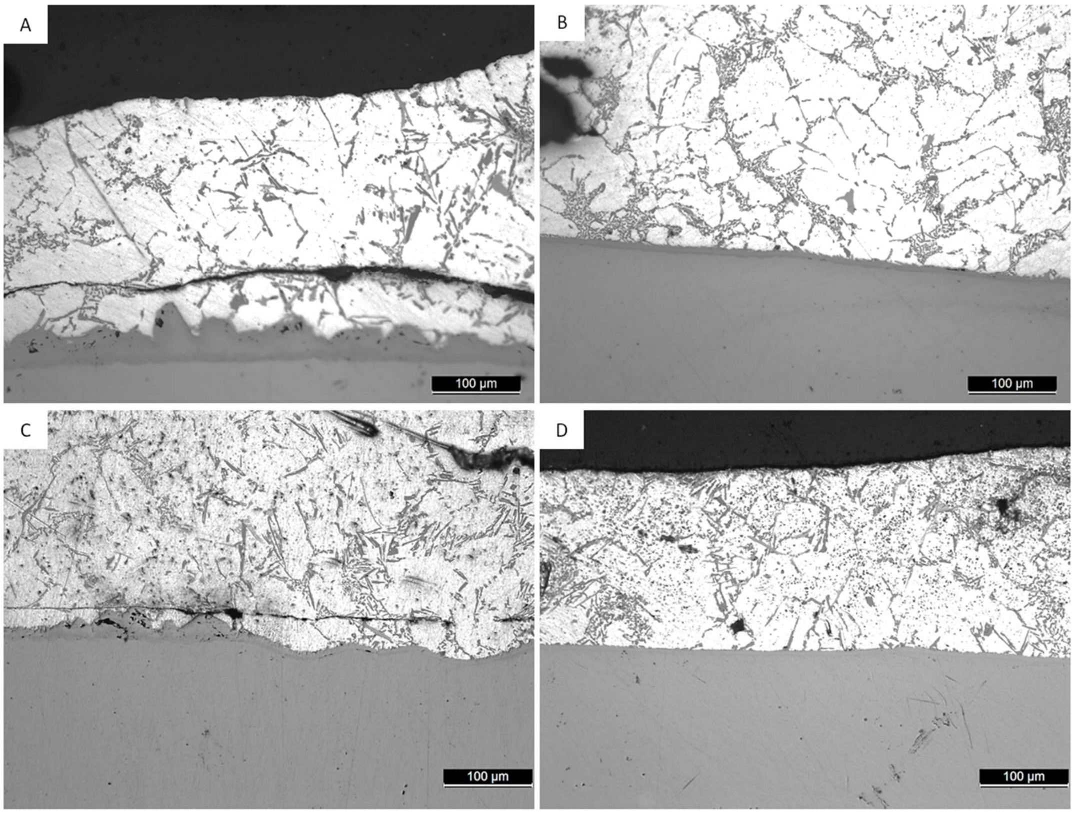

Figure 33 - Microstructures from samples A to D. A – Galvanized sheet; B – Galvanized sheet with NH_4Cl treatment; C – Non-Galvanized sheet; D – Non-Galvanized sheet with NH_4Cl treatment

Since sample A has similar conditions to the previous hot dipped composite, an extensive analysis was not carried out on this sample. Starting off with the analysis of sample B, EDS maps can be seen in Figure 34. As previously stated on other samples, Zn seems to have been lost from the insert during the hot dipping. However, the (IML) seems to be thinner, as well as the Si eutectic, something that will be further confirmed with the following SEM images.

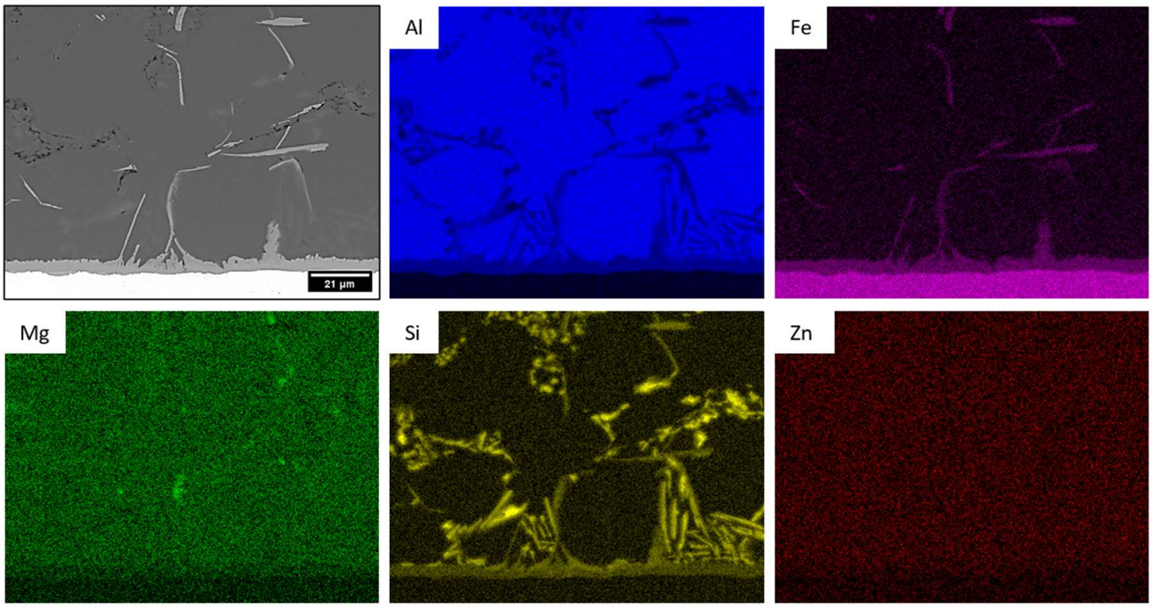

Figure 34 - Galvanized and NH_4Cl treated sample EDS color maps.

Figure 35 shows approximately the middle of the insert, demonstrating an uneven aluminum adhesion on both sides, which can be attributed to some difficulties during the dipping procedure, such as physical contact between sheets. However, the application of the NH_4Cl treatment appears to not only decrease the IML thickness, but also regularize its morphology. Simultaneously a discontinuity line on the aluminum matrix was not evidenced in these images.

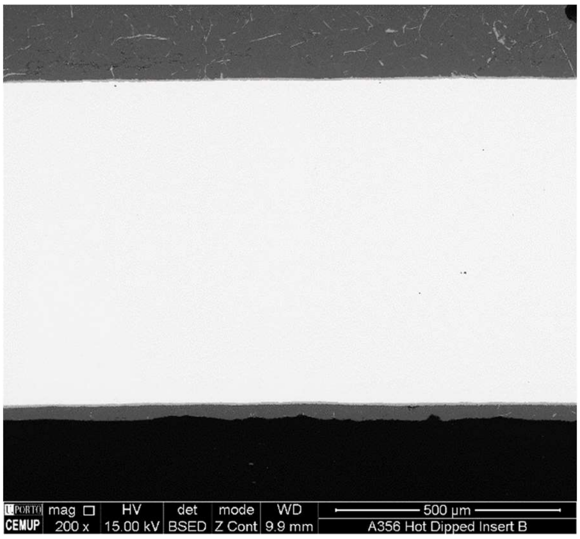

Figure 35 - Galvanized and NH_4Cl treated sample SEM microstructure.

Going through the EDS chemical analysis of the zones on Figure 36 and presented on Table 7, Z1 and Z2 correspond to the α-Al matrix, and to α-Al and Si eutectic respectively [54]. Furthermore, areas Z3 to Z5 appear AlSiFe ternary phases, more precisely τ_4-Al_3FeSi_2, τ_5-$Al_{7.4}Fe_2Si$ and η-Al_5Fe_2 [55, 56, 58]. All three of these ternary intermetallics were previously seen on either the T6 heat treated base alloy or the hot dipped insert. Bearing this, at first sight the ammonium chloride treatment appears to not only grant the forementioned benefits, but also leads to the absence of the tongue-like τ_2-Al_3FeSi phase on the intermetallic layer. Also, Z6 corresponds to the steel insert.

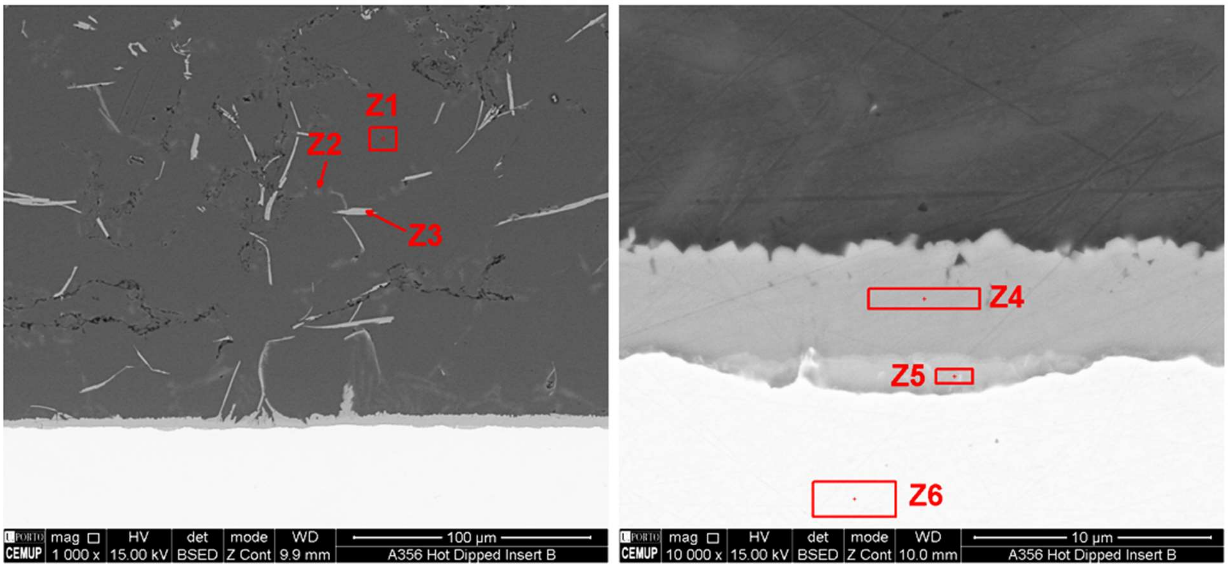

Figure 36 - Galvanized and NH_4Cl treated sample SEM/EDS microstructures.

Table 7 - Galvanized and NH_4Cl treated sample EDS chemical analysis on zones Z1 to Z5

Element (at %)	Al	Si	Fe
Z1	98.74	1.26	-
Z2	26.08	73.92	-
Z3	51.55	29.98	18.48
Z4	65.68	12.28	22.04
Z5	63.94	5.72	30.35

EDS maps of sample C can be viewed in Figure 37. Since the Zn was previously removed, once again lack of Zn on the maps is evidenced and also the appearance of a discontinuity line close to the interface of both materials, which was not present on sample B. However, with these maps, it appears that discontinuities have a preferential site to occur, more precisely on the silicon eutectic zones, which also seem to be coarser and less plate-like.

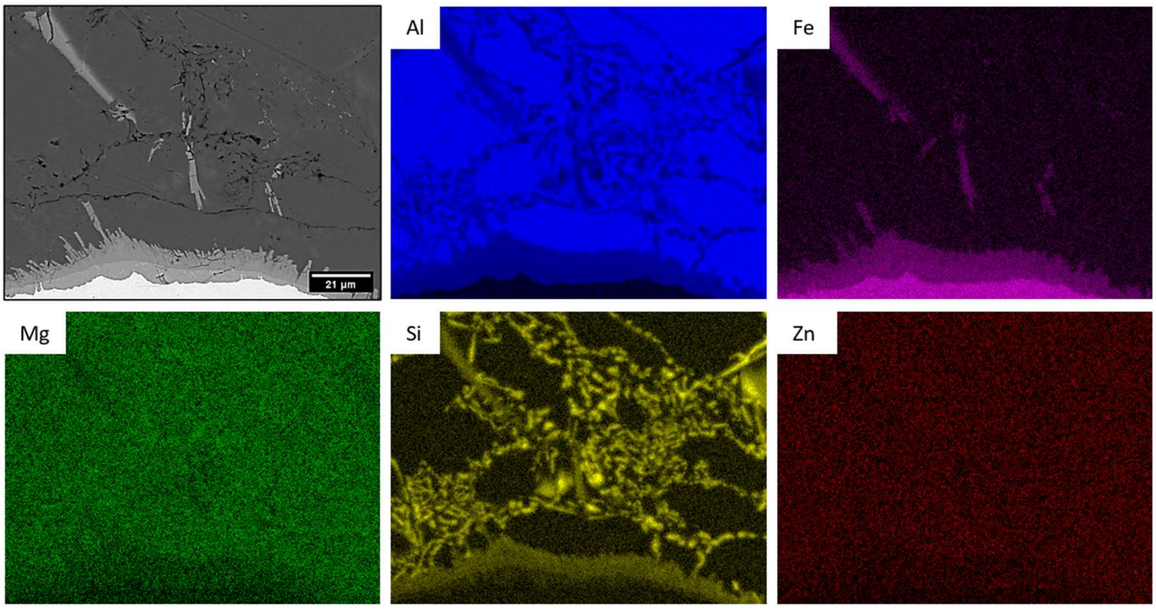

Figure 37 - Non-Galvanized and untreated with NH$_4$Cl sample EDS color maps.

Figure 38 shows SEM images of this sample, demonstrating an IML way more irregular than in sample B, be it in morphology and thickness across the section. Since this sample, as well as the one that will be analyzed next, lacks the galvanized layer on the steel sheet, chemical analysis was done to better evaluate what compounds were formed and if any of them are new.

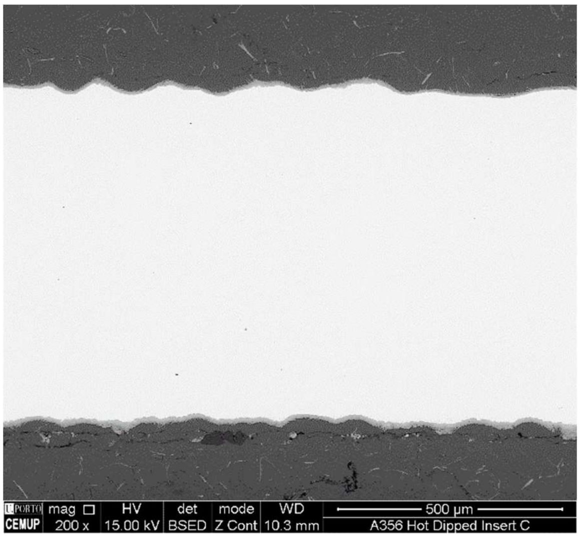

Figure 38 - Non-Galvanized and untreated with NH$_4$Cl sample SEM microstructure.

Looking at Table 8, corresponding to the semi quantitative EDS analysis of the zones in Figure 39, Z1 and Z2 are, similarly to sample B, α-Al, and to α-Al and Si eutectic [54]. On the other hand, Z3 is τ_6-Al$_{4.5}$FeSi, Z4 is τ_2-Al$_3$FeSi and Z5 is τ_5-Al$_{7.4}$Fe$_2$Si [55, 56, 58, 62]. At last, area Z6 pertains to η-Al$_5$Fe$_2$ and Z7 to the steel insert [55]. With this in mind, the lack of galvanized layer and treatment seems to have led to the formation of different intermediate intermetallic compounds, and also to a more irregular morphology and thicker IML.

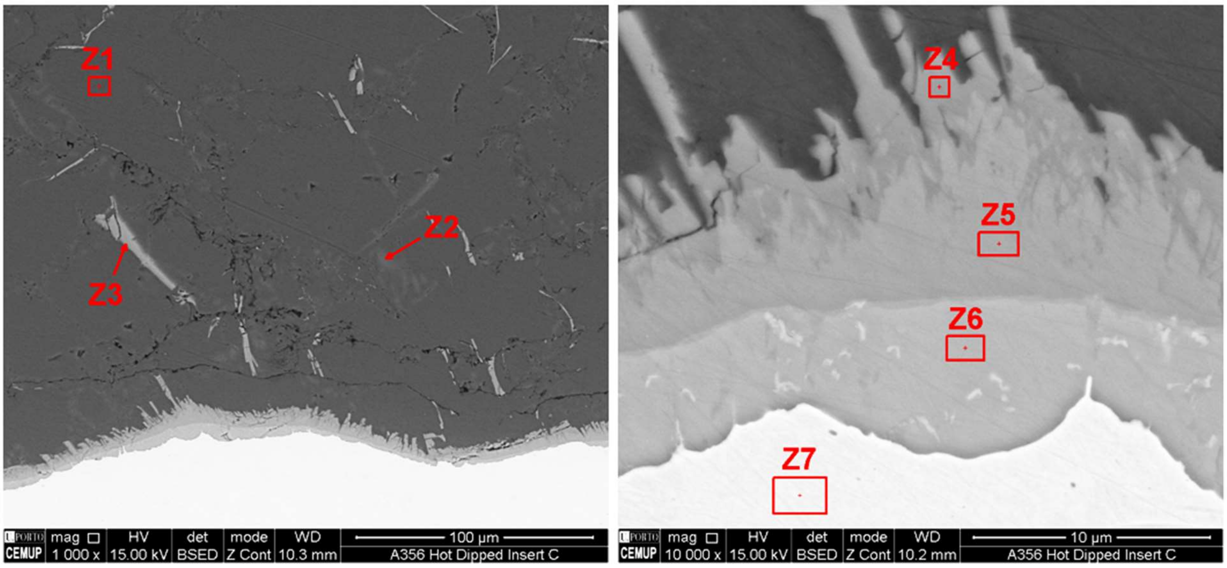

Figure 39 - Non-Galvanized and untreated with NH_4Cl sample SEM/EDS microstructure.

Table 8 - Non-Galvanized and untreated with NH_4Cl sample EDS chemical analysis on zones Z1 to Z6

Element (at %)	Al	Si	Fe
Z1	98.60	1.40	-
Z2	29.92	70.08	-
Z3	63.21	20.30	16.49
Z4	56.36	16.79	16.51
Z5	66.46	11.82	21.71
Z6	65.62	4.18	30.20

Moving on to the last sample, sample D, EDS maps can be seen in Figure 40. Comparing these with the previous sample, both the insert and the IML are more regular but also a needle-like morphology of the eutectic seems to be favored. Going back to sample B, there is also a more needle-like eutectic morphology, which seems to point out that the application of the treatment might be the cause of this. This contrasts with sample C, in which the eutectic has a more globular shape and is also more agglomerated. Looking back at the cold inserted and hot dipped samples, the discontinuity line also surges on the eutectic sites, pointing that this might be the actual cause of these defects, either due to poor alloy quality or lack of inert atmosphere control. Once again, lack of zinc was verified.

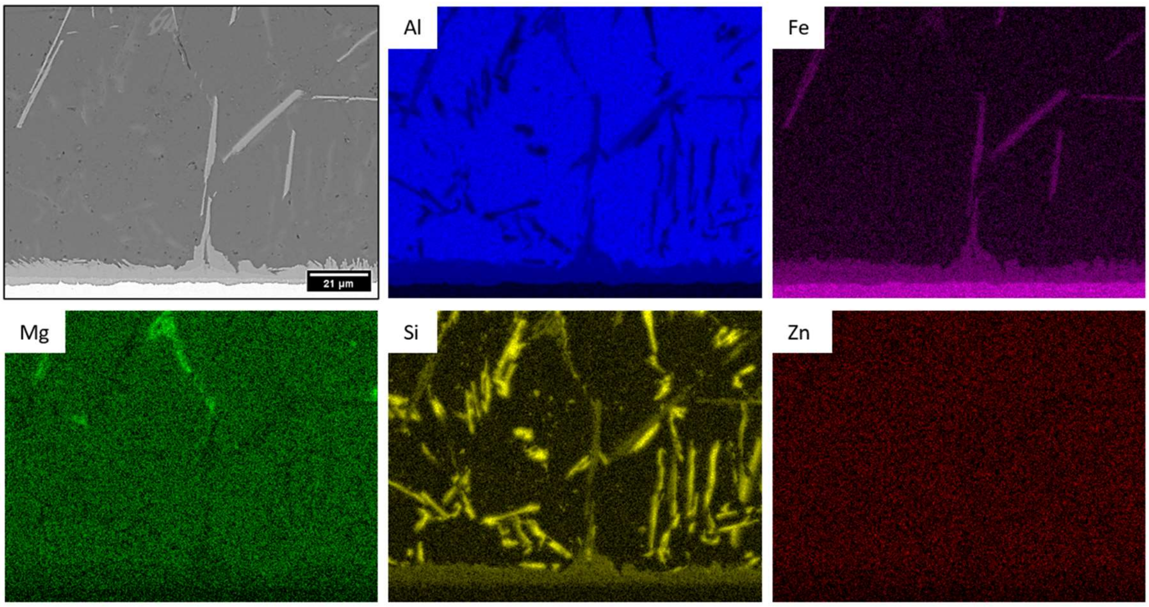

Figure 40 - Non-galvanized and NH_4Cl treated sample EDS color maps.

Figure 41 represents the SEM images that were taken from this sample. Similar to the other treated sample, the thickness of the IML layer is lower. However, the IML is way more irregular than the one in the galvanized B sample. This is reported due to the fact that this sample also demonstrates the presence of needle-like τ_2-Al_3FeSi intermetallics such as the ones seen in every other sample except B.

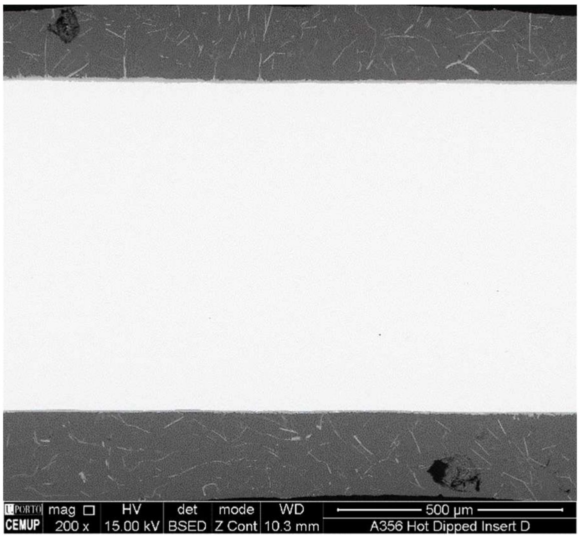

Figure 41 - Non-galvanized and NH_4Cl treated sample SEM microstructure.

As for the EDS chemical analysis, Figure 42, alongside Table 9, were retrieved. Areas Z1 and Z2 correspond to α-Al, and the eutectic [54], and Z3 to τ_6-$Al_{4.5}FeSi$ [55, 58]. On the other hand, Z4 pertains to $Al_{18}Fe_2Mg_7Si_{10}$, a phase also seen in the base aluminum alloy with the T6 treatment [54]. When it comes to Z5 and Z6, these are the ternary phases τ_2-Al_3FeSi and τ_5-$Al_{7.4}Fe_2Si$, respectively [55, 56, 58, 62]. Finally, area Z7 corresponds to η-Al_5Fe_2 [55] and Z8 to the steel insert. Bearing this, the application of the ammonium chloride treatment did not lead to the formation of any phases that were not previously seen.

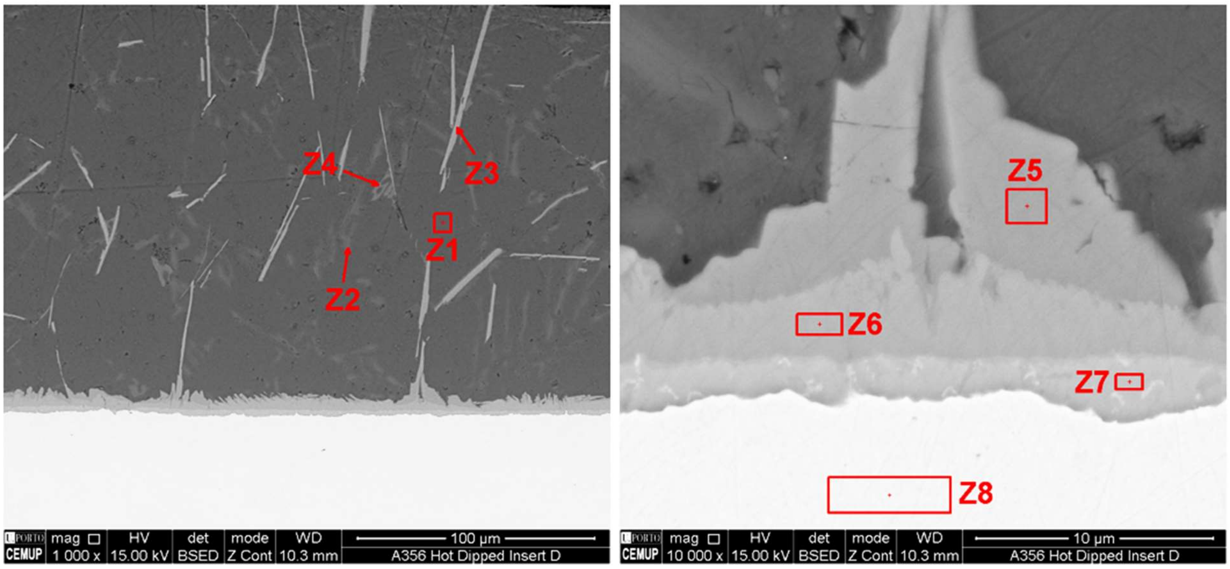

Figure 42 - Non-galvanized and NH_4Cl treated sample SEM/EDS microstructures.

Table 9 - Non-galvanized and NH_4Cl treated sample EDS chemical analysis on zones Z1 to Z7

Element (at %)	Al	Si	Fe	Mg
Z1	98.13	1.87	-	-
Z2	15.15	83.96	-	0.89
Z3	65.31	18.19	15.15	1.34
Z4	63.85	21.11	4.44	10.60
Z5	64.11	19.16	16.73	-
Z6	66.56	12.20	21.24	-
Z7	66.14	4.12	29.75	-

To confirm the IML thickness reduction, measurements on the different sample microstructures of the interface were done. The results can be seen in Table 10. According to what would be expected, the samples without the treatment have a significantly thicker IML layer. Also, comparing the cold inserted composite with the hot dipped one, the slight difference on the length of the layer can be due to the employment of the hot dipping procedure, which would cause a higher molten aluminum contact time with the insert, allowing the layer to grow.

Table 10 - IML thickness of the different samples

Sample	IML Thickness (µm)
Cold Insert	10.6 ± 2.1
Hot Dipped / A	12.7 ± 2.7
Galvanized and Treated (B)	6.1 ± 0.4

Non-Galvanized and Untreated (C)	10.4 ± 1.8
Non-Galvanized and Treated (D)	8.6 ± 1.5

To summarize these results, the ammonium chloride treatment seems to reduce the thickness of the IML and its irregularity. However, the treatment also seems to lead to a eutectic needle-like morphology, instead of a more rounded, globular, one, which might be the cause for the lack of a discontinuity line on the aluminum matrix. Although this absence of the discontinuity line may also have happened due to a lack of Si segregation, which also might have occurred because of the ammonium chloride treatment. The best results were found in sample B, with the galvanized treated insert, since in this sample, not only the thickness of the IML is the lowest, but it also is the most regular of all the samples. One other thing that is worth mentioning is that the η-Al_5Fe_2 intermetallic layer is the smallest in sample B, which is a positive outcome since this compound is very brittle. Also, the galvanized and treated sample seems to lack the presence of the tongue-like τ_2-Al_3FeSi phase in the interface between aluminum and steel.

4.1.2 Mechanical Properties

4.1.2.1 Tensile Tests

Figure 43 shows examples of tensile stress curves of the structural composites through which tensile properties were determined. These include the YS, the UTS and the A% which can be more accurately seen in Figure 44.

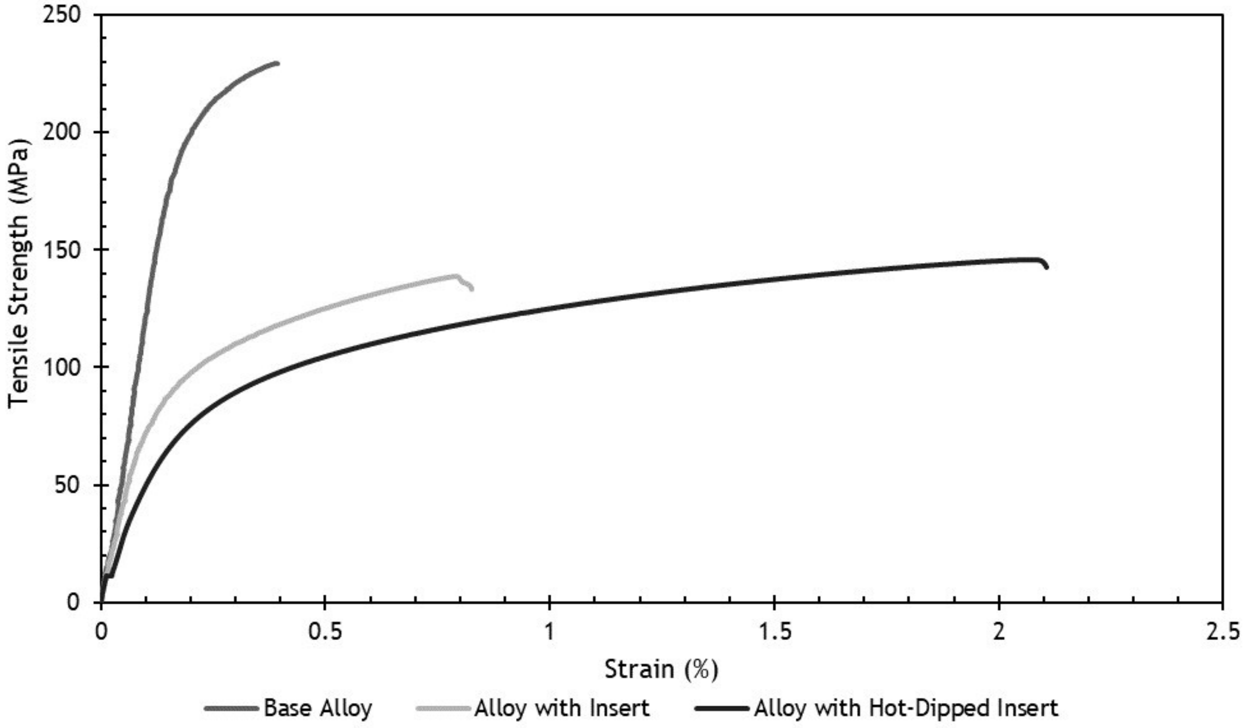

Figure 43 - Tensile stress curves of structural composites.

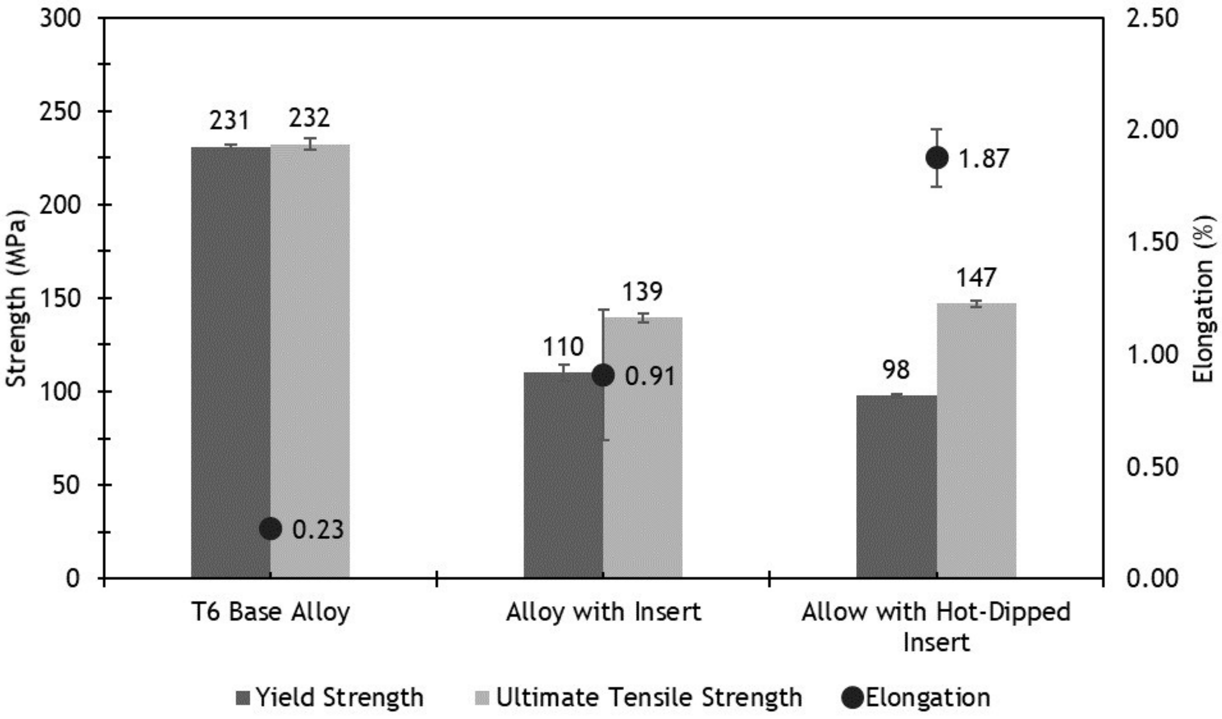

Figure 44 - YS, UTS and A% of the structural composites.

With the observation of the curves, it is possible to perceive straight away that the use of reinforcement increased the A% and decreased the UTS and YS. More accurately, the use of reinforcement caused a 52 % decrease in YS, which is amplified to 58 % when the reinforcement was previously hot dipped, and a 40 % decrease in UTS. This allows the conclusion that the insertion of a steel reinforcement decreases overall strength and increases ductility. Having this said, the failure of a fiber-reinforced composite is usually determined by the fracture of the fiber, under longitudinal monotonic tension [63]. This provides an explanation as to why the overall strength diminished in these fiber-reinforced aluminum composites. Also, the steel fibers had holes throughout their length to promote a better infiltration of the aluminum. These holes proved to be the preferential sites for fracture, due to a lower section area, across the different reinforced samples, thus supporting the forementioned idea that the fibers' properties were the determining factor for the tensile tests. On the other hand, defects introduced on the machining of the holes could also be at fault for the strength decrease. However, it is also important to note that the discontinuity line present in between the eutectic may also be the reason the properties of the composites were not higher. As for the hot dipped sample, the YS was even lower than the non-hot dipped reinforced samples. This can be due to the fact that a brittle alloy layer is formed in the holes of the steel inserts, limiting the degree of possible deformation, which could potentially diminish the YS [10]. When it comes to the A%, these values are lower than what was expected, which should be higher than 3.5% for the T6 base alloy and higher than 2% for the non-heat-treated samples [64, 65]. This could be due to big porosities present in the previously seen microstructures, which was discovered to be around 2% through density measurements. Also, as previously mentioned, Yang et al. [17], noticed that pores have a noticeably negative impact in both the A% and

UTS due to higher strain accumulation on the eutectic, which by itself is a preferential zone for microcrack propagation, as seen in Figure 3.

As for the specific strength (SS) of the composites, compared to the heat-treated base alloy, the measurement and results can be seen in Table 11. These revealed to be non-advantageous for strength related applications when compared to the A356 + T6 alloy, since not only there is a decrease of the UTS but also an increase of the specific mass for the composites, which ultimately leads to SS values of almost half.

Table 11 - Specific strength of the structural composites

Sample	Specific Mass (kg/m^3)	UTS (MPa)	SS (kN*m/Kg)	Variation
A356 + T6	2655	232	87	-
Cold Insert	2838	139	49	-44 %
Hot Dipped Insert	2827	147	52	-41 %

4.1.2.2 Hardness Tests

Figure 45 shows the Vickers microhardness test results and Figure 46 two of the hardness profiles made. When it comes to the aluminum matrix (20 μm distance), the hardness values are pretty much the same across all the samples, around 73 ± 18 HV. On the same note, the insert hardness values (0 μm distance) are very consistent and according to expected, rounding 205 ± 14 HV, since the steel material was the same. On the interfacial zone next to the steel insert, at 5 μm distance, this zone presented quite high hardness values, namely 1346 ± 189 HV. This is due to the fact that the indented phase in these samples was η-Al_5Fe_2, a very hard and brittle phase with reported hardness values of around 1000 HV [35]. However, for sample B, since this compound layer is very thin, it is believed that the high hardness values pertain to τ5-$Al_{7.4}Fe_2Si$, another brittle phase [66–69]. Finally, at the 10 μm distance, there are quite different hardness values, varying between samples. For samples A and C, without the NH_4Cl treatment, the values are consistent with the brittle phase, which is present in all the samples, namely τ5-$Al_{7.4}Fe_2Si$, which seems to possess hardness values of around 1130 ± 253 HV [66–69]. Moreso, for the cold inserted and D sample, these lower values, averaging 410 ± 124 HV, are believed to pertain to the tongue-like τ2-Al_3FeSi intermetallic compound. As for sample B, since this has a very thin IML layer, the low values could be due to faulty indentations in between the aluminum matrix and the IML τ5-$Al_{7.4}Fe_2Si$ layer phase, since there is an absence of τ2-Al_3FeSi in the interface.

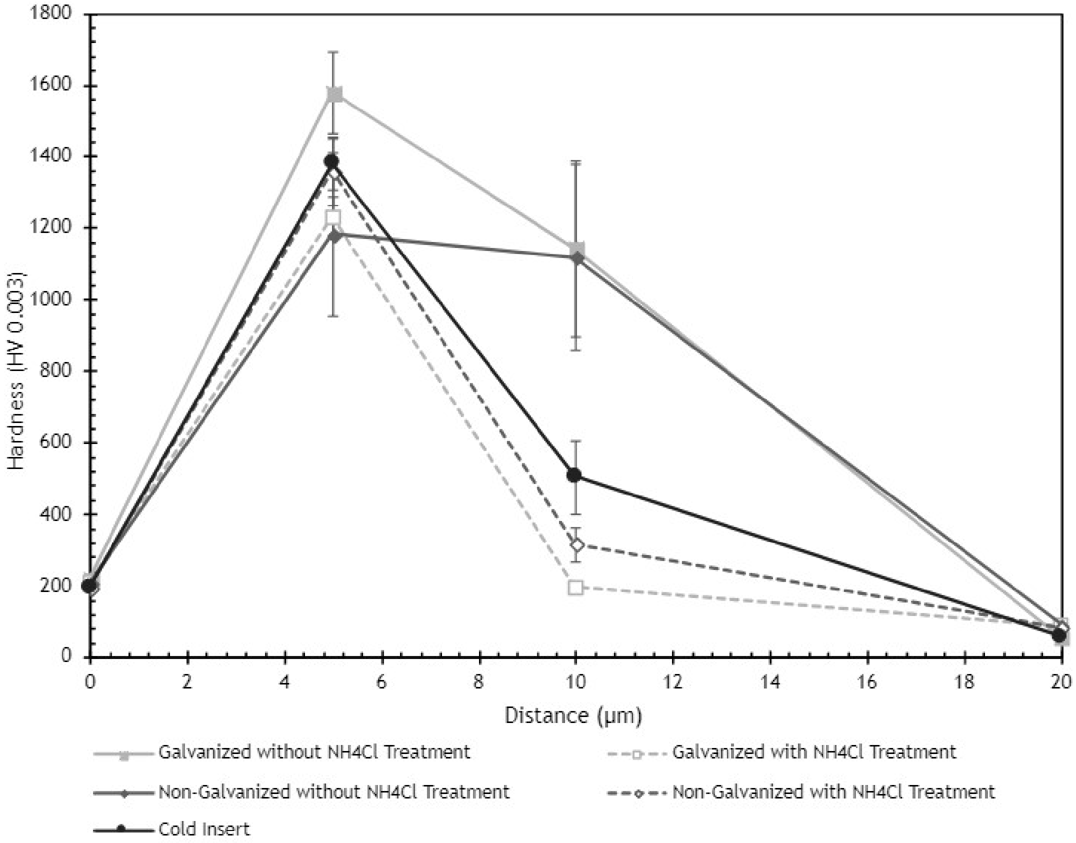

Figure 45 - Vickers Hardness results on the structural composites (0 µm distance corresponds to the steel insert, 5 and 10 µm to the interface and 20 µm to the aluminum matrix).

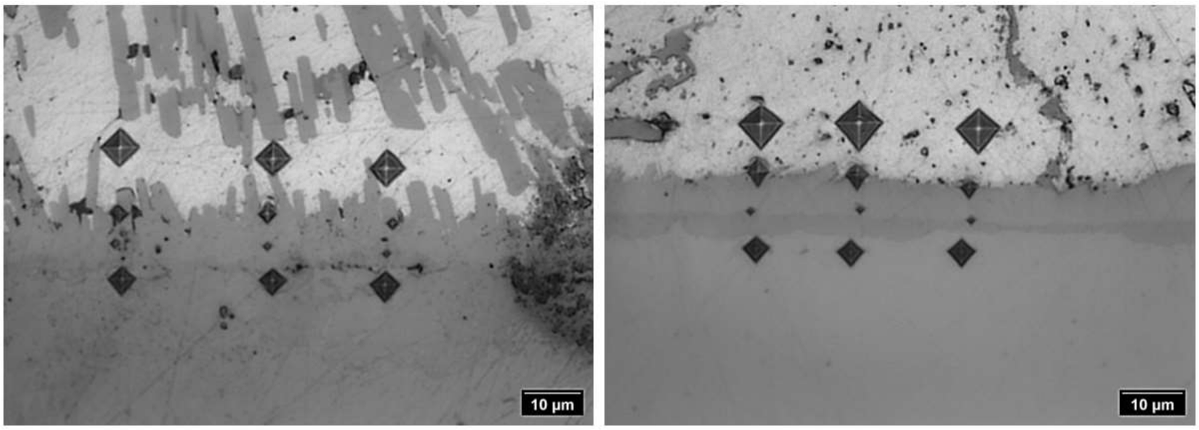

Figure 46 - Hardness profiles from cold inserted sample (left) and non-galvanized with NH_4Cl treatment sample (right). The aluminum matrix corresponds to the upper bright portion, while the lower part corresponds to the steel insert. In-between is the interface.

4.1.3 Fractography Characterization

4.1.3.1 A356 Base Alloy

SEM analysis was also carried out for the fracture surfaces of the samples. Starting off with the T6 heat treated A356 sample, non-reinforced, fracture surfaces can be seen in Figure 47. In Figure 47a, the dendritic structure can be easily recognizable, along with some large porosities that suggest having been the main cause of fracture. Taking a closer look, in Figures 47b and 47c, both fracture mechanisms, dimples and cleavage planes, can be seen. However, there is a higher emphasis on the cleavage planes, which goes accordingly to the expected due to the very low A% of this sample presented in the tensile tests. Moreso, a very high quantity of large porosities can also be evidenced, which may also provide an explanation as to why this alloy fractured at such low A% values.

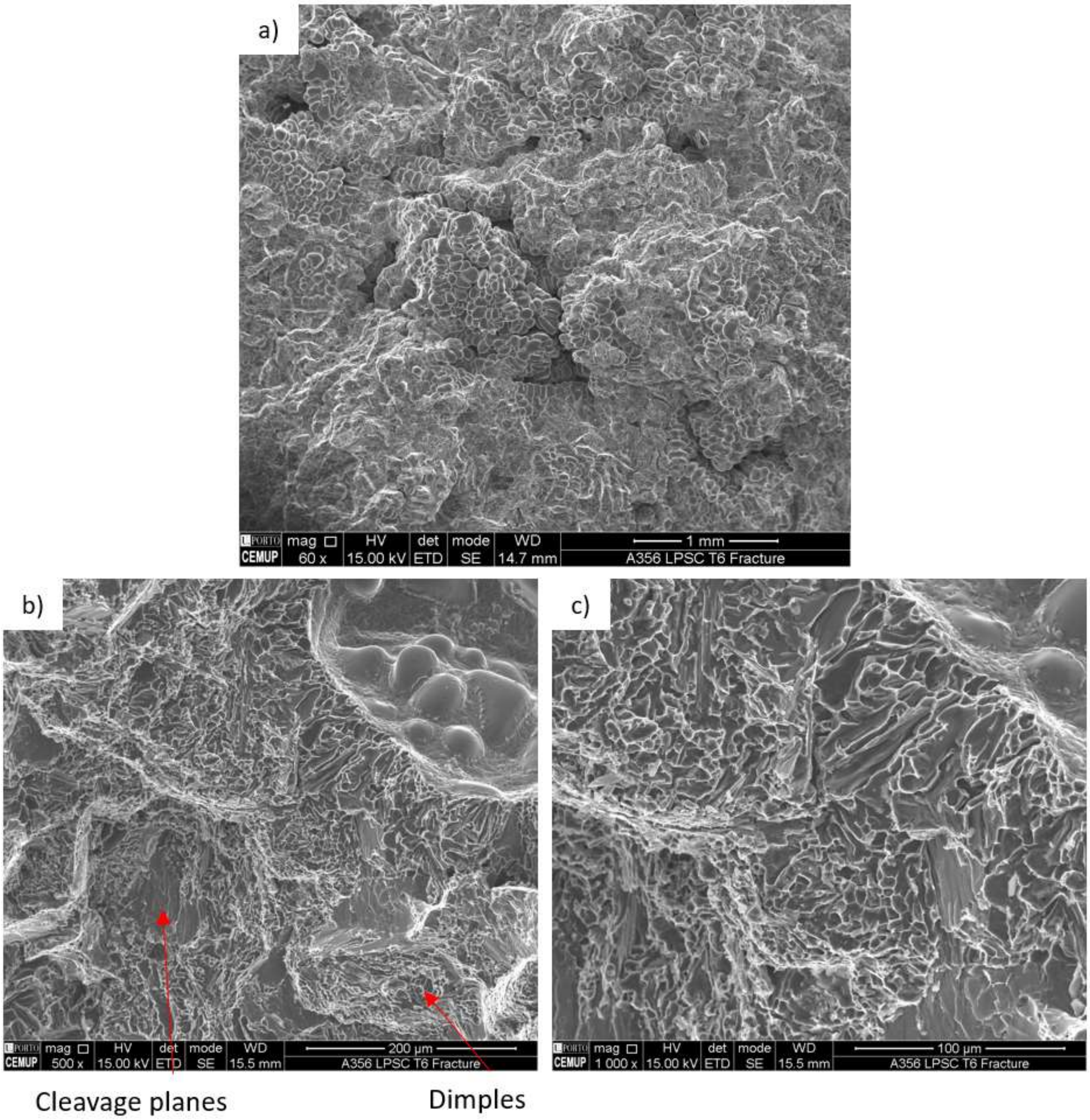

Figure 47 - T6 A356 fracture surfaces obtained with SEM.

4.1.3.2 Bimetallic Composites

Moving on to the reinforced sample without previous hot dipping, the fracture images can be seen in Figure 48. With a lower magnification, Figure 48a, in the aluminum zone, the fracture was similar to the T6 fracture, namely fragile, which can be evidenced due to the cleavage planes. On the other hand, in Figure 48b, the steel insert clearly presents a ductile fracture, due to the existence of dimples all across its section. At last, analyzing the iron aluminide layer that formed between the insert and the aluminum, in Figure 48c, it presented only cleavage planes, which coincides with the expected, since these compounds are very brittle [10].

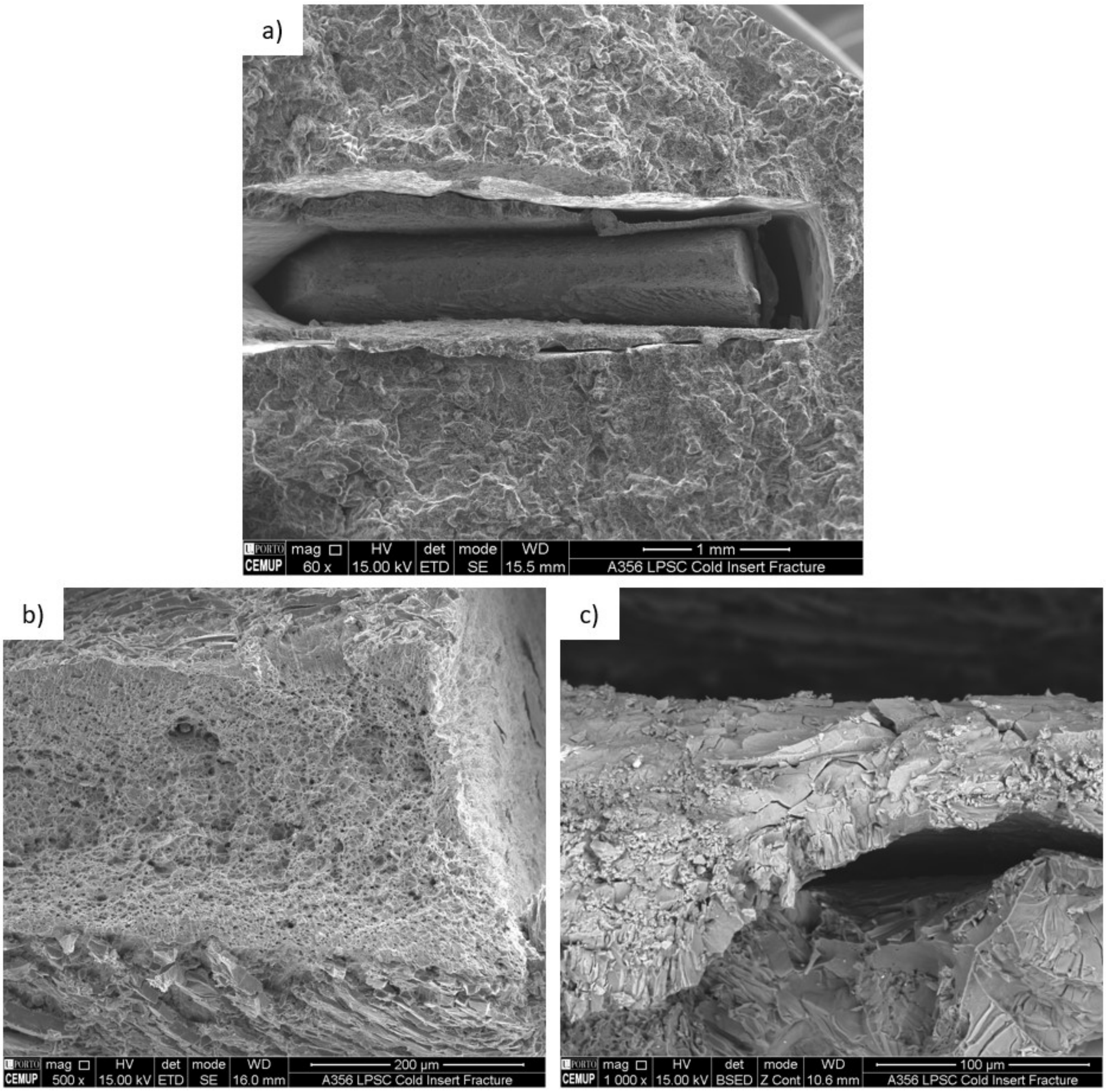

Figure 48 - Cold inserted composite fracture surfaces obtained with SEM.

When it comes to the hot dipped insert sample, the fractography results are very similar to the non-hot dipped. In Figure 49, the overall fracture, with a zoom in on the steel insert and the aluminide compound correspondingly can be observed. Once again, cleavage planes can be observed on the α-Al matrix and the aluminide, meaning these zones behaved in a brittle manner, and dimples all across the steel insert, corresponding to a ductile fracture.

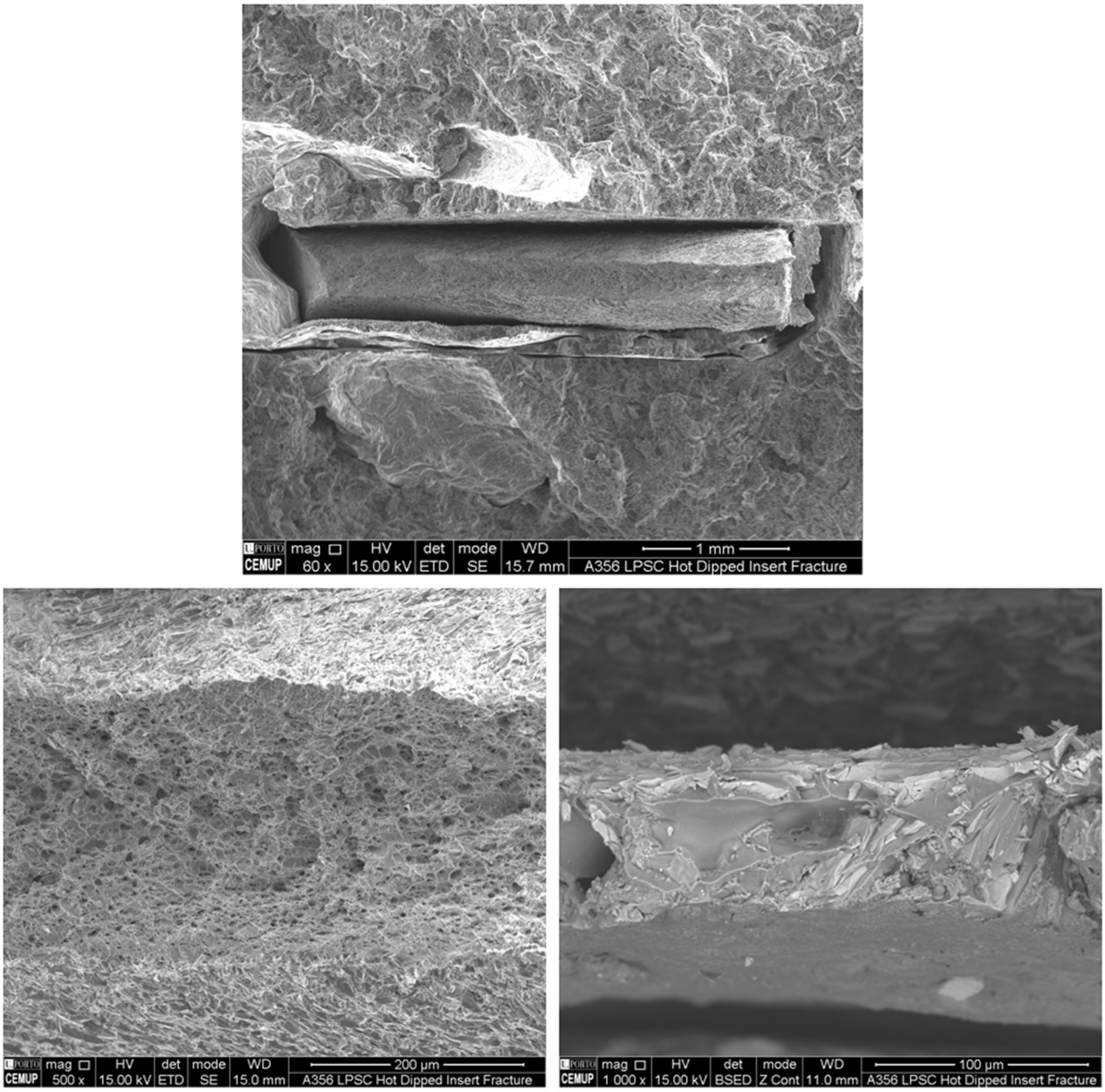

Figure 49 - Hot dipped composite fracture surfaced obtained with SEM.

4.2 DRA Composites

4.2.1 Microstructural Characterization

After the milling procedure mentioned before, microstructures of the powder obtained were taken. These can be seen in Figure 50. The black dots on the white surface are believed to pertain to the Al_2O_3 particles, which goes according to results from some authors [29, 32]. Although, this is something that should be further confirmed by chemical analysis. However, as opposed to what would be expected, the microstructures appear to have the presence of distorted aluminum dendrites and the eutectic Al-Si compound. This can be due to the milling procedure, the lack of liquid processing post-milling, or both. As for the Al_2O_3 distribution across the matrix, in figure 50B it seems there might be some agglomeration of these particles on the upper part of the microstructure.

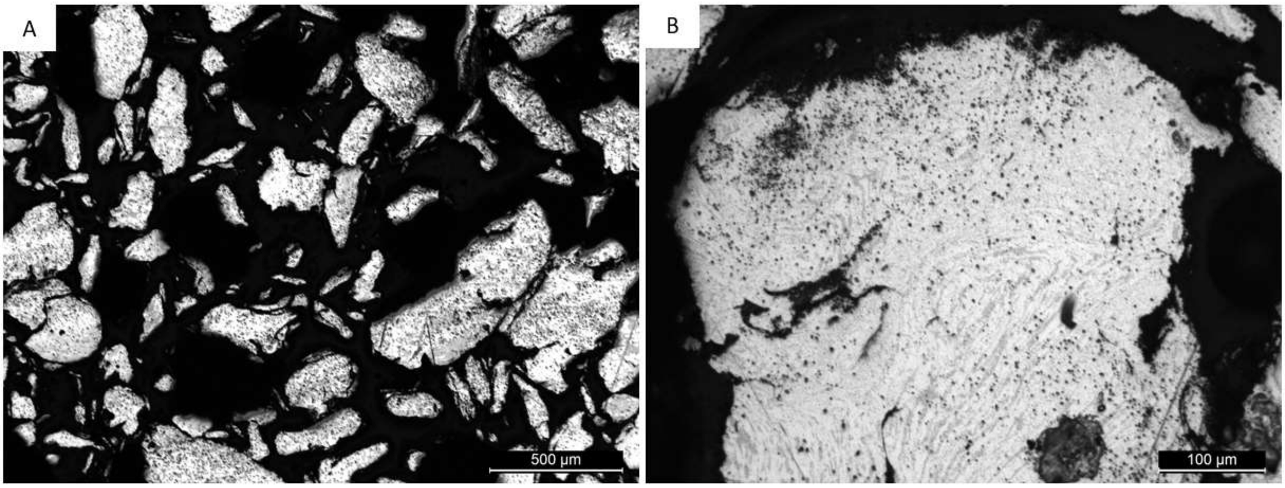

Figure 50 - Powder composite microstructure.

Recurring to SEM, micrographs were also taken from these samples. These can be seen in Figure 51. Starting off with Figure 51C, to better evaluate what the greyish particles in the aluminum matrix correspond to, an EDS semi-quantitative analysis allowed to reach the conclusion that those are Al_2O_3 particles. This is represented in Table 12. Bearing this, on Figure 51A and 51B there seems to be a tendency for Al_2O_3 particles to be agglomerated near the edges of the milled A356 chips. With this in mind, it is important to mention that the milling process needs optimization to achieve a better distribution of the Al_2O_3 across the matrix.

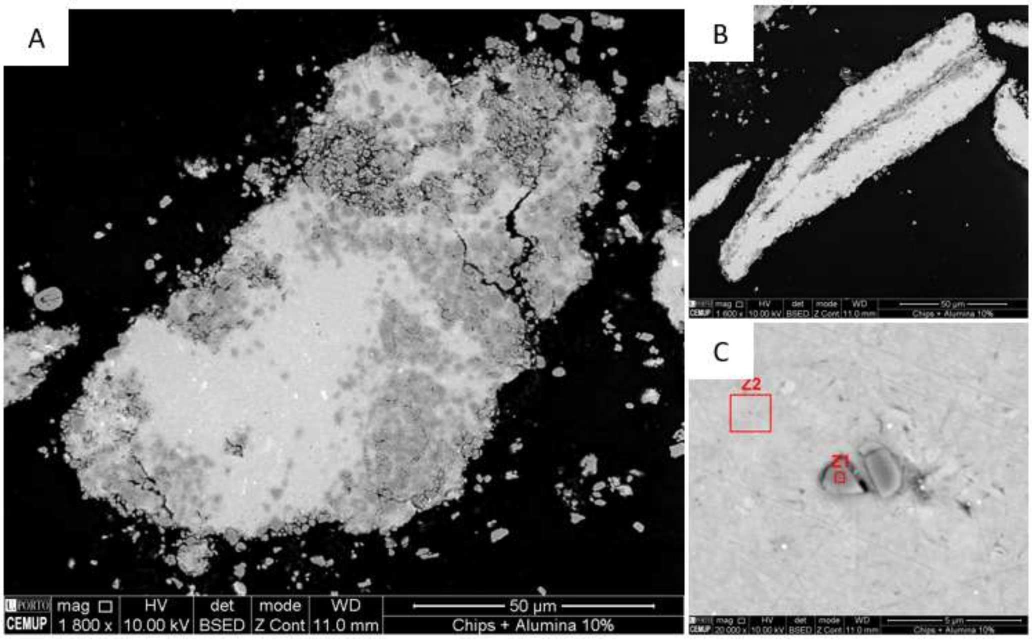

Figure 51 – Powder composite SEM/EDS microstructure.

Table 12 – Powder composite sample EDS chemical analysis on zones Z1 and Z2

Element (at %)	Al	O	Si	C
Z1	49.26	47.96	1.29	1.49
Z2	88.09	4.43	4.67	2.82

4.2.2 Mechanical Tests

4.2.2.1 Hardness Tests

To better understand the effect of the Al_2O_3 on the mechanical properties of the powder composite, more specifically on the hardness, microhardness tests were performed. The results from the powder measurements were compared with the block from which the A356 alloy chips were taken. These can be seen in Table 13.

Table 13 - Hardness values of powder composite and A356 chips

Sample	Hardness
A356 block	81.7 ± 2.2 HV 0.003
Powder composite	157.3 ± 8.6 HV 0.003

Starting off with the alloy block, the values are relatively high, which might be due to either some natural aging of the aluminum, or to the low force applied. Also, for the block, macrohardness examination to better evaluate its' hardness should have been conducted. As for the powder, the hardness values seem to practically double, which leads to believe that the milling procedure carried out allowed the formation of a strengthened composite powder.

5 Conclusions and Future Works

5.1 Conclusions

The main objectives of this study, namely producing aluminum composites and powder composite, were achieved. Furthermore, these composites were also successfully characterized through microstructural analysis, fractography examination and mechanical tests such as tensile and microhardness.

The aluminum-steel bimetallic composites presented an IML layer with multiple ternary, and occasionally quaternary, compounds, as well as binary phases. Hot dipping the inserts seems to lead to a slight increase in IML thickness but also a somewhat more regular layer. However, the composites presented a discontinuity line propagating through the eutectic α-Al and Si compounds in the aluminum matrix along the insert. Silicon segregation that caused different strength zones in the material is believed to be the cause of this. Furthermore, in order to try and improve the bond quality between aluminum and steel, an ammonium chloride treatment was performed. It was found that the application of this treatment caused a reduction in both the thickness and irregularity of the IML layer, and also seemed to prevent the installation of the discontinuity line. The cause of the latter benefit may be due to either the prevention of silicon segregation or the modification of the eutectic compound morphology, which appears to have become less rounded and more needle-like.

As for the mechanical properties, the bimetallic composites do not appear to have enhanced the strength of the base material, despite increasing its ductility. In fact, the composites had a decrease of approximately 50% in YS and UTS of the base alloy. This is believed to have been caused by the pre-existing holes in the inserts, that were created to try and improve aluminum adhesion to the steel. When mechanically loaded, due to a decreased section area, greater tension was being applied on those zones, which led to a premature fracture of the tensile specimens. Nonetheless, both the composites and the T6 A356 base alloy presented very low A% values, which are believed to have been caused by existing porosities.

Hardness profiles were also obtained on the IML of the composites. With these, it was evidenced that the closer to the insert, the higher the hardness due to a more prevalent formation of brittle intermetallic compounds such as η-Al_5Fe_2 and τ5-$Al_{7.4}Fe_2Si$. Both of these compounds presented microhardness values around 1300 HV 0.003.

Finally, the fractography examination presented both fracture mechanisms in the composites. In the aluminum matrix, as well as in the IML, cleavage planes were mostly evident, pointing to fragile behavior. On the other hand, the steel insert had dimples all over its' fracture surface, exhibiting a ductile behavior. Also, it was confirmed that in the T6 A356 base alloy, porosities are at fault for the very low A% values, despite the relatively low porosity percentage, which was found to be around 2%.

On the other hand, a discontinuously reinforced A356/Al_2O_3 powder composite was produced through milling. In turn, this powder was observed in OM and SEM, and underwent microhardness examination. The microstructures revealed the presence of unevenly distributed Al_2O_3 particles across the aluminum matrix, more specifically agglomeration on the edges of the A356 chips. These also presented distortion of both the eutectic and aluminum dendrites, possibly due to either the milling procedure or the absence of liquid processing post-milling. As for the mechanical properties, hardness test results have shown that the powder composite has twice the hardness values of the A356 alloy block from which the chips were taken.

Also, it was not possible to produce cast composites with milled powder due to a lack of fusion in the available furnace and malfunctioning centrifugal equipment.

5.2 Future Works

After the realization of the present work, some things can still be done to improve or complete it. Some suggestions follow:

- Verify and complete the microstructural analysis with the assistance of EBSD or TEM techniques on the IML layer.
- Produce a steel inserted A356 aluminum cast with a previous ammonium chloride treatment and hot dipping to evaluate mechanical properties.
- Produce a steel inserted A356 aluminum cast without holes in the steel sheets to check if it is possible to achieve strength improvement.
- Perform optimization of the milling procedure to achieve better Al_2O_3 distribution.
- Produce a composite cast with powder composite.
- Test the composite powder in additive manufacturing techniques such as direct energy deposition (DED).
- Perform mechanical tests and microstructural analysis on the composite made with the powder composite.

References

[1] D. S. L. Miracle Daniel B., “1. Introduction to Composites,” *ASM Handbook, Volume 21 - Composites*. ASM International, 2001. [Online]. Available: https://app.knovel.com/hotlink/khtml/id:kt007PRMG1/asm-handbook-volume-21/asm-handbo-introduction

[2] F. Nturanabo, L. Masu, and J. B. Kirabira, “Novel Applications of Aluminium Metal Matrix Composites,” in *Aluminium Alloys and Composites*, K. O. Cooke, Ed., Rijeka: IntechOpen, 2019. doi: 10.5772/intechopen.86225.

[3] P. Mallick, “Fiber Reinforced Composites Materials, Manufacturing, and Design.”

[4] F. C. Campbell, “33.1 Aluminum-Matrix Composites,” *Elements of Metallurgy and Engineering Alloys*. ASM International, 2008. [Online]. Available: https://app.knovel.com/hotlink/khtml/id:kt00URM2Y1/elements-metallurgy-engineering/aluminum-matrix-composites

[5] A. S. M. I. H. Committee, “122.1 Classification of MMCs,” in *ASM Handbook, Volume 15 - Casting*, ASM International. [Online]. Available: https://app.knovel.com/hotlink/pdf/id:kt008I4MO4/asm-handbook-volume-15/classification-mmcs

[6] O. Emadinia, “Processing Metal Powders & Reinforcements,” in *Metal Matrix Composites and Advanced Metallic Materials curricular unit appointments*, 2021.

[7] F. C. Campbell, “20.1 Aluminum Matrix Composites,” *Structural Composite Materials*. ASM International, 2010. [Online]. Available: https://app.knovel.com/hotlink/khtml/id:kt008N7PB1/structural-composite/aluminum-matrix-composites

[8] T. William Clyne, “Thermal and electrical conduction in metal matrix composites,” in *Comprehensive Composite Materials II*, Elsevier, 2017, pp. 188–212. doi: 10.1016/B978-0-12-803581-8.09970-7.

[9] Yi X., Du S., and Zhang L., “Composite Materials Engineering, Volume 1_ Fundamentals of Composite Materials”.

[10] T. J. D. R. Talbot David E. J., “6.3 Hot-Dip Coatings,” *Corrosion Science and Technology (3rd Edition)*. CRC Press, 2018. [Online]. Available: https://app.knovel.com/hotlink/khtml/id:kt011MIGR2/corrosion-science-technology/hot-dip-coatings

[11] D. S. L. Miracle Daniel B., “20. Metallic Matrices,” *ASM Handbook, Volume 21 - Composites*. ASM International, 2001. [Online]. Available: https://app.knovel.com/hotlink/khtml/id:kt007PRUU5/asm-handbook-volume-21/metallic-matrices

[12] W. J. K. J. G. Anderson Kevin, “22. Processing of Aluminum Metal-Matrix Composites,” *ASM Handbook, Volume 02A - Aluminum Science and Technology*. ASM International, 2018. [Online]. Available: https://app.knovel.com/hotlink/khtml/id:kt00CYUTL6/asm-handbook-volume-02a/processing-aluminum-metal

[13] S. M. Lee, “29. Metal Matrix Composites, Discontinuously Reinforced, Microstructure and Mechanical Property Correlations,” *Handbook of Composite Reinforcements*. John Wiley & Sons, 1993. [Online]. Available: https://app.knovel.com/hotlink/khtml/id:kt00CRB5L1/handbook-composite-reinforcements/handbook-c-metal-matrix-3

[14] S. M. Lee, “26. Metal Matrix Composites, Aluminum,” *Handbook of Composite Reinforcements*. John Wiley & Sons, 1993. [Online]. Available:

https://app.knovel.com/hotlink/khtml/id:kt00CRB4NF/handbook-composite-reinforcements/metal-matrix-composites

[15] N/A, "1.2 Introduction to MMC Materials," in *Military Handbook - MIL-HDBK-17-4A: Composite Materials Handbook, Volume 4 - Metal Matrix Composites*, U.S. Department of Defense. [Online]. Available: https://app.knovel.com/hotlink/pdf/id:kt0056OJG8/military-handbook-mil/introduction-mmc-materials

[16] S. A. Sajjadi, H. R. Ezatpour, and M. Torabi Parizi, "Comparison of microstructure and mechanical properties of A356 aluminum alloy/Al2O3 composites fabricated by stir and compo-casting processes," *Mater Des*, vol. 34, pp. 106–111, 2012, doi: https://doi.org/10.1016/j.matdes.2011.07.037.

[17] B.-C. Yang *et al.*, "Effects of microstructure coarsening and casting pores on the tensile and fatigue properties of cast A356-T6 aluminum alloy: A comparative investigation," *Materials Science and Engineering: A*, vol. 857, p. 144106, 2022, doi: https://doi.org/10.1016/j.msea.2022.144106.

[18] E. Sequeiros, "Powder Characterization," in *Aditive Manufacturing and Powder Metallurgy curricular unit appointments*,

[19] D. R. J. J. A. M. N. M. E. V. V. G. F. Y. D. Bruno Thomas J., "6. Introduction to Characterization of Powders," *ASM Handbook, Volume 10 - Materials Characterization (2019 edition)*. ASM International, 2019. [Online]. Available: https://app.knovel.com/hotlink/khtml/id:kt012EHZ27/asm-handbook-volume-10/asm-handbo-introduction-2

[20] L. Castanheira, "Production of Sustainable Powders for Direct Energy Deposition (DED)."

[21] Powder Metallurgy - Vocabulary, ISO 3252:2019, 2019.

[22] N. S. S. M. I. V. G. V. G. F. I. V. L. D. V Neikov Oleg D., "1.4 Techniques of Chemical Analysis for Powders," *Handbook of Non-Ferrous Metal Powders - Technologies and Applications*. Elsevier, 2009. [Online]. Available: https://app.knovel.com/hotlink/khtml/id:kt006QPW82/handbook-non-ferrous/techniques-chemical-analysis

[23] M. Kok, "Production and mechanical properties of Al2O3 particle-reinforced 2024 aluminium alloy composites," *J Mater Process Technol*, vol. 161, no. 3, pp. 381–387, 2005, doi: https://doi.org/10.1016/j.jmatprotec.2004.07.068.

[24] E. M. F. N. A. W. Harnby N., "6.1 Introduction," *Mixing in the Process Industries (2nd Edition)*. Elsevier, 1992. [Online]. Available: https://app.knovel.com/hotlink/khtml/id:kt00C5YSN6/mixing-in-process-industries/dispersion-introduction

[25] H. S. S. Peker Sümer M., "7.1.1 Phenomena Involving Surface and Interfacial Tensions," *Solid-Liquid Two Phase Flow*. Elsevier, 2008. [Online]. Available: https://app.knovel.com/hotlink/khtml/id:kt00C50522/solid-liquid-two-phase/phenomena-involving-surface

[26] S. Ebnesajjad, "5.5 Wetting Theory," *Surface Treatment of Materials for Adhesion Bonding*. William Andrew Publishing, 2006. [Online]. Available: https://app.knovel.com/hotlink/khtml/id:kt003XMN81/surface-treatment-materials/wetting-theory

[27] S. A. Sajjadi, H. R. Ezatpour, and H. Beygi, "Microstructure and mechanical properties of Al–Al2O3 micro and nano composites fabricated by stir casting," *Materials Science and Engineering: A*, vol. 528, no. 29, pp. 8765–8771, 2011, doi: https://doi.org/10.1016/j.msea.2011.08.052.

[28] F. Viana, “Ciência dos Materiais - Solidificação.” [Online]. Available: https://youtu.be/jq8pCThPIjo

[29] A. Vencl, I. Bobic, S. Arostegui, B. Bobic, A. Marinković, and M. Babić, “Structural, mechanical and tribological properties of A356 aluminium alloy reinforced with Al2O3, SiC and SiC+graphite particles,” *J Alloys Compd*, vol. 506, no. 2, pp. 631–639, 2010, doi: https://doi.org/10.1016/j.jallcom.2010.07.028.

[30] J. F. D. H. H. L. R. H. H. M. C. J. B. L. Oberg Erik, “7.3.23 Centrifugal Casting,” *Machinery’s Handbook (31st Edition)*. Industrial Press, 2020. [Online]. Available: https://app.knovel.com/hotlink/khtml/id:kt012F3TZ1/machinerys-handbook-31st/metal-cast-centrifugal

[31] N. Janco, “1.4.1 Method I-True Centrifugal Casting,” *Centrifugal Casting*. American Foundry Society (AFS), 1988. [Online]. Available: https://app.knovel.com/hotlink/khtml/id:kt00CY8I11/centrifugal-casting/method-i-true-centrifugal

[32] H. Sevik and S. C. Kurnaz, “Properties of alumina particulate reinforced aluminum alloy produced by pressure die casting,” *Mater Des*, vol. 27, no. 8, pp. 676–683, 2006, doi: https://doi.org/10.1016/j.matdes.2005.01.006.

[33] A. Bouayad, C. Gerometta, A. Belkebir, and A. Ambari, “Kinetic interactions between solid iron and molten aluminium,” *Materials Science and Engineering: A*, vol. 363, no. 1, pp. 53–61, 2003, doi: https://doi.org/10.1016/S0921-5093(03)00469-6.

[34] H. Nunes *et al.*, “Infiltration of aluminum in 3D-printed metallic inserts,” *Applied Research*, vol. 2, no. 1, Feb. 2023, doi: 10.1002/appl.202200062.

[35] S. Kobayashi and T. Yakou, “Control of intermetallic compound layers at interface between steel and aluminum by diffusion-treatment,” *Materials Science and Engineering: A*, vol. 338, no. 1, pp. 44–53, 2002, doi: https://doi.org/10.1016/S0921-5093(02)00053-9.

[36] Xiangfan Fang, “Evaluation of Coating Systems for Steel Aluminum Hybrid Casting,” *J Mater Sci Eng A*, vol. 7, no. 2, Apr. 2017, doi: 10.17265/2161-6213/2017.3-4.001.

[37] Q. Wang, C.-Z. Zhao, H.-X. Zhang, H. Li, and X.-K. Yang, “Microstructure and Mechanical Properties of Al/Steel Bimetal Composite Produced by Compound Casting,” *International Journal of Materials Science and Engineering*, vol. 6, pp. 72–79, Sep. 2019, doi: 10.17706/ijmse.2018.6.3.72-79.

[38] F. Mao *et al.*, “Interface Microstructure and Mechanical Properties of Al/Steel Bimetallic Composites Fabricated by Liquid-Solid Casting with Rare Earth Eu Additions,” *Materials*, vol. 15, no. 19, 2022, doi: 10.3390/ma15196507.

[39] J. G. Bralla, “4.B2a Plunger Molding,” *Handbook of Manufacturing Processes - How Products, Components and Materials are Made*. Industrial Press, 2007. [Online]. Available: https://app.knovel.com/hotlink/khtml/id:kt006HS3L1/handbook-manufacturing/a-plunger-molding

[40] R. Guo, D. Zeng, and F. Li, “Promoting of metallurgical bonding by ultrasonic insert process in steel–aluminum bimetallic castings,” vol. 41, no. 1, pp. 289–295, 2022, doi: doi:10.1515/htmp-2022-0009.

[41] W. J. K. J. G. Anderson Kevin, “22.2 Metal-Matrix Composite Infiltration Processes,” *ASM Handbook, Volume 02A - Aluminum Science and Technology*. ASM International, 2018. [Online]. Available: https://app.knovel.com/hotlink/khtml/id:kt00CYUTX2/asm-handbook-volume-02a/processing-metal-matrix

[42] J. Campbell, “Rule 2. Avoid Turbulent Entrainment (the Critical Velocity Requirement),” *Castings Practice - The Ten Rules of Castings*. Elsevier, 2004.

[Online]. Available: https://app.knovel.com/hotlink/khtml/id:kt009FHZG5/castings-practice-ten/rule-2-avoid-turbulent

[43] F. C. Campbell, “9. Metal-Matrix Composites,” *Lightweight Materials - Understanding the Basics*. ASM International, 2012. [Online]. Available: https://app.knovel.com/hotlink/khtml/id:kt00AW59PB/lightweight-materials/lightweigh-metal-matrix

[44] J. F. D. H. H. L. R. H. H. M. C. J. B. L. Oberg Erik, “7.3.24 Squeeze Casting,” *Machinery’s Handbook (31st Edition)*. Industrial Press, 2020. [Online]. Available: https://app.knovel.com/hotlink/khtml/id:kt012F3U34/machinerys-handbook-31st/squeeze-casting

[45] R. P. K. Gupta Nikhil, “3.1.5 Centrifugal Casting and Infiltration,” *Metal Matrix Syntactic Foams - Processing, Microstructure, Properties and Applications*. DEStech Publications, 2015. [Online]. Available: https://app.knovel.com/hotlink/khtml/id:kt011EPEC1/metal-matrix-syntactic/centrifugal-casting-infiltration

[46] G. E. Totten, “41.4 Strengthening Mechanisms of Aluminum Alloys,” *ASM Handbook, Volume 18 - Friction, Lubrication, and Wear Technology (2017 Revision)*. ASM International, 2017. [Online]. Available: https://app.knovel.com/hotlink/khtml/id:kt00CY9LP1/asm-handbook-volume-18/strengthening-mechanisms

[47] M. A. T. Olander Donald R., “11.3.2 Strengthening Mechanisms,” *Light Water Reactor Materials, Volume I - Fundamentals*. American Nuclear Society (ANS), 2017. [Online]. Available: https://app.knovel.com/hotlink/khtml/id:kt011ILCA1/light-water-reactor-materials/strengthening-mechanisms

[48] Q. J. S. J. X. G. N. D. T. P. F. S. H. L. Shi Cai Jun, “16.5.2 Strengthening Mechanism,” *Materials in Machinery and Construction*. Trans Tech Publications, 2021. [Online]. Available: https://app.knovel.com/hotlink/khtml/id:kt012ZBYN2/materials-in-machinery/strengthening-mechanism

[49] M. A. T. Olander Donald R., “7.12.4 Obstacles,” *Light Water Reactor Materials, Volume I - Fundamentals*. American Nuclear Society (ANS), 2017. [Online]. Available: https://app.knovel.com/hotlink/khtml/id:kt011IL9S2/light-water-reactor-materials/obstacles

[50] W. Jiang, Z. Fan, and C. Li, “Improved steel/aluminum bonding in bimetallic castings by a compound casting process,” *J Mater Process Technol*, vol. 226, pp. 25–31, 2015, doi: https://doi.org/10.1016/j.jmatprotec.2015.06.032.

[51] B. Yang, H. Song, S. Wang, S. Chen, and S. Zhang, “Tension-compression mechanical behavior and corresponding microstructure evolution of cast A356-T6 aluminum alloy,” *Materials Science and Engineering: A*, vol. 821, p. 141613, 2021, doi: https://doi.org/10.1016/j.msea.2021.141613.

[52] T. Haskel, G. O. Verran, and R. Barbieri, “Rotating and bending fatigue behavior of A356 aluminum alloy: Effects of strontium addition and T6 heat treatment,” *Int J Fatigue*, vol. 114, pp. 1–10, 2018, doi: https://doi.org/10.1016/j.ijfatigue.2018.04.012.

[53] J. Yu, “Formation of Intermetallic Phases in Al-10Si-0.3Fe based Alloys,” 2016. doi: 10.14279/depositonce-5679.

[54] M. Petrič, B. Zeka, P. Mrvar, A. Nagode, M. Vončina, and T. Balaško, “Solidification behaviour and microstructure of AlSi7Mg cast alloy with addition of Li,” *Journal of Materials Research and Technology*, vol. 19, pp. 2084–2092, 2022, doi: https://doi.org/10.1016/j.jmrt.2022.05.171.

[55] A. O. Bakke, L. Arnberg, J.-O. Løland, S. Jørgensen, J. Kvinge, and Y. Li, “Formation and evolution of the interfacial structure in al/steel compound castings during solidification and heat treatment,” *J Alloys Compd*, vol. 849, p. 156685, 2020, doi: https://doi.org/10.1016/j.jallcom.2020.156685.

[56] M. C. J. Marker, B. Skolyszewska-Kühberger, H. S. Effenberger, C. Schmetterer, and K. W. Richter, “Phase equilibria and structural investigations in the system Al-Fe-Si,” *Intermetallics (Barking)*, vol. 19, no. 12, pp. 1919–1929, 2011, doi: https://doi.org/10.1016/j.intermet.2011.05.003.

[57] L. F. (Lucio F.) Mondolfo, *Aluminum alloys : structure and properties*. Butterworths, 1976.

[58] T. Maitra and S. P. Gupta, “Intermetallic compound formation in Fe–Al–Si ternary system: Part II,” *Mater Charact*, vol. 49, no. 4, pp. 293–311, 2002, doi: https://doi.org/10.1016/S1044-5803(03)00005-6.

[59] W. Yi, J. Gao, Y. Tang, and L. Zhang, “Thermodynamic descriptions of ternary Al–Si–Sr system supported by key experiments,” *Calphad*, vol. 68, p. 101732, 2020, doi: https://doi.org/10.1016/j.calphad.2019.101732.

[60] M. A. Baghchesara and H. Abdizadeh, “Production and microstructural investigation of A356 aluminum alloy based Magnesium oxide particles reinforced metal-matrix nanocomposites,” 2014.

[61] J. L. Murray, “The Al−Zn (Aluminum-Zinc) system,” *Bulletin of Alloy Phase Diagrams*, vol. 4, no. 1, pp. 55–73, 1983, doi: 10.1007/BF02880321.

[62] K. Zhang, X. Bian, Y. Li, Y. Liu, and C. Yang, “New evidence for the formation and growth mechanism of the intermetallic phase formed at the Al/Fe interface,” *J Mater Res*, vol. 28, no. 23, pp. 3279–3287, 2013, doi: 10.1557/jmr.2013.345.

[63] B. S. Majumdar, “Engineering Mechanics and Analysis of Metal-Matrix Composites,” 2001, doi: 10.1361/asmhba0003399.

[64] Aluminum A356.0-T6, Sand Cast, https://www.matweb.com/search/datasheet_print.aspx?matguid=d524d6bf305c4ce99414cabd1c7ed070.

[65] Aluminum 356.0-F, Sand Cast, https://www.matweb.com/search/DataSheet.aspx?MatGUID=4625707f449a43b59a6dbdbf9617526b.

[66] M. Tupaj, A. Orlowicz, M. Mróz, A. Trytek, A. Dolata, and A. Dziedzic, “A Study on Material Properties of Intermetallic Phases in a Multicomponent Hypereutectic Al-Si Alloy with the Use of Nanoindentation Testing”.

[67] M. Karim and Y.-D. Park, “A Review on Welding of Dissimilar Metals in Car Body Manufacturing,” *Journal of Welding and Joining*, vol. 38, Feb. 2020, doi: 10.5781/JWJ.2020.38.1.1.

[68] S. Tabibian, E. Charkaluk, A. Constantinescu, G. Guillemot, and F. Szmytka, “Influence of process-induced microstructure on hardness of two Al-Si alloys,” *Materials Science and Engineering: A*, vol. 646, pp. 190–200, 2015, doi: 10.1016/j.msea.2015.08.051ï.

[69] J. R. Davis, “28.4.1.3 Intermetallic Constituents,” *ASM Specialty Handbook - Aluminum and Aluminum Alloys*. ASM International, 1993. [Online]. Available: https://app.knovel.com/hotlink/khtml/id:kt00URKH21/asm-specialty-handbook/intermetallic-constituents

Appendix: Al-Si-Fe Ternary Phase Diagrams

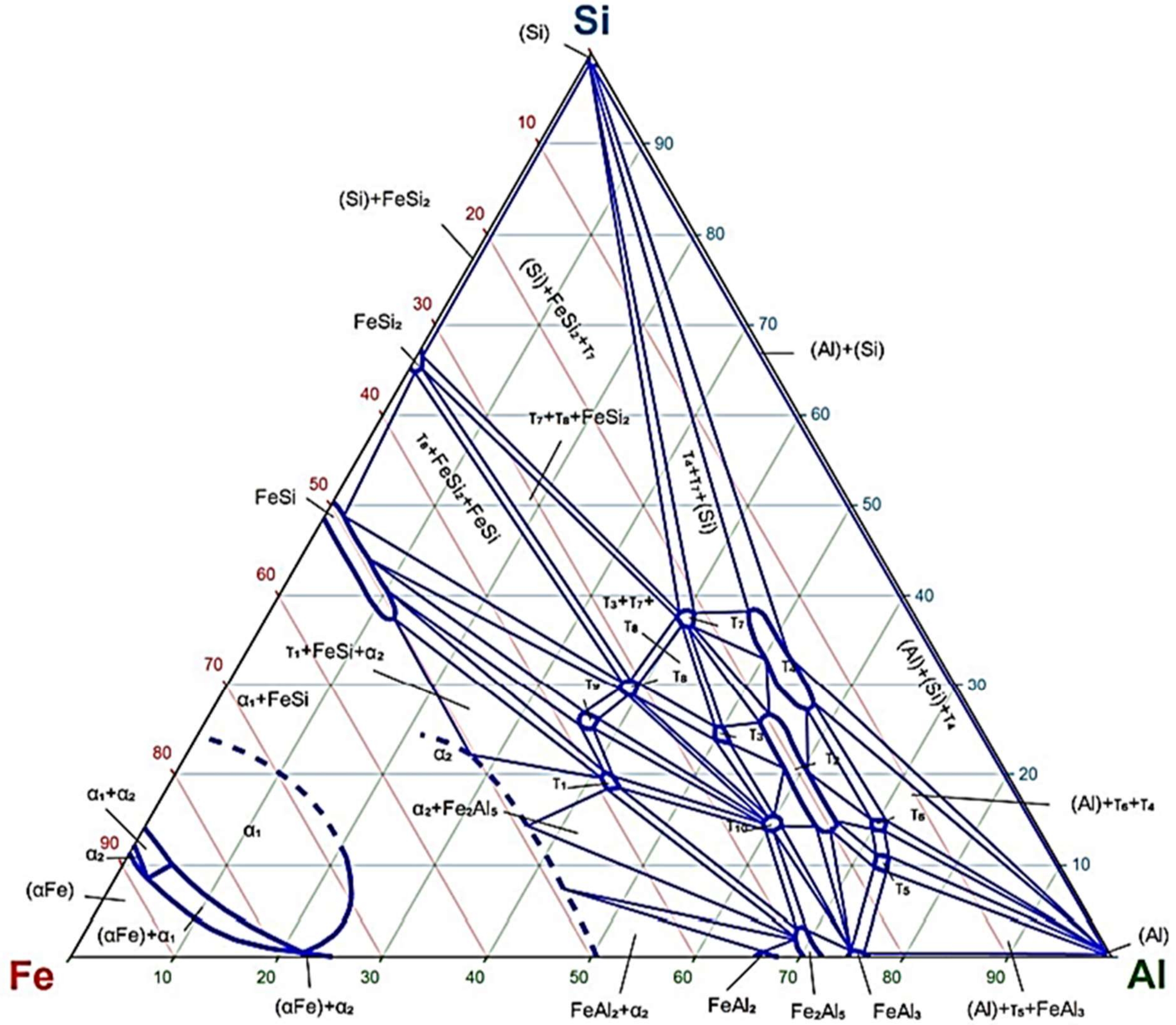

Figure 52 - Al-Si-Fe ternary phase diagram at 600 ºC [53].

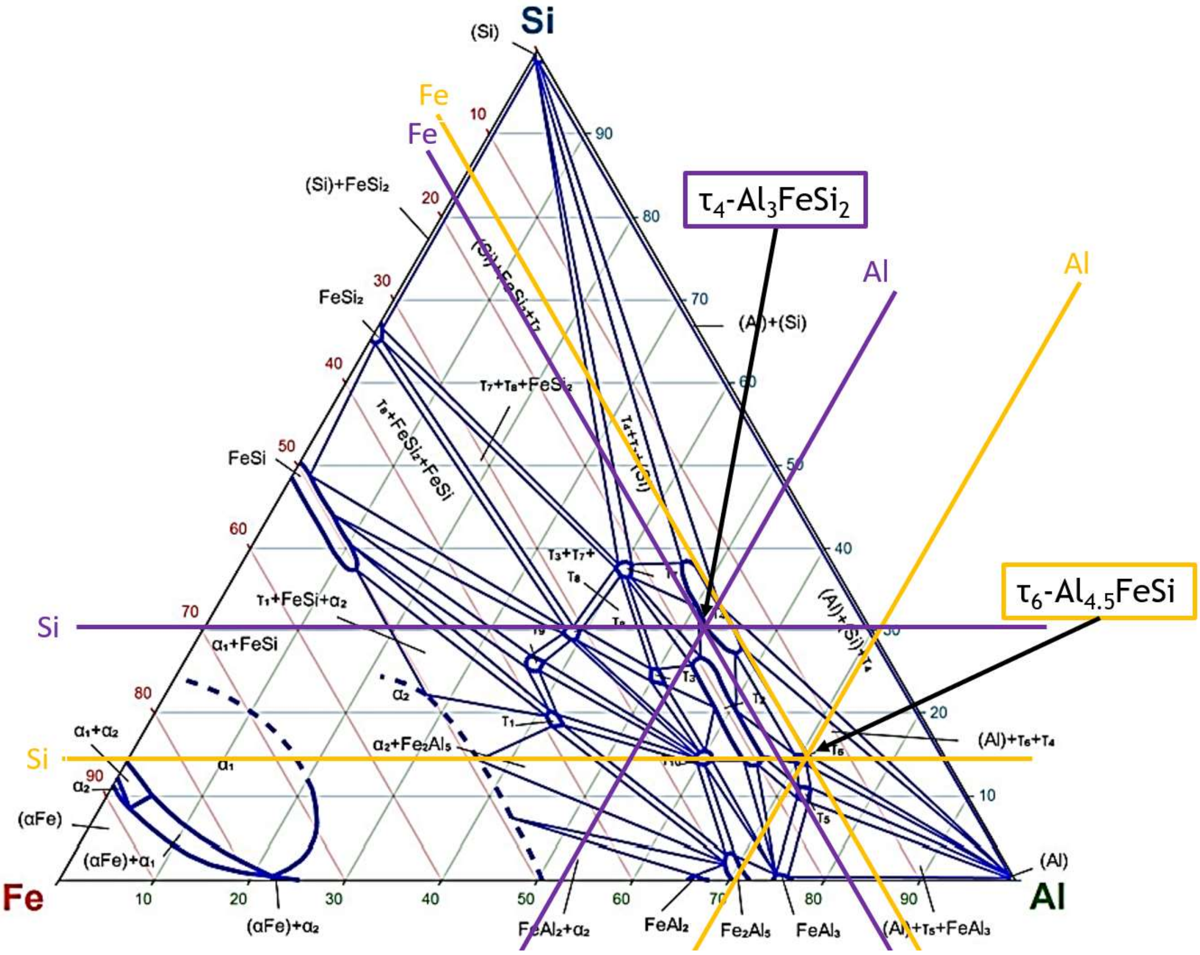

Figure 53 - Al-Si-Fe ternary phase diagram at 600 ºC with the chemical composition for A356 base alloy Z4 - τ6-$Al_{4.5}FeSi$ and Z5 - τ4-Al_3FeSi_2. Adapted from [53].

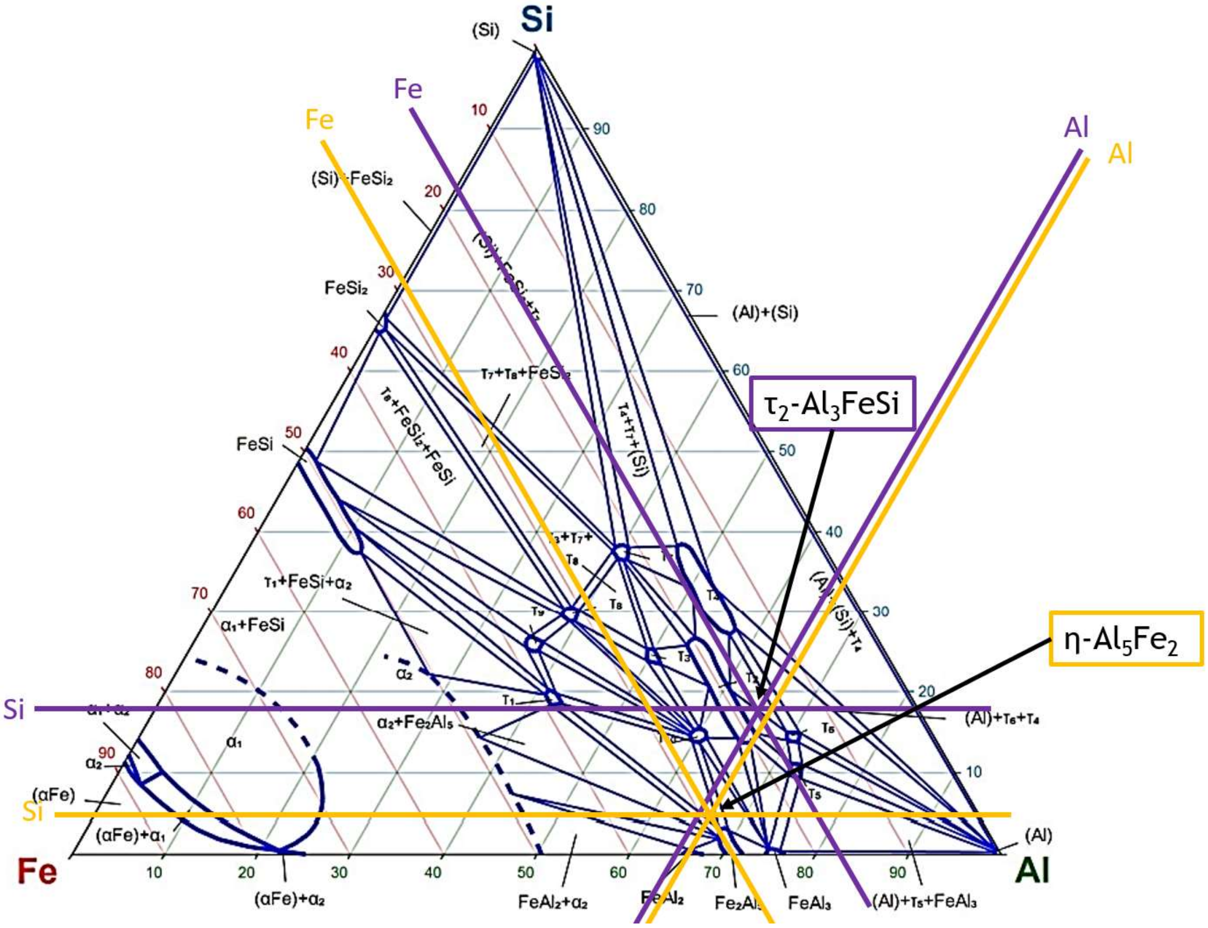

Figure 54 - Al-Si-Fe ternary phase diagram at 600 ºC with the chemical composition for cold inserted composite Z4 - τ2-Al_3FeSi and Z5 - η-Al_5Fe_2. Adapted from [53].

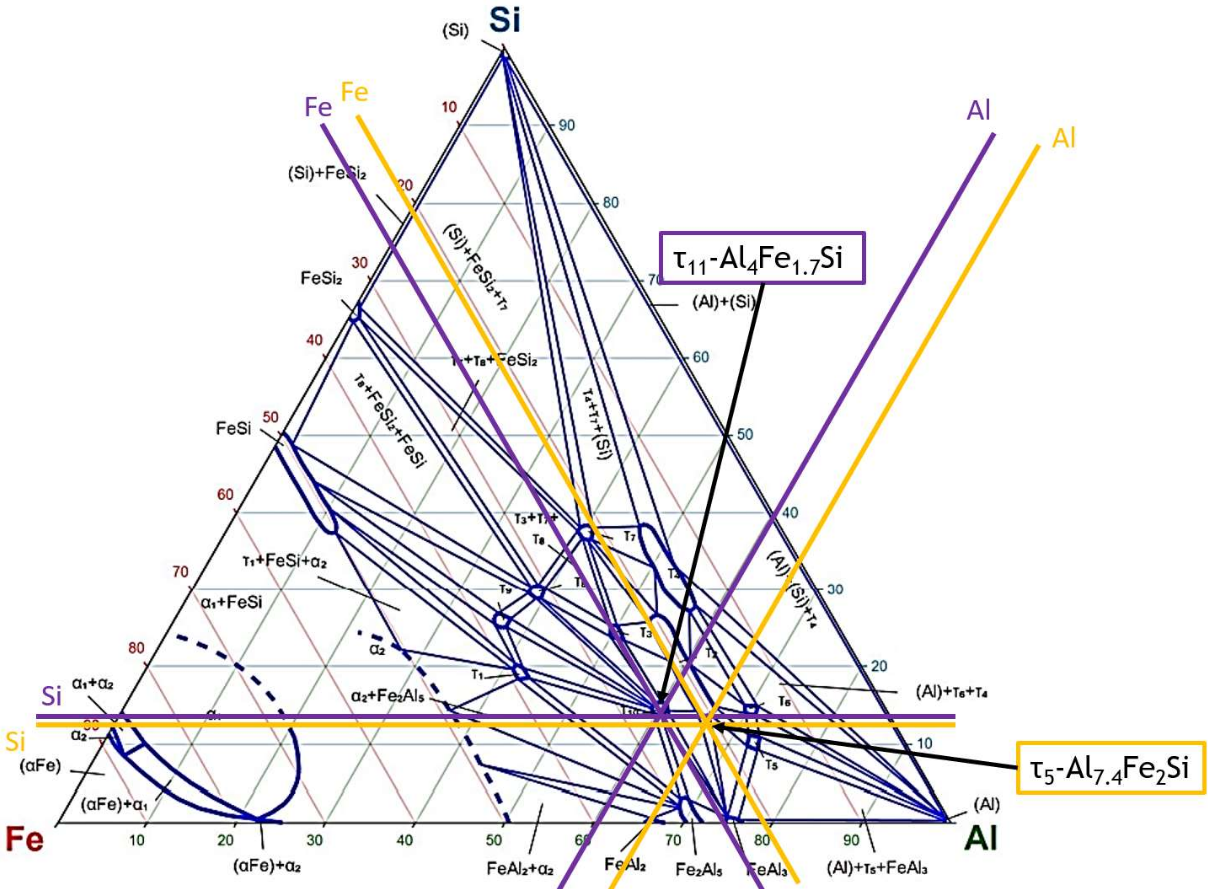

Figure 55 - Al-Si-Fe ternary phase diagram at 600 ºC with the chemical composition for hot dipped composite Z3 - τ11-Al$_4$Fe$_{1.7}$Si and Z4 - τ5-Al$_{7.4}$Fe$_2$Si. Adapted from [53].